

Copyright

by

MING DING

2004

The Dissertation Committee for MING DING
certifies that this is the approved version of the following dissertation:

**Channel Equalization To Achieve High Bit Rates
In Discrete Multitone Systems**

Committee:

Brian L. Evans, Supervisor

Ross Baldick

Melba M. Crawford

Robert W. Heath, Jr.

Edward J. Powers

**Channel Equalization To Achieve High Bit Rates
In Discrete Multitone Systems**

by

MING DING, B.S., M.ENG.

Dissertation

Presented to the Faculty of the Graduate School of

The University of Texas at Austin

in Partial Fulfillment

of the Requirements

for the Degree of

Doctor of Philosophy

The University of Texas at Austin

August 2004

to my family

Acknowledgments

Life is a journey. I just finished an exciting ride. The happiness from this one will last for a long long time and I feel obligated to show my gratitude to the persons accompanying me during this wonderful trip.

I would like to start by thanking my supervisor Prof. Brian L. Evans. This dissertation could not have been written without him who not only recruited and sponsored me to the program but also encouraged and challenged me throughout the whole process.

I wish to express sincere appreciation to Dr. Rick Martin and Professor Richard Johnson, Jr. for their nice hosting of my visiting study at Cornell University and for their long term cooperation in the joint research which consists of core of this manuscript. Also, many thanks to Dr. K. Vanbleu and Dr. G. Ysebaert for their endless effort and valuable input to the joint research.

I want to thank Dr. Arthur Redfern and Dr. Murtaza Ali at Texas Instruments DSPS center. With their assistance and friendship, I had very pleasant experience during my internships at their group. What I learned from them contributes a lot to my Ph.D. work. Knowing how to think from a developer's perspective really narrows the gap between academia and industry. I believe it will benefits my future career definitely.

My gratitude goes to three of my former group members, Dr. Guner Arslan, Dr. Lu Biao and Dr. Milos Milosevic. Without their hard work and great results

to jump start and form a solid base of this project, I cannot continue this research smoothly and successfully. Special thank to my current group member Zukang Shen for his sincere friendship, great personality and nice cooperation. The thanks also go to rest of my group members of the Embedded Signal Processing Laboratory: Gregory E. Allen, Dogu Arifler, Serene Banerjee, Kyungtae Han, Vishal Monga, Ian Wong, Wade C. Schwartzkopf and K. Clint Slatton. They made the lab a warm, family-like environment for a great stay.

Last but not least, I would like to thank my entire family for their always accessible support from the day I was born.

MING DING

The University of Texas at Austin

August 2004

Channel Equalization To Achieve High Bit Rates In Discrete Multitone Systems

Publication No. _____

MING DING, Ph.D.

The University of Texas at Austin, 2004

Supervisor: Brian L. Evans

Multicarrier modulation (MCM) techniques such as orthogonal frequency division multiplexing (OFDM) and discrete multi-tone (DMT) modulation are attractive for high-speed data communications due to the ease with which MCM can combat channel dispersion. With all the benefits MCM could give, DMT modulation has an extra ability to perform dynamic bit loading, which has the potential to exploit fully the available bandwidth in a slowly time-varying channel. In broadband wireline communications, DMT modulation is standardized for asymmetric digital subscribe line (ADSL) and very-high-bit-rate digital subscriber line (VDSL) modems. ADSL and VDSL standards are used by telephone companies to provide high speed data service to residences and offices.

In an ADSL receiver, an equalizer is required to compensate for the channel's dispersion in the time domain and the channel's distortion in the frequency domain of the transmitted waveform. This dissertation proposes design methods for linear equalizers to increase the bit rate of the connection. The methods are amenable

to implementation on programmable fixed-point digital signal processors, which are employed in ADSL/VDSL transceivers.

A conventional ADSL equalizer consists of a time-domain equalizer, a fast Fourier transform, and a frequency domain equalizer. The time domain equalizer (TEQ) is a finite impulse response filter that when coupled with a discretized channel produces an equivalent channel whose impulse response is shorter than that of the discretized channel. This channel shortening is required by the ADSL standards. In this dissertation, I first propose a linear phase TEQ design that exploits symmetry in existing eigen-filter approaches such as minimum mean square error (MMSE), maximum shortening signal to noise ratio (MSSNR) and minimum intersymbol interference (Min-ISI) equalizers. TEQs with symmetric coefficients can reach the same performance as non-symmetric ones with much lower training complexity.

Second, I improve Min-ISI design. I reformulate the cost function to make long TEQs design feasible. I remove the dependency of transmission delay in order to reduce the complexity associated with delay optimization. The quantized weighting is introduced to further lower the complexity. I also propose an iterative optimization procedure of Min-ISI that completely avoids Cholesky decomposition hence is better suited for a fixed-point implementation.

Finally I propose a dual-path TEQ structure, which designs a standard single-FIR TEQ to achieve good bit rate over the entire transmission bandwidth, and designs another FIR TEQ to improve the bit rate over a subset of subcarriers. Dual-path TEQ can be viewed as a special case of a complex valued filter bank structure that delivers the best bit rate of existing DMT equalizers. However, dual-path TEQ provides a very good tradeoff between achievable bit rate vs. implementation complexity on a programmable digital signal processor.

Contents

Acknowledgments	v
Abstract	vii
Chapter 1 Introduction	1
1.1 Broadband Wireline Communications	1
1.1.1 Evolving from Voice to Broadband	3
1.1.2 xDSL Transmission Technologies	5
1.2 Multicarrier Modulation	8
1.3 Channel Equalization	11
1.3.1 Single Carrier Equalization	11
1.3.2 Multicarrier Equalization	13
1.4 Nomenclature and Notation	18
1.5 Thesis Statement and Organization of the Dissertation	22
Chapter 2 Unification of Channel Equalization in Discrete Multitone	
Systems	24
2.1 Introduction	24
2.2 Common Mathematical Framework	26
2.2.1 System Model	26
2.2.2 Unified Framework	28

2.3	Single Quotient Cases	30
2.3.1	Single Filter	30
2.3.2	Multiple Filters	38
2.4	Products of Quotients Cases	42
2.4.1	Maximum Geometric Signal-to-noise Ratio Method	43
2.4.2	Maximum Bit Rate method	45
2.4.3	Maximum Data Rate TEQ	46
2.4.4	Bitrate Maximizing TEQ	46
2.5	Conclusion	48
Chapter 3 Symmetric Equalizer Design		49
3.1	Introduction	49
3.2	Infinite Length Results	50
3.2.1	Magnitude Response	50
3.2.2	Symmetry in Eigenvectors	54
3.3	Design Implication for Finite Length Cases	56
3.3.1	Exploiting Symmetry	56
3.3.2	Exploiting Linear Phase Property	61
3.4	Conclusion	62
Chapter 4 Improving Minimum Intersymbol Interference Methods		63
4.1	Introduction	63
4.2	Original Methods	64
4.2.1	Review	64
4.2.2	Evaluation	66
4.3	Reformulation of the Cost Function	69
4.4	Quantized Weighting Function	71
4.5	Iterative Implementation	73

4.6	Conclusion	75
Chapter 5 Filter Bank Equalization		77
5.1	Introduction	77
5.2	Complex Filter Bank Equalization: A Performance Bound	78
5.2.1	Structure	78
5.2.2	Design	82
5.3	Dual Path Equalizer: A Practical Implementation	85
5.3.1	Model	87
5.3.2	Design	88
5.4	Conclusion	89
Chapter 6 Performance Evaluation		90
6.1	Introduction	90
6.2	Physical Channel Characteristics	90
6.3	Noise Environment	93
6.3.1	Crosstalk noise	93
6.3.2	Other impairments	96
6.4	Achievable Bit Rates On Synthesized Loops	97
6.5	Achievable Bit Rates on Measured Real Channels	105
6.6	Conclusion	107
Chapter 7 Conclusions		109
7.1	Summary	109
7.2	Future Directions	113
Appendix A Applied Signal Technology Data Study		117
A.1	Observations of Provided ADSL Demonstration	117
A.2	Description of Data Under Study	118

A.2.1	Accessing the data	119
A.2.2	Resampling the data	119
A.2.3	Short review of ADSL initialization sequence	120
A.2.4	Channel estimation based on real data	123
Appendix B	Effect of Channel Estimation Error to Performance	130
B.1	Bit Rate Loss Model	131
B.1.1	General Formulation	131
B.1.2	Case Studies	134
B.2	Simulations	137
Bibliography		142
Vita		154

Chapter 1

Introduction

1.1 Broadband Wireline Communications

The broadband era is here. For both home users and businesses, communication is now more about acquiring and distributing information than it is about conversation over old fashioned telephones. Data transmission occupies more of the communications market share than voice communications. Even in telephone networks, more traffic is due to data than to voice. Data communications usually demands higher transmission speed, namely, more bandwidth, than voice communications. Recent technologies, such as Internet telephony and real-time video broadcasting, will further increase the demand for bandwidth. This transformation is challenging the achieved connection speeds being delivered by current communications networks. The future lies with broadband technologies that can move vast amounts of information to and from households and businesses.

Although emerging wireless technologies share part of the burden to build an entirely interconnected world, wireline communications offers most broadband access in today's market through its core networks: cable TV or telephony. On one hand, the user demand for transmission and handling of all the different types of

communications is growing. On the other hand, service providers expect to save money by using the same facilities for all kinds of communications. This demand of convergence actually pushes the development of new technologies that fully utilize the available bandwidth on wired network infrastructure.

Traditionally, cable television distributors used a tree-structured high-speed network that broadcasts television programs from a head to the individual users [1]. The network can carry up to 500 different television channels. To incorporate other types of communications, cable network operators assign available channels to transmit data other than television signals. Conventional cable networks carry one-way traffic going from the hub to the nodes. Modern cable networks have two-way communications for traffic other than TV broadcasting. Modern cable networks establish connections with the Internet, the telephone network and other networks. This turns the head of a cable network into a switching node for many types of traffic going in different directions.

In a cable network, users connect to the Internet via a special cable modem that works as a bridge between a computer and the cable network. According to the Data Over Cable Service Interface Specifications (DOCSIS) standards [2], the downstream channel (from service provider to customer) uses 64 or 256 quadrature amplitude modulation (QAM) on a carrier of 6 MHz to offer either 27 or 36 Mbps bit rate. The upstream (from customer to service provider) adopts quadrature phase shift keying (QPSK) modulation or 16 QAM on a variable carrier between 200 kHz and 3.2 MHz to reach a data rate between 320 kbps and 10 Mbps.

The problem associated with cable networks is that it is shared access. The bandwidth is distributed among all cable users on the same local area cable network. In central Austin, Texas, for example, a local area network might cover a geographic area as large as a square kilometer. Each user can experience deteriorating data rate performance during peak usage periods. In the contrast, telephone line based

technologies provide dedicated access to the individual users. It is reported that even a 384 kbps downstream/128 kbps upstream asymmetric digital subscriber line (ADSL) transmission outperforms cable modem in terms of bit rate in the evening in some test neighborhoods [1].

Despite the fact that ADSL is a point-to-point communications standard, an ADSL line can experience interference from other telephone lines in the same bundle going to the central office. The twisted pair copper wires in the bundle are unshielded. Due to electromagnetic coupling, DSL services running on other lines in the bundle can dramatically reduce the achievable bit rate on one's ADSL line. In the rest of this section, I will focus on high-speed access to the telephone network.

1.1.1 Evolving from Voice to Broadband

The first effort to transmit data over voice channels was made in the 1950s via dial-up modems. The basic idea is to fit the data into the voice band via modulation. The data appears to be a voice signal to the telephone channel although it sounds meaningless. With available voice bandwidth being limited to 3.4 kHz, the highest achievable bit rate of a commercial modem is 56.6 kbps in practice [2]. Since the data transmission occupies the voice channel, it is not possible to simultaneously transmit both voice and data signals.

As one of the earliest efforts to integrate the transmission and switching of data over existing user access lines without interruption of voice communications, the International Telegraph and Telephone Consultative Committee (CCITT), now known as the Telecommunication Standardization Sector of the International Telecommunication Union (ITU-T), formed a group to study the possibility. In 1984, it resulted in a series of CCITT Recommendations concerning the Integrated Services Digital Network (ISDN). Each digital data channel can support 64 kbps (56 kbps on some systems) of bi-directional data and the two data channels of an

ISDN basic rate interface (BRI) line can be combined together to achieve rates of up to 128 kbps. Because user demand in some markets was advancing faster than the recommendations of the CCITT/ITU-T, the agency introduced broadband-ISDN (B-ISDN) to its recommendations in 1990. The agency also recommended the use of asynchronous transfer mode (ATM) for the implementation of B-ISDN. As an ISDN primary rate interface (PRI) line, B-ISDN is composed of 23 data channels, which can support up to 1.5 Mbps in total. As a result, it is much more expensive than the 2-channel BRI ISDN line installed in a typical end user's home and is mainly used by business subscribers [3].

In the meantime, other broadband transmission, switching and routing facilities were being developed. They served as wide area network (WAN) protocols to regulate interconnection between many different data transmission networks. These inventions include X.25, frame relay, and switched megabit data service (SMDS). The CCITT/ITU-T Recommendation X.25 refers to a packet switching standard that includes error detection on each transmission link to be more resilient to low-quality transmission links. Later, the quality of transmission links had been improved, and as a result, frame relay, which essentially abandoned the error-detection feature, emerged as a substitute for X.25. Frame relay is also considered a derivative of ISDN since it was originally designed for connection of ISDN interfaces. SMDS was proposed by Bell Communications Research, Inc. (Bellcore, now called Teleordia). SMDS provides access to telecommunications networks at bit rates from 1.2 Mbps to 34 Mbps. SMDS is based on the user-network interface distributed-queue dual-bus described in the IEEE 802.6 standard [4].

Meanwhile, back at the telephone industry, digital voice channels were often multiplexed into 24 channels to form what is called a T1 line. Outside of North America and Japan, 30 voice channels and 2 control channels are bundled together to form an E1 line. These systems use a protocol called alternate mark inversion

(AMI). They offer a higher bit rate connection than ISDN for business. T1 and E1 systems support digital signal transmission at 1.544 Mbps and 2.048 Mbps, respectively, in many applications besides voice transmissions.

There are several problems associated with AMI. Transmission systems using AMI require a repeater at 3,000 feet from the central telephone office and a repeater every 6,000 feet thereafter. Second, several T1 lines cannot be put on the same cable unless the pairs are shielded. Normally, no more than a single T1 line can be put on a 50-pair cable and two cables with T1 cannot be next to each other. Moreover, all bridged taps should be removed before a T1/E1 line can properly operate. Last but not least, the installation and maintenance are time and financially consuming. These rule out the possibility of using T1/E1 links for household users.

Fortunately, a cheaper alternative to T1/E1 lines was developed. It is so called digital subscribe line (DSL) technology. It will be covered in depth in next subsection.

1.1.2 xDSL Transmission Technologies

xDSL is a family of public network technologies that delivers high bandwidth over traditional existing twisted pairs at limited distances. It realizes the dream that converts the household telephone line from a voice lane into an information highway. The various siblings in the xDSL family – HDSL, ADSL, and VDSL – are all provisioned by modem pairs, with one modem located at the central office and the other at the premises. Most DSL technologies operate over the plain old telephone service (POTS) lines by using a splitter at the customer’s premises to separate voice and data channels. For instance, users browsing the Internet over an ADSL connection can still make and receive telephone calls at the same time. Frequency division multiplexing could enable coexistence of various DSL applications on the same line, although it is rarely seen in current practice.

High-data-rate digital subscriber line (HDSL) delivers a full duplex T1 (1.544 Mbps) or E1 (2.048 Mbps) in each direction over *two* copper twisted pairs without repeaters. Its transmission bandwidth ranges from 80 kHz to 240 kHz. This high-performance technology is a cost-effective alternative for providing T1/E1 access. HDSL's operating range, however, is limited to carrier service areas (CSA) in which lines only extend up to 12,000 feet. HDSL is applied primarily in private branch exchange network connections, digital loop carrier systems, interexchange post office protocols, Internet servers, and private data networks.

Single-line digital subscriber line (SDSL) is similar to HDSL in that it transmits 1.544 Mbps both downstream and upstream, but it provides T1/E1 rates over a single copper twisted pair only. In practice, SDSL operates within 10,000 feet range due to the use of a single twisted pair. But it could be used in such applications as residential video conference or remote local area network (LAN) access because of its symmetric data rates.

Other members in HDSL family include HDSL-2, which also utilizes one pair of wires to deliver T1/E1 rates, and HDSL4, which achieves greater loop reach using two pairs of wires. Those different standards bring issues of interoperability and spectral compatibility. Recently, single pair HDSL (SHDSL) is a new recommendation from ITU (G. 991.2) that addresses these issues and includes all the latest development for symmetric DSL technology as well. Compare to other HDSL technologies, SHDSL provides full symmetric service rates at greater distances and with lower power [5].

Asymmetric digital subscriber line (ADSL) technology was originally intended to support video-on-demand services, but was reshaped to offer Internet access. ADSL is built to deliver much more data going downstream (from the central office to the subscriber) than upstream. Downstream rates range from 1.5 Mbps to 9 Mbps, while upstream bandwidth ranges from 16 kbps to 640 kbit/s. Range

extended ADSL (READSL) can work outside the CSA on lines up to 18,000 feet over a single copper twisted pair. The project of long reach DSL is still on-going at the ITU [6].

Recent developments in ADSL technology include ADSL2 and ADSL2+. ADSL2, which is standardized by ITU G.992.3 and G.992.4, adds new features and functionality aimed at improving communication performance and interoperability. It also defines new applications, services and deployment scenarios. Among the changes are improvements in data rate performance, reach distance, rate adaptation, and diagnostics. ADSL2+, which is standardized by ITU G.992.5, doubles the bandwidth used for downstream data transmission, thereby effectively doubling the maximum downstream data rates, and achieving rates of 20 Mbps on phone lines up to 5,000 feet. ADSL2+ solutions will most commonly be multi-modal by interoperating with ADSL, ADSL2, and ADSL2+ chipsets.

As the latest xDSL standard, very-high-data-rate digital subscriber line (VDSL) can be operated in either asymmetric or symmetric mode. Its asymmetric mode operates at higher data rates than ADSL: 13/22 Mbps downstream and 3 Mbps upstream. The symmetric mode offers upstream the same bit rates as downstream. The operating distance is limited to 1000 to 4500 feet of line length. VDSL is proposed to connect the end point of a fiber network and customer premise. The much wider bandwidth enables central office to deliver high bandwidth services such as high-definition television (HDTV).

The development of xDSL techniques also gives rebirth to the multicarrier modulation (MCM) technique which originated from the idea of the Collins Kineplex system in the 1950's [7]. Discrete multitone (DMT), one of the various MCM methods, has been chosen as the standard line code for both ADSL [8] and VDSL. A detailed introduction of multicarrier modulation is given in the next section.

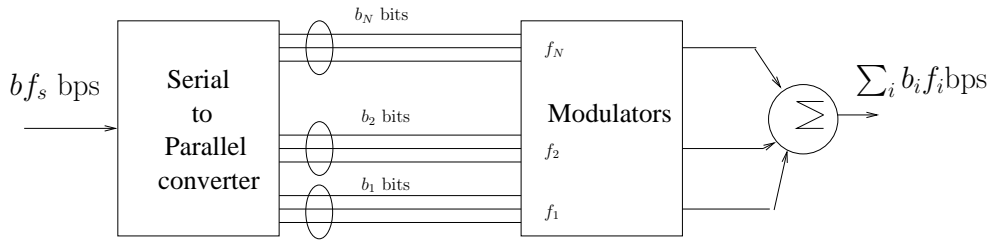


Figure 1.1: Simplified block diagram of a multicarrier transmitter

1.2 Multicarrier Modulation

Multicarrier modulation is a novel approach to design a bandwidth-efficient communication system in the presence of channel distortion. The basic idea is to divide the available channel bandwidth into a set of subchannels, such that independent information streams are transmitted on different subchannels [9]. Although multicarrier modulation is a form of frequency-division multiplexing (FDM), it has some unconventional characteristics. A simplified multicarrier transmitter is shown in Fig. 1.1.

Suppose that a given channel with bandwidth W were divided into $\tilde{N} = W/\Delta f$ subchannels of equal width Δf , where \tilde{N} is chosen so that the frequency response of each subchannel is approximately constant across its bandwidth. This creates a set of nearly ideal memoryless subchannels. Each of the subchannels is independently modulated to a carrier frequency $f_i = i\Delta f$, for $i = 1, \dots, \tilde{N}$. Input data are grouped into blocks of b bits at a block rate of f_s . For the subcarrier at f_i , b_i bits are used to form the sub-signals under the constraint $\sum_i b_i = b$. Note that the number of bits allocated to the different subchannels need not be the same in contrast to the traditional FDM case. The allocation of bits in a subchannel is determined by the signal-to-noise ratio in that subchannel. If a subchannel suffers severe channel attenuation, i.e. has low SNR, then it can be turned off. This

flexibility offers the possibility of putting more bits on higher SNR subchannels and not using low SNR subchannels in order to improve the achievable bit rate. The modulated subcarriers are superimposed for transmission.

Several methods have been used to implement multicarrier modulation. The earliest attempts used filters to separate the bands. But since sharp narrow band filters were difficult to obtain, the band usage efficiency would decrease [7]. Efficient implementation of multicarrier modulation is performed digitally through a special discrete Fourier transform (DFT) based multiplexing scheme called discrete multitone (DMT) modulation. With the help of modern digital signal processors and efficient implementations of the fast Fourier transform (FFT), the DFT approach has become dominant in standards for multicarrier modulation communication systems. Although variations of DMT have been proposed, such as discrete wavelet multitone modulation (DWMT) [10], vector coding [11], and nonuniform multitone modulation [12], most commercial implementations chose either DMT or its sibling orthogonal frequency division multiplexing (OFDM), due to their advantages in implementation complexity.

While OFDM is widely exploited in broadband wireless communication systems (IEEE 802.11a/g, Digital Video Broadcasting (DVB) and Digital Audio Broadcasting (DAB)), DMT is extensively used in broadband wireline communication systems. It has been chosen as standard line code in asymmetric digital subscriber line (ADSL) systems and very-high speed DSL (VDSL) systems. Fig 1.2 shows a standard ADSL transceiver architecture with DMT modulation/demodulation.

Basically, OFDM and DMT are quite similar. The major difference is that DMT has extra ability to perform dynamic bit loading. As the name suggests, OFDM is a more traditional FDM scheme with fixed bit allocation. But for DMT, subchannel SNR is slow varying due to the stable wireline channel. A receiver can send a bit allocation table determined according to the measured subchannel

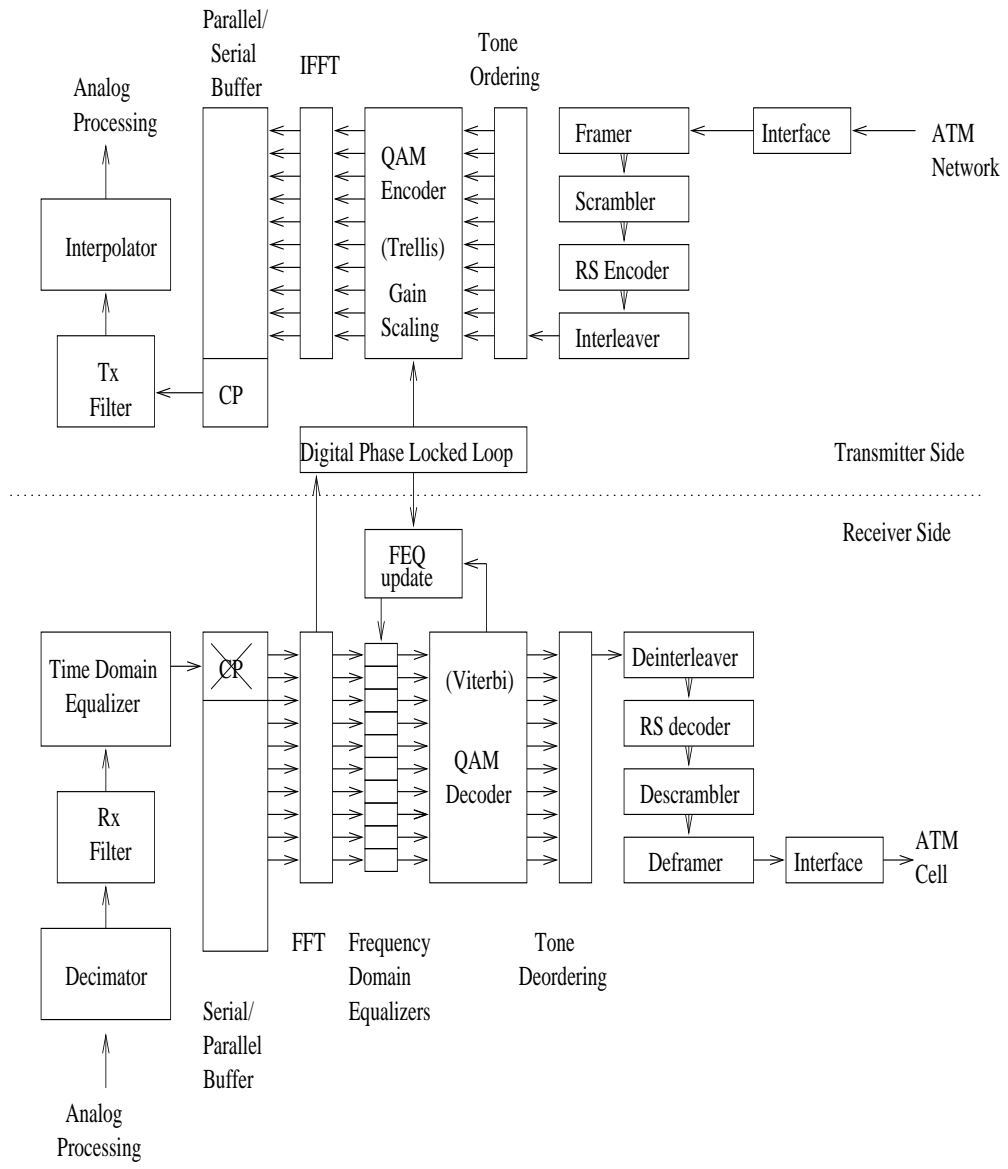


Figure 1.2: A typical single-chip ADSL transceiver architecture. (Physical layer digital signal processing with interface to an ATM network.)

SNR through a relatively reliable feedback channel to the transmitter. Bit loading is easily implemented. This flexibility maximizes DMT's bit rate performance. If some subchannels have been shut down due to bad transmission conditions, then the transmitted energy can be redistributed to those good subchannels.

1.3 Channel Equalization

The capacity of reliable information transmission over any physical communication channel would be limited by non-ideal characteristics of the channel. Among those impairments encountered in a discrete time channel, intersymbol interference (ISI) due to channel memory corrupts the current received data by previous data symbol(s). Severe ISI will significantly downgrade the achievable bit rate. Some form of channel equalization is typically employed by a digital transmission system to mitigate the ISI.

1.3.1 Single Carrier Equalization

Major equalizer structures in a conventional single carrier digital communication system can be classified into two categories: linear or decision feedback.

A zero-forcing linear equalizer (ZF-LE) is the simplest form of equalizer structure. It ignores the noise and shapes the received signal so that it is free of ISI. Ideally without additive noise, it ends up with the reciprocal of the channel transfer function. Since the design of ZF-LE ignores the effects of noise, this oversight can lead to noise enhancement [13]. The noise power after the ZF-LE could be unacceptably large, thereby leading to poor communication performance.

The minimum mean-square error linear equalizer (MMSE-LE) is widely used for its tradeoff of ISI reduction and noise enhancement. The MMSE-LE performs at least as well as the ZF-LE. Usually the MMSE-LE obtains better communication performance with the same implementation complexity. MMSE-LE tries to minimize

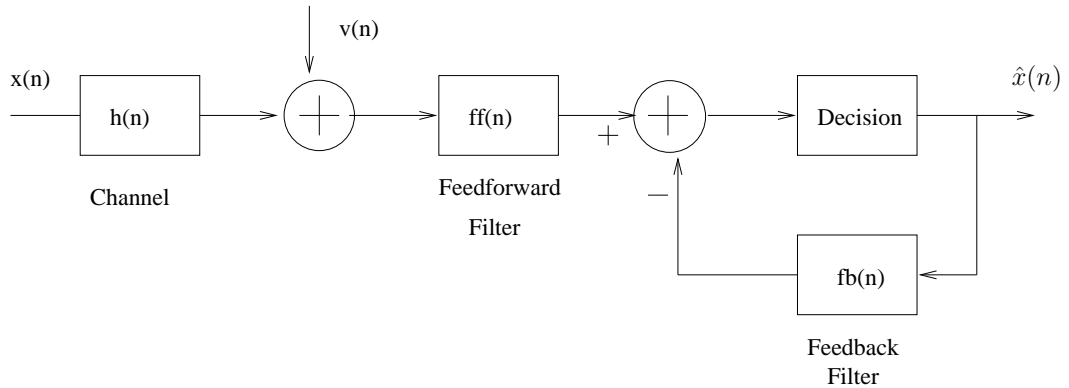


Figure 1.3: Basic Structure of a MMSE-DFE equalizer.

the mean square error between the transmitted signal and the equalized channel output. The orthogonality principle of the signal and noise subspaces is used to solve this linear estimation problem. The consideration of additive noise during training usually guarantees a well-defined transfer function even when the channel gain is zero in some frequency bands. It prevents the noise enhancement in those bands that would have occurred by the ZF-LE.

Fig. 1.3 shows another equalizer structure called decision feedback equalizer (DFE). DFE makes use of previous decisions to estimate current symbol. Basically, it reconstructs and subtracts any ISI caused by previous symbols. Due to the feedback, it is nonlinear in nature. Similar to the linear case, both ZF-DFE and MMSE-DFE can be designed. A decision feedback equalizer usually outperforms the corresponding linear equalizer because past decisions are used to aid the current decision [14]. Conceptually, a DFE contains a feedforward filter, which will try to shape the channel output signal to be minimum phase and whitened, and a feedback filter, which will then subtract (without noise enhancement) any trailing ISI [13]. MMSE-DFE is obtained through a spectral factorization of related autocorrelation functions. ZF-DFE can be developed from MMSE-DFE. However, DFE assumes

that all past decisions are correct and no error propagation will occur through the feedback filter, which is not achieved in practice. The error propagation may be eliminated by moving the feedback section of the DFE to the transmitter, which is known as Tomlinson-Harashima precoding.

In the case that an infinite length equalizer is adopted, the training is easily performed by calculating related coefficients in the transform domain [13] according to different criteria. However, equalization filters are almost always implemented as finite impulse response (FIR) filters in practice. FIR filters are always stable and usually have better numerical properties than infinite impulse response (IIR) filters. However, the performance of FIR equalizers are generally worse than the corresponding IIR equalizers with the same number of coefficients.

Theoretically, a single carrier modulated transceiver with ideal MMSE-DFE equalization can achieve virtually the same bit rates as a multicarrier receiver because a infinite length equalizer can be designed to take care of any kind of channel frequency response [15]. But in practice, it is very difficult for a finite length equalizer to handle partially-occupied bandwidth [15]. The implementation of the transmission filter that contains a number of bandpass filters leads to unacceptable implementation complexity. Therefore, multicarrier modulation systems seem to be more suitable for broadband transmission over telephone lines because disjoint frequency regions usually exist due to unterminated bridge taps, crosstalk, and unused bandwidth. From now on, I will focus on multicarrier equalization.

1.3.2 Multicarrier Equalization

Ideally, all multicarrier modulation techniques partition a data transmission channel with ISI into a set of orthogonal, memoryless subchannels. In other words, within each independent subchannel, the channel impulse response is ideally flat and only has one tap. The equalization is performed in each subchannel by scaling back the

received signal by an appropriate factor.

The prerequisite for this subchannel equalization is that orthogonality between subchannels must be maintained. The aforementioned two popular DFT-based partition schemes, OFDM and DMT, use a cyclic prefix (CP) as a guard band. If the CP is longer than the channel memory, then orthogonality will also be present in the received waveform. In a typical wireless transceiver with OFDM modulation, it is usually assumed that the CP is longer than the channel memory, which is realized by installing enough transmitters in the coverage area, and equalization in the DFT domain fully reverses the channel distortion. However, the CP is usually shorter than channel length in a wireline system. It forces a typical DMT based wireline transceiver to implement a more complicated equalizer than the one in a wireless system. Practically the equalization performs in two steps: (1) using a FIR time domain equalizer (TEQ) before the FFT to shorten the channel length to be at most length of CP plus one; and (2) using a bank of 1-tap complex frequency domain equalizers (FEQ) following the FFT to compensate for the magnitude and phase distortion within each subchannel.

The design of the FEQ is relatively easy. A complex least mean square (LMS) adaptive algorithm is commonly used. TEQ design turns out to be challenging when an extra goal, maximizing the bit rate, is incorporated into the design in addition to channel shortening. Optimization of a bit rate maximizing TEQ usually leads to a computationally-prohibitive non-linear optimization problem. Sometimes it is impossible to obtain a near-optimal design in a real-time fixed-point implementation in commercial modems. Hence, a reliable and cost effective TEQ design to achieve high bit rates becomes an important topic in the area of DMT-based communications.

Minimum mean squared error (MMSE) design, which has its roots in [16], was revived in the early stages of ADSL research [17, 18]. MMSE TEQ design minimizes the mean square error between the output of the physical path consisting of the

channel and FIR filter and the output of a virtual path consisting of a transmission delay Δ and a target impulse response (TIR). An iterative implementation of the MMSE TEQ design method [17] shipped in many of the ADSL modems in the late 1990s. The drawbacks of the MMSE TEQ method include sensitivity to the transmission delay parameter and nulling of subcarriers [19]. Bit rate performance varies widely with TEQ length. At some point, longer MMSE TEQs start killing subcarriers [20].

The maximum shortening SNR (MSSNR) [21] method attempts to minimize intersymbol interference (ISI) in the time domain. The MSSNR method maximizes the ratio of the energy of the effective channel impulse response inside a target window of $\nu + 1$ samples to that outside the target window. Alternate objective functions include maximizing the ratio of the energy inside the target window to the total energy [22, 23], and minimizing (maximizing) the energy outside (inside) the target window while holding the energy inside (outside) the target window fixed. Finite-length MSSNR TEQs are approximately symmetric [20]. A blind, adaptive MSSNR algorithm is reported in [24]. Drawbacks of the MSSNR TEQ method include sensitivity to the transmission delay parameter and lack of control of where the ISI resides in the frequency domain. Bit rate performance varies widely with TEQ length. At some point, longer MSSNR TEQs start killing subcarriers [20].

The first attempt at TEQ design to maximize the bit rate was Al-Dhahir and Cioffi's work on the maximum geometric SNR (MGSNR) TEQ [25]. MGSNR TEQ design is formulated as a nonlinear constrained optimization problem. This method does not have a closed-form solution. By choosing appropriate numerical technique and starting with a certain initial condition obtained by the MMSE method, a local optimum solution can be found. The MGSNR TEQ method is not optimum in the sense of maximizing bit rate due to several unrealistic approximations: (1) its SNR definition does not include the effect of ISI; (2) its objective function assumes target

impulse response and TEQ are independent; and (3) it relies on user intervention to set a key parameter.

Farhang-Boroujeny and Ding addressed the impact of nulling of subcarriers in MMSE TEQ designs on bit rate performance [19]. They gave several guidelines to design bit rate maximizing TEQs. A suboptimum eigen-approach design is proposed based on the guidelines. However, the guidelines are relatively vague.

The first closed-form solution for bit rate maximization TEQ design was proposed by Arslan, Evans and Kiaei [26]. They partition an equalized multicarrier channel into its equivalent signal, noise and intersymbol interference (ISI) paths to develop a new subchannel SNR definition. Then they derive a maximum bit rate (MBR) method to optimize a nonlinear function of TEQ taps that measures bit rate. Calculating the MBR TEQ requires solving a nonlinear optimization problem. The expensive implementation cost makes it an impractical solution. Other direct bit rate maximizing methods such as maximum data rate (MDR) [27] and Bitrate Maximizing method (BM) [28] face the same obstacle.

Inspired from the MBR cost function, the authors of [26] proposed the Minimum-ISI (Min-ISI) as well. This method generalizes the MSSNR method by weighting the ISI in the frequency domain [26]. Implementations of the Min-ISI method on TI and Motorola fixed-point programmable digital signal processors (DSPs) satisfy real-time requirements in ADSL for 15-tap TEQs [29]. Drawbacks of the Min-ISI method include (1) sensitivity to transmission delay, (2) inability to design TEQs longer than $\nu + 1$ taps, and (3) sensitivity to the fixed-point computation in the Cholesky decomposition. Ding, Evans, Martin and Johnson proposed an updated version of the Min-ISI method [30], which successfully addressed these three issues.

Both MSSNR and Min-ISI use a rectangular window to separate ISI-free and ISI-inducing taps of the channel impulse response. It sees no difference among

the taps outside the window. However, ISI and ICI induced by the taps outside the window is proportional to the distance between the tap and the window edge even though all taps have the same energy [31]. To truly minimize the ISI/ICI, the positions of the taps outside the window must also be taken into consideration. Some windows other than rectangular have been considered in the minimum interblock (Min-IBI) method [32] and minimum delay spread (MDS) method [22] to impose different weights to taps according to their position. The overall effect of these methods is to concentrate channel energy as closely as possible.

Besides the single FIR TEQ structure, at least three alternate equalizer structures have been proposed. The dual-FIR TEQ [33] uses a standard single-FIR TEQ design algorithm to achieve good performance over the entire transmission bandwidth, and uses a second-FIR TEQ design algorithm to achieve better performance over a subset of subcarriers. A second alternate structure is the per-tone equalizer [34]. The per-tone equalizer essentially moves the single-FIR TEQ into the FEQ, which makes the FEQ become a linear combiner for each subcarrier. For data transmission, the per tone equalizer requires several times more memory but slightly lower computational complexity than the conventional equalizer. For training, however, the implementation complexity can increase by up to a factor equal to the number of subcarriers, over the conventional equalizer. A third alternate structure is a filter bank TEQ, in which a different FIR TEQ is designed for each tone. The FFT becomes a bank of Goertzel filters [27]. As reported in [27], the filter bank TEQ method has nine times the computational complexity of the per-tone equalizer for ADSL data transmission. Further, the latest activity in investigation of an alternative equalization structure will be reported in this thesis as a form of complex-valued filter bank.

I have limited the survey to linear equalization techniques for DMT systems. Multiple MMSE-DFEs could be applied to a multicarrier system, but such proposals

available in literature are only targeted to a filter-bank based multicarrier system.

1.4 Nomenclature and Notation

ABR	: Achievable Bit Rate
ADSL	: Asymmetric Digital Subscriber Lines
AMI	: Alternate Mark Inversion
AST	: Applied Signal Technology
ATM	: Asynchronous Transfer Mode
AWGN	: Additive White Gaussian Noise
B-ISDN	: Basic Rate ISDN
BM	: Bitrate Maximizing
CAP	: Carrierless Amplitude/Phase
CCITT	: Comite Consultatif Internationale de Telegraphie et Telephonie
CP	: Cyclic Prefix
CSA	: Carrier Serving Area
CTEQFB	: Complex TEQ Filter Bank
DC	: Divide And Conquer
DFE	: Decision Feedback
DFT	: Discrete Fourier Transform
DMT	: Discrete Multitone Modulation
DSL	: Digital Subscriber Line
FDM	: Frequency Division Multiplexing
FEXT	: Far-End Crosstalk
FFT	: Fast Fourier Transform
FIR	: Finite Impulse Response
FSK	: Frequency Shift Keying
GSNR	: Geometric Signal-to-Noise Ratio

GUI	: Graphical User Interface
HDSL	: High-bit-rate Digital Subscriber Line
ICI	: Intercarrier Interference
IEEE	: Institute of Electrical and Electronics Engineers
IFFT	: Inverse Fast Fourier Transform
IIR	: Infinite Impulse Response
ISDN	: Integrated Services Digital Network
ISI	: Intersymbol Interference
ITU	: International Telecommunication Union
LAN	: Local Area Network
LE	: Linear Equalizer
LMS	: Least Mean Squares
LU	: Lower Upper
MAC	: Multiply and Accumulate
MBR	: Maximum Bit Rate
MDR	: Maximum Data Rate
MDS	: Minimum Delay Spread
MFB	: Matched Filter Bound
MGSNR	: Maximum Geometric Signal-to-Noise Ratio
Min-IBI	: Minimum Interblock Interference
Min-ISI	: Minimum Intersymbol Interference
MIPS	: Million Instructions per Second
ML	: Maximum Likelihood
MMSE	: Minimum Mean Squared Error
MSE	: Mean Squared Error
MSSNR	: Maximum Shortening Signal-to-noise Ratio
NEXT	: Near-End Crosstalk

OFDM	: Orthogonal Frequency Division Multiplexing
PCM	: Pulse Code Modulation
PTEQ	: Pertone TEQ
POTS	: Plain Old Telephone System
PSD	: Power Spectral Density
PSK	: Phase Shift Keying
PSTN	: Public Switched Telephone Network
QAM	: Quadrature Amplitude Modulation
QPSK	: Quadrature Phase Shift Keying
RADSL	: Rate-adaptive Asymmetric Digital Subscriber Line
RAS	: Remote Access Service
SIR	: Shortened Impulse Response
SNR	: Signal-to-noise Ratio
SSNR	: Shortening Signal-to-noise Ratio
TCM	: Trellis Coded Modulation
TEQ	: Time-Domain Equalizer
TEQFB	: Time-Domain Equalizer Filter Bank
TIR	: Target Impulse Response
UEC	: Unit-Energy Constraint
UTC	: Unit-Tap Constraint
VDSL	: Very-high-speed Digital Subscriber Lines
WAN	: Wide Area Network
ZF	: Zero Forcing

Table 1.4 describes the notation used throughout the dissertation.

Table 1.1: Thesis Notation

Notation	Meaning
$x(n)$	transmitted signal
$y(n)$	received signal (channel output)
$v(n)$	channel noise
$z(n)$	signal after TEQ
N	size of FFT/IFFT
ν	size of CP
N_c	number of data carrying subchannels
Δ	propagation delay
$\mathbf{h} = [h(0), \dots, h(L_h - 1)]$	channel impulse response
$\mathbf{w} = [w(0), \dots, w(L_w - 1)]$	TEQ impulse response
$\mathbf{d} = [d(0), \dots, d(\nu)]$	desired impulse response
L_h	length of channel
L_w	length of TEQ
\mathbf{H}	channel convolution matrix
\mathbf{Y}	received signal matrix
\mathbf{D}, \mathbf{G}	windowing matrix
\mathbf{A}, \mathbf{B}	TEQ design matrix
\mathbf{U}, \mathbf{V}	bit rate calculation matrix
\mathbf{I}	identity matrix
X	transmitted QAM signal point
\hat{X}	demodulated QAM signal point
R	achievable data rate
b	number of bits assigned
J	cost function
S_x, S_n	signal power and noise power
λ	eigenvalue
$E[.]$	expectation
\mathbf{q}	one row of DFT matrix
ϕ	a complex scalar FEQ
$(.)^T, (.)^H, (.)^*$	transpose, Hermitian and complex conjugate
\star	convolution
$(.)_i$	i th subchannel
$(.)_t$	t th DMT symbol

1.5 Thesis Statement and Organization of the Dissertation

In this dissertation, I defend the following thesis statement:

Complexity-reduced discrete multitone time domain equalizer designs, which exploit symmetry, quantization, or/and subchannel grouping, give comparable performance to optimal discrete multitone time domain equalizer design that maximizes bit rate.

Showing this statement to be true would enable the design of optimal TEQs without directly optimizing a measure of achievable bit rate. Bit rate maximization generally involves nonlinear programming which is not suitable for real-time implementation due to its computational complexity. Moreover, nonlinear programming methods cannot guarantee to reach the global optimum.

This dissertation is organized as follows. Chapter 2 presents a unified treatment of optimal equalizer designs for multicarrier receivers. It is shown that nearly all equalizer designs share a common mathematical framework that is based on the maximization of a product of generalized Rayleigh quotients. This framework is used to give an overview of existing designs, apply a unified notation, and present various common strategies to obtain a solution. Moreover, the unification emphasizes the differences between the methods, which enables a comparison of their advantages and disadvantages. In addition, an extensive literature survey is given.

Chapter 3 reports infinite length TEQ results and their design implications. I show that for infinite length TEQs, minimum mean squared error target impulse responses have all zeros on the unit circle, which can lead to poor bit rate performance due to the nulling of subcarriers. Also, maximum shortening SNR TEQs and MMSE target impulse responses are perfectly symmetric. As a result, I propose symmetric design for TEQs. Symmetric TEQs greatly reduced design and

implementation complexity with little loss in achievable bit rate.

Chapter 4 develops an alternate min-ISI cost function. From it, I derive (1) a fast search method for the optimal transmission delay, (2) extensions to design min-ISI TEQs with length up to 512, and (3) an iterative Min-ISI method. The iterative Min-ISI method avoids Cholesky decomposition by calculating the eigenvector using a steepest descent searching, and achieves the bit rate performance of the original Min-ISI method.

Chapter 5 shows a complex-tap filter bank structure for channel equalization in multicarrier modulation systems appears to benchmark the bit rate performance among existing wireline multicarrier equalization methods. A special case of this filter bank structure, which has only two paths, is also proposed as a complexity-reduced practical solution.

Chapter 6 details the simulation environment and its parameters used in the comparative performance analysis of the leading TEQ design methods. Simulation results show that the proposed reduced complexity methods give matchable performance to the optimal design methods both in synthetic channels and real channels as claimed in the thesis statement.

Chapter 7 summarizes this dissertation and points out possible areas for further research. Appendix A presents details of the study of data provided by Applied Signal Technology for TEQ design. Appendix B shows how channel estimation error could affect the bit rate performance of a wireline multicarrier transceiver.

Chapter 2

Unification of Channel Equalization in Discrete Multitone Systems

2.1 Introduction

Channel equalization tries to restore the orthogonality between signal basis functions and hence enables match filter detection over bandlimited channels. In a DMT receiver, detection is performed in a block fashion. The orthogonality of signal basis functions is destroyed by both intersymbol interference (ISI) and intercarrier interference (ICI). Equalization is first performed to remove the ICI and the ISI by a time domain equalizer (TEQ). With successful time domain equalization, orthogonality of basis functions in each subcarrier is restored. Second, scaling is performed in the frequency domain to assure orthonormality of the basis functions. Then the received signal is decoded.

The evaluation of multicarrier channel equalization is application-dependent. In a wireless scenario, with no reliable feedback channel to do bit loading, fixed bit

allocation with bit-error rate minimization and fast adaptation to non-stationary environments is desired. In a wireline setup, bit-rate maximization in a quasi-stationary environment is targeted. This dissertation focuses on the DSL context, in which the ultimate performance measure is the achievable bit rate. Designing of a TEQ that directly maximizes the bit rate leads to a highly non-linear optimization problem, which is attractive to researchers who love to pursue the beauty of theory. However, practical considerations demand simplified procedures, which are primarily based on *time domain channel shortening*. Here, the TEQ is designed so that the convolution of a channel impulse response \mathbf{h} (modeled as a discrete-timed FIR filter combining responses of a transmit filter, a channel and a receive filter) and the TEQ \mathbf{w} produces an overall impulse response with almost all of its nonzero samples contained in a window of cyclic prefix length plus one samples.

Because the TEQ is preprocessing the input to an FFT, all frequency bins are treated in a superimposed fashion. Moreover, non-perfect spectral partition of the FFT demodulation generates a difficult interference structure and may lead to noise enhancement combined with “noise pick-up” from out-of-band noise [35]. It is a tough job to satisfy highly frequency selective demands without biased treatment for all subchannels. Alternatively, one could exploit a bank of equalizers, one per subcarrier. This approach is a generalization of the TEQ, which means that its performance should be at least equivalent to or better than an optimal TEQ. Considering the poor frequency containment of the FFT, some propose channel partitioning and synthesizing with a set of parallel filters [36], [37], [38] to replace the cascade of the FFT and the equalizer filter bank. The set of parallel filters act directly on the time domain samples to estimate the transmitted frequency domain symbols, without performing an FFT. In these proposals, multiple DFE equalizers are usually implemented for their better performance than linear equalizers.

This chapter presents an overview of the various DMT equalizer designs. It

provides a unified mathematical framework and a unified notation for different equalizer designs to the single-input, single-output (SISO) transmission model. Most of the material presented in this chapter has been included in transaction submissions [39, 40].

2.2 Common Mathematical Framework

2.2.1 System Model

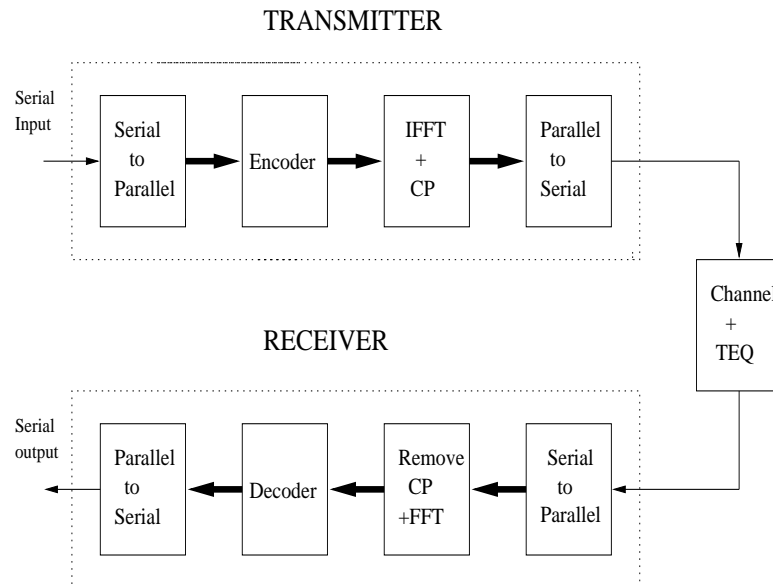


Figure 2.1: Block diagram of a standard discrete multitone transceiver

Fig. 2.1 depicts a block diagram of a standard DMT transceiver. In the transmitter, the data sequence is partitioned into a number of parallel streams. Each stream of data is modulated via a particular subcarrier. The modulated subcarriers are summed to obtain the transmit signal. The use of an inverse FFT (IFFT) in a DMT transmitter allows an efficient realization of the subcarrier modulators in a

parallel processing structure. Similarly, an FFT is used for an efficient realization of the subcarrier demodulators in a DMT receiver. As mentioned in Chapter 1, ISI and ICI could be ideally removed by cyclically extending the output of the inverse FFT modulator so that the input sequence looks periodic to the channel. The length of the cyclic prefix should be at least equal to the duration of the channel impulse response, L_h , minus one. However, the addition of the cyclic prefix (CP) reduces the throughput of the channel as it only carries redundant information. To minimize this reduction of throughput, a TEQ is applied to reduce the overall duration of the system (channel plus equalizer) impulse response to a predefined length.

In explaining the function of the TEQ, let t indicate the DMT symbol index and $n = 0, 1, \dots, N + \nu - 1$ indicate the samples within the given symbol plus the CP. The TEQ output is given as

$$z_t(n) = \sum_{\tau=0}^{L_w-1} w(\tau)y_t(n - \tau) \quad (2.1)$$

where $w(\tau)$ denotes the τ th coefficient of the length L_w TEQ and $y_t(\cdot)$ is the received sequence. The TEQ operations in a DMT receiver can be written as

$$\begin{aligned} \mathbf{z}_t &= \begin{bmatrix} y_t(\nu) & y_t(\nu - 1) & \dots & y_t(\nu - L_w + 1) \\ y_t(\nu + 1) & y_t(\nu) & \dots & y_t(\nu - L_w + 2) \\ \vdots & \vdots & \ddots & \vdots \\ y_t(N + \nu - 1) & \dots & \dots & y_t(N + \nu - L_w) \end{bmatrix} \\ &\quad \times \begin{bmatrix} w(0) \\ w(1) \\ \vdots \\ w(L_w) \end{bmatrix} \\ &= \mathbf{Y}_t \mathbf{w} \end{aligned} \quad (2.2)$$

where \mathbf{Y}_t is a Toeplitz matrix that contains the received signal for detection of t th symbol. TEQ outputs are grouped into length $N + \nu$ blocks. The first ν samples

in a given block have been discarded because they are corresponding to the cyclic prefix.

The rest of the functions of a receiver are explained as follows. The CP-removed TEQ output is then transferred to frequency domain by means of an FFT. To recover the transmitted data, a one-tap FEQ is applied to each tone of the FFT output to undo the equalized channel attenuation. Let \mathbf{Q} denote the $N \times N$ DFT matrix and the diagonal matrix $\mathbf{\Phi}$ denote the FEQ matrix with the i th diagonal entry corresponding to the complex one-tap FEQ for the i th tone. I express the estimated DMT symbol as

$$\begin{aligned}
\hat{\mathbf{X}}_t &= \begin{bmatrix} \hat{X}_{t,0} \\ \hat{X}_{t,1} \\ \vdots \\ \hat{X}_{t,N-1} \end{bmatrix} \\
&= \begin{bmatrix} \phi_0 & & & \\ & \phi_1 & & \\ & & \ddots & \\ & & & \phi_{N-1} \end{bmatrix} \begin{bmatrix} \mathbf{q}_0^H \\ \mathbf{q}_1^H \\ \vdots \\ \mathbf{q}_{N-1}^H \end{bmatrix} \mathbf{Y}_t \mathbf{w} \\
&= \mathbf{\Phi} \mathbf{Q} \mathbf{Y}_t \mathbf{w}
\end{aligned} \tag{2.3}$$

where \mathbf{q}_i^H denotes the i th row of the DFT-matrix. Using (2.3), I write the estimated data for tone i as

$$\hat{X}_{t,i} = \phi_i \mathbf{q}_i^H \mathbf{Y}_t \mathbf{w} = \phi_i \mathbf{s}_{t,i}^T \mathbf{w} \tag{2.4}$$

where $\mathbf{s}_{t,i} = \mathbf{q}_i^H \mathbf{Y}_t$.

2.2.2 Unified Framework

The problem of conventional channel shortening in DMT transceivers may be formulated as the following TEQ design problem: Given a channel with the impulse

response samples $h_0, h_1, \dots, h_{L_h-1}$ and corrupted with some additive noise, I wish to find the coefficients $w_0, w_1, \dots, w_{L_w-1}$ of an FIR equalizer that results in a combined channel-equalizer response, which is shortened to a duration of L_s samples, where L_s can be at most equal to the length of cyclic prefix ν plus one. In this design, the known parameters are the channel response, the channel noise (usually its autocorrelation coefficients), and the expected duration, L_s , of the equalized impulse response. Recent research suggests that channel shortening can also be performed by different approaches including multiple TEQs and integration with FEQs. However, almost all of the algorithms fit into the same formulation: the maximization of a generalized Rayleigh quotient or a product of generalized Rayleigh quotients.

Consider the optimization problem

$$\hat{\mathbf{w}}^{opt} = \arg \max_{\hat{\mathbf{w}}} \prod_{j=1}^M \frac{\hat{\mathbf{w}}^T \mathbf{B}_j \hat{\mathbf{w}}}{\hat{\mathbf{w}}^T \mathbf{A}_j \hat{\mathbf{w}}} \quad (2.5)$$

In general, the solution to (2.5) is not well-understood when $M > 1$. However, for $M = 1$,

$$\hat{\mathbf{w}}^{opt} = \arg \max_{\hat{\mathbf{w}}} \frac{\hat{\mathbf{w}}^T \mathbf{B} \hat{\mathbf{w}}}{\hat{\mathbf{w}}^T \mathbf{A} \hat{\mathbf{w}}}, \quad (2.6)$$

the solution is the generalized eigenvector of the matrix pair (\mathbf{B}, \mathbf{A}) corresponding to the largest generalized eigenvalue [41]. Equivalently, the inverse of the ratio in (2.6) is minimized by the eigenvector of (\mathbf{A}, \mathbf{B}) corresponding to the smallest generalized eigenvalue. Most TEQ designs fall into the category of (2.6), although several have $M \gg 1$ as in (2.5). The vector $\hat{\mathbf{w}}$ to be optimized is usually the TEQ taps, but it may also be e.g. the (shortened) target impulse response (TIR) [16], the per-tone equalizer taps [34], or half of the taps of a symmetric TEQ [20].

The generalized eigenvector problem requires computation of the $\hat{\mathbf{w}}$ that satisfies [41], [42]

$$\mathbf{B} \hat{\mathbf{w}} = \lambda \mathbf{A} \hat{\mathbf{w}}, \quad (2.7)$$

where $\hat{\mathbf{w}}$ corresponds to the largest generalized eigenvalue λ . If \mathbf{A} is invertible, the

problem can be reduced to finding an eigenvector of $\mathbf{A}^{-1}\mathbf{B}$ [41]. When \mathbf{A} is positive definite, another approach is to form the Cholesky decomposition $\mathbf{A} = \sqrt{\mathbf{A}}\sqrt{\mathbf{A}}^T$, and define $\hat{\mathbf{v}} = \sqrt{\mathbf{A}}^{-T}\hat{\mathbf{w}}$, as in [21]. Then

$$\hat{\mathbf{v}}^{opt} = \arg \max_{\hat{\mathbf{v}}} \frac{\hat{\mathbf{v}}^T \overbrace{\left(\sqrt{\mathbf{A}}^{-1} \mathbf{B} \sqrt{\mathbf{A}}^{-T} \right)}^{\mathbf{C}} \hat{\mathbf{v}}}{\hat{\mathbf{v}}^T \hat{\mathbf{v}}}. \quad (2.8)$$

The solution for $\hat{\mathbf{v}}$ is the eigenvector of \mathbf{C} associated with the largest eigenvalue, and $\hat{\mathbf{w}} = \sqrt{\mathbf{A}}^{-T}\hat{\mathbf{v}}$, assuming that \mathbf{A} is invertible. If \mathbf{A} is not invertible, then it has a non-zero null space, so the ratio is maximized (to infinity!) by choosing $\hat{\mathbf{w}}$ to be a vector in the null space of \mathbf{A} .

2.3 Single Quotient Cases

2.3.1 Single Filter

The Maximum Shortening SNR Design Method

The maximum shortening SNR (MSSNR) TEQ design proposed by Melsa, Younce and Rohrs in [21] attempts to maximize the ratio of the energy in a window of the effective channel over the energy in the remainder of the effective channel. The MSSNR design was reformulated for numerical stability by Yin and Yue in [43]. Adaptive and iterative implementations have been proposed in [24] and [44], respectively. Following [21], I define

$$\mathbf{H}_{win} = \begin{bmatrix} h(\Delta) & h(\Delta - 1) & \cdots & h(\Delta - L_w + 1) \\ \vdots & & \ddots & \vdots \\ h(\Delta + \nu) & h(\Delta + \nu - 1) & \cdots & h(\Delta + \nu - L_w + 1) \end{bmatrix} \quad (2.9)$$

as the middle $\nu + 1$ rows of the (tall) channel convolution matrix \mathbf{H} , and \mathbf{H}_{wall} as the remaining rows of \mathbf{H} . Thus, $\mathbf{c}_{win} = \mathbf{H}_{win}\mathbf{w}$ yields a length $\nu + 1$ window of the effective channel, and $\mathbf{c}_{wall} = \mathbf{H}_{wall}\mathbf{w}$ yields the remainder of the effective

channel. The MSSNR design problem can be stated as “maximize $\|\mathbf{c}_{win}\|$ subject to the constraint $\|\mathbf{c}_{wall}\| = 1$,” [21], [43] which reduces to

$$\max_{\mathbf{w}} \left(\mathbf{w}^T \underbrace{\mathbf{H}_{win}^T \mathbf{H}_{win}}_{\mathbf{B}} \mathbf{w} \right) \text{ subject to } \mathbf{w}^T \underbrace{\mathbf{H}_{wall}^T \mathbf{H}_{wall}}_{\mathbf{A}} \mathbf{w} = 1. \quad (2.10)$$

Solving (2.10) leads to a TEQ that satisfies the generalized eigenvector problem,

$$\mathbf{B}\mathbf{w} = \lambda\mathbf{A}\mathbf{w}. \quad (2.11)$$

The solution for \mathbf{w} is the eigenvector corresponding to the largest generalized eigenvalue [42].

MSSNR only considers energy distribution in the time domain and ignores frequency domain characteristics of the TEQ and the additive noise. Djokovic [45] adds the contribution of the noise by defining $\mathbf{A} = \mathbf{H}_{wall}^T \mathbf{H}_{wall} + \mathbf{R}_n$, where \mathbf{R}_n is a noise covariance matrix. Wang, Adali, Liu, and Vlatnic [46] also introduce a second term by forming \mathbf{A} as $\mathbf{H}_{wall}^T \mathbf{H}_{wall} + \mathbf{S}$, where \mathbf{S} contains suppression coefficients to shape the spectrum of the TEQ. It has been pointed out in [35] that TEQ suppression at some frequency bins is desirable when a transmission does not occupy the full bandwidth.

Some variations of MSSNR have been proposed for a real-time implementation. Chiu *et al.* [47] apply the inverse power method to find minimum eigenvalue and corresponding eigenvector in an iterative algorithm. The proposed algorithm has a super-linear convergence rate with iteration $\mathbf{A}\mathbf{w}_i = \mathbf{B}\mathbf{w}_{i-1}$. Lu, Clark, Arslan, and Evans [48] use a divide and conquer approach to design a series of two-tap TEQs that iteratively achieve MSSNR shortening. Divide and conquer design only requires two orders of magnitude fewer computations because it needs neither matrix inversion nor Cholesky decomposition.

Martin *et al.* [24] propose a blind, adaptive, stochastic gradient descent algorithm called multicarrier equalization by restoration of redundancy (MERRY)

to nicely exploit the repetition between CP and data symbol. The cost function defined as $\mathbf{J}_\Delta = E[|y(\nu + \Delta) - y(\nu + N + \Delta)|]$ is proportional to the energy of the combined impulse response outside of a length ν window, plus a noise gain term. It means MERRY tries to converge to a solution similar to MSSNR.

The Minimum Mean-Squared Error Design Method

Chow, Tu and Cioffi introduce channel shortening for DSL applications in [49]. In [50], Chow and Cioffi propose minimum mean-squared error (MMSE) design for channel shortening, which resurrects the channel memory truncation solution in [16]. As shown in Fig. 2.2, the MMSE design creates a virtual target impulse response (TIR) \mathbf{b} of length $\nu + 1$ such that the MSE (measured between the output of the effective channel and the output of the TIR) is minimized.

A thorough description of MMSE approach is given by Al-Dhahir and Cioffi [18]. The MMSE design uses a target impulse response (TIR) \mathbf{b} that must satisfy

$$\mathbf{R}_{yx}\mathbf{b} = \mathbf{R}_y\mathbf{w} \quad (2.12)$$

where

$$\mathbf{R}_{yx} = E \left[\begin{bmatrix} y(k) \\ \vdots \\ y(k - L_w + 1) \end{bmatrix} [x(k - \Delta) \quad \dots \quad x(k - \Delta - \nu)] \right] \quad (2.13)$$

is the channel input output cross-correlation matrix and

$$\mathbf{R}_r = E \left[\begin{bmatrix} y(k) \\ \vdots \\ y(k - L_w + 1) \end{bmatrix} [y(k) \quad \dots \quad y(k - L_w + 1)] \right] \quad (2.14)$$

is the channel output autocorrelation matrix. Typically, \mathbf{b} is computed first, and then (2.12) is used to determine \mathbf{w} . The goal is for $\mathbf{h} \star \mathbf{w}$ to approximate a delayed version of \mathbf{b} . If I enforce unit norm constrain $\mathbf{b}^T \mathbf{b} = 1$ on the target impulse

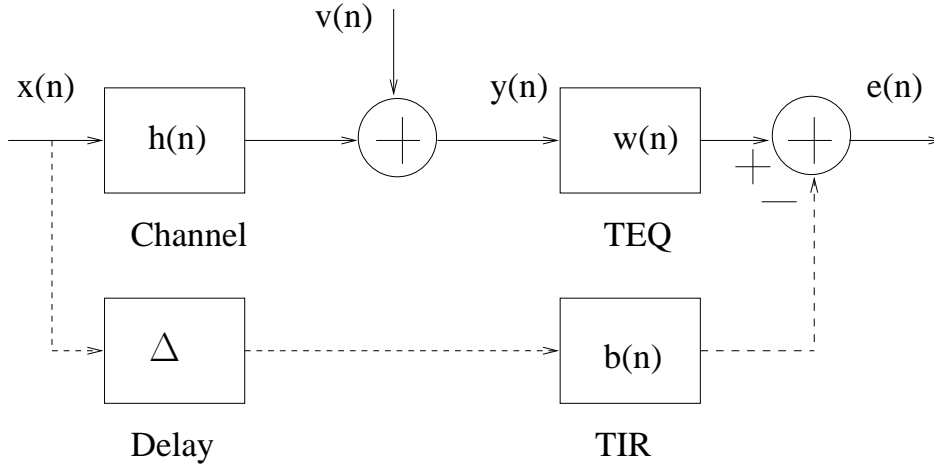


Figure 2.2: Minimum mean-squared error system model: $h(n)$, $w(n)$, and $b(n)$ are the impulse responses of the channel, time domain equalizer, and target, respectively; and Δ is a delay. The dashed lines indicate a virtual path, which is used only for analysis.

response, \mathbf{b} is the generalized eigenvector corresponding to the maximum eigenvalue of matrix pair

$$\begin{aligned} \mathbf{A} &= \mathbf{R}_x - \mathbf{R}_{xy} \mathbf{R}_y^{-1} \mathbf{R}_{yx} \\ \mathbf{B} &= \mathbf{I}_{\nu+1} \end{aligned} \quad (2.15)$$

which indeed a normal eigenvalue problem.

In the absence of noise, if the input signal is white, then the optimal MMSE and MSSNR solutions are identical [51]. This result was generalized to the noisy case in [20].

Fast and cost effective implementations of the MMSE method are available including Chow and Cioffi's iterative algorithm [17], off-line least mean squares (LMS) based iterative method and inverse power method from Nafie and Gatherer [44], and a fast computation method based on circulant approximation of \mathbf{A} from Lee, Chow, and Cioffi [52].

Wang [53] calculates MSE in the frequency domain so that only error energy on used portion of Nyquist bandwidth has been included, which achieves a MMSE solution on a partially bandwidth-occupied system. (This is the case for ADSL and VDSL applications.)

Van Kerchove and Spruyt [35] point out potential noise leaking from upstream band due to the weak channel partition of the FFT in a FDM-ADSL system if an MMSE TEQ has high magnitude response in the upstream bins. They inject virtual noise to suppress TEQ magnitude response in the undesired bands.

Farhang-Boroujeny and Ding [19] analyze the effect on the data rate due to a badly shaped TEQ spectrum with nulls in the transmission band. They propose a method to combine weighted eigenvectors of \mathbf{A} in a MMSE algorithm to form a TEQ without any nulls and maintain relatively low MSE. In a quite different approach, Warke *et al.* [54] augment the MSE cost function to include a flatness measure to obtain the desired “spectral flatness” in the TEQ frequency response.

The Minimum Intersymbol Interference Design Method

The TEQ output $h(n) \star w(n)$ can be decomposed into the desired part and the ISI-corrupted part by windowing

$$g(n) = \begin{cases} 1 & \text{if } \Delta \leq n \leq \Delta + \nu \\ 0 & \text{otherwise} \end{cases} \quad (2.16)$$

where Δ is the delay. The TEQ output is then written as

$$\begin{aligned} z(n) &= h(n) \star w(n) \star x(n) + w(n) \star \nu(n) \\ &= h^{signal}(n) \star x(n) + h^{ISI}(n) \star x(n) \\ &\quad + w(n) \star \nu(n) \end{aligned} \quad (2.17)$$

For each tone, a following definition of SNR can be formed

$$\text{SNR}_i = \frac{|H_i^{signal}|^2 S_{x,i}}{|H_i^{ISI}|^2 S_{x,i} + |W_i|^2 S_{n,i}} \quad (2.18)$$

where H_i^{signal} , H_i^{ISI} and W_i are i th DFT sample of h^{signal} , h^{ISI} and \mathbf{w} , respectively. In matrix form, (2.18) becomes

$$\text{SNR}_i = \frac{|\mathbf{q}_i^H \mathbf{G} \mathbf{H} \mathbf{w}|^2 S_{x,i}}{|\mathbf{q}_i^H \mathbf{D} \mathbf{H} \mathbf{w}|^2 S_{x,i} + |\mathbf{q}_i^H \mathbf{Q} \mathbf{H} \mathbf{w}|^2 S_{n,i}} \quad (2.19)$$

where

$$\begin{aligned} \mathbf{G} &= \text{diag}[g(0)g(1)\dots g(N-1)]^T \\ \mathbf{D} &= \mathbf{I} - \mathbf{G} \\ \mathbf{H} &= \begin{bmatrix} h(0) & 0 & \dots & 0 \\ h(1) & h(0) & \dots & 0 \\ \vdots & \vdots & \ddots & \vdots \\ h(N-1) & h(N-2) & \dots & h(-(N-L_w)) \end{bmatrix} \\ \mathbf{q}_i &= [1 \quad e^{j2\pi i/N} \quad \dots \quad e^{j2\pi i(N-1)/N}]^T \end{aligned} \quad (2.20)$$

Here, $\mathbf{q}_i^H \mathbf{Q} \mathbf{H} \mathbf{w}$ is the i th N -point FFT coefficient of \mathbf{w} . The idea behind the min-ISI method can be explained from (2.19) [26]. Both the numerator and the denominator of (2.19) are power terms. Because a power term is always nonnegative, minimizing the distortion power in each subchannel is equivalent to minimizing the sum of the distortion powers over all subchannels:

$$P_d(\mathbf{w}) = \sum_{i \in \mathcal{S}} (\mathbf{w}^T \mathbf{F}^T \mathbf{q}_i S_{n,i} \mathbf{q}_i^H \mathbf{F} \mathbf{w} + \mathbf{w}^T \mathbf{H}^T \mathbf{D}^T \mathbf{q}_i S_{x,i} \mathbf{q}_i^H \mathbf{D} \mathbf{H} \mathbf{w})$$

After normalizing by $S_{n,i}$,

$$P_d^{norm}(\mathbf{w}) = \sum_{i \in \mathcal{S}} \mathbf{w}^T \mathbf{F}^T \mathbf{q}_i \mathbf{q}_i^H \mathbf{F} \mathbf{w} + \sum_{i \in \mathcal{S}} \mathbf{w}^T \mathbf{H}^T \mathbf{D}^T \mathbf{q}_i \left(\frac{S_{x,i}}{S_{n,i}} \right) \mathbf{q}_i^H \mathbf{D} \mathbf{H} \mathbf{w} \quad (2.21)$$

which is equal to

$$P_d^{norm}(\mathbf{w}) = \mathbf{w}^T \mathbf{w} + \mathbf{w}^T \mathbf{H}^T \mathbf{D}^T \sum_{i \in \mathcal{S}} \left(\mathbf{q}_i \frac{S_{x,i}}{S_{n,i}} \mathbf{q}_i^H \right) \mathbf{D} \mathbf{H} \mathbf{w} \quad (2.22)$$

due to Parseval's Theorem.

The first term does not affect the minimization of (2.22) for a constant norm \mathbf{w} (the optimal \mathbf{w} can always be scaled to force $\mathbf{w}^T \mathbf{w} = 1$). While minimizing the distortion power, a constraint is required to prevent the minimization of the signal power as well. Therefore, the Min-ISI TEQ design is defined as

$$\arg \min_{\mathbf{w}} \left(\mathbf{w}^T \mathbf{H}^T \mathbf{D}^T \sum_{i \in \mathcal{S}} \left(\mathbf{q}_i \frac{S_{x,i}}{S_{n,i}} \mathbf{q}_i^H \right) \mathbf{D} \mathbf{H} \mathbf{w} \right) \text{ s.t. } \|\mathbf{h}^{signal}\|^2 = 1 \quad (2.23)$$

Alternatively, Min-ISI can be generalized from MSSNR method [21]. MSSNR minimizes the norm of the ISI path impulse response, whereas Min-ISI minimizes the weighted sum of the ISI power. The Min-ISI cost function can be written as

$$\begin{aligned} J(\mathbf{w}) &= \frac{\mathbf{w}^T \mathbf{H}^T \mathbf{D}^T \sum_i \left(\mathbf{q}_i \frac{S_{x,i}}{S_{n,i}} \mathbf{q}_i^H \right) \mathbf{D} \mathbf{H} \mathbf{w}}{\mathbf{w}^T \mathbf{H}^T \mathbf{G}^T \mathbf{G} \mathbf{H} \mathbf{w}} \\ &= \frac{\mathbf{w}^T \mathbf{B} \mathbf{w}}{\mathbf{w}^T \mathbf{A} \mathbf{w}} \end{aligned} \quad (2.24)$$

where $S_{x,i}$ and $S_{n,i}$ are the transmitted signal power and channel noise power for i th tone, respectively. The design problem is defined as

$$\arg \max_{\mathbf{w}} (\mathbf{w}^T \mathbf{A} \mathbf{w}) \text{ s.t. } \mathbf{w}^T \mathbf{B} \mathbf{w} = 1 \quad (2.25)$$

It perfectly falls into the common framework in (2.6).

Wu, Arslan and Evans [55] outline procedure to reduce redundant computations of optimum Min-ISI for different delays. Martin *et al.* describe additional complexity reductions in [56] by introducing a fast matrix reconstruction routine, which is applicable to the MSSNR method as well.

Methods to Minimize ISI/ICI energy

It has been shown in [57] that ISI can be calculated as

$$y_{ISI}(n) = \sum_{\rho=\nu+1+n}^{L_h-1} h(\rho)x(n-\rho), \text{ with } 0 \leq n \leq L_h - \nu - 2 \quad (2.26)$$

where index $n = 0$ denotes the start point of current symbol excluding CP. The power spectral density (PSD) of ISI is then

$$P_{ISI}(i) = \sigma_x^2 \sum_{m=\nu+1}^{L_h-1} \left| \sum_{\mu=m}^{L_h-1} h(\mu) e^{-j\frac{2\pi}{N}\mu i} \right|^2. \quad (2.27)$$

ICI is computed as a negative signal of a part of a fake circular convolution of which CP length is assumed to be long enough:

$$y_{ICI}(n) = - \sum_{\rho=\nu+1+n}^{L_h-1} h(\rho)x((n-\rho) \bmod N), \quad 0 \leq n \leq L_h - \nu - 2 \quad (2.28)$$

It turns out that PSD of ICI is exactly the same as P_{ISI} given by (2.27).

The taps of \mathbf{h} exceeding the CP length cause ISI and ICI, and the interference levels depend on both the taps' distances to the prefix and their energy [22]. The contributions of interblock interference (IBI) from tails of impulse responses grow linearly as the samples move away to the edges [31]. This fact is partially ignored by MSSNR approach since a rectangular window is used without bias on the distance issue. Therefore, Schur and Speidel [22] propose to use an exponential window instead to minimize the square of the delay spread of \mathbf{h} , where the delay spread is defined as

$$D = \sqrt{\frac{1}{E} \sum_{n=0}^{L_h} (n - \bar{n})^2 |\mathbf{c}[n]|^2}. \quad (2.29)$$

Here, $E = \mathbf{h}^T \mathbf{h}$, and \bar{n} is a user-defined "center of mass." This results in (2.6) with

$$\mathbf{A} = \mathbf{H}^T \mathbf{Q} \mathbf{H}, \quad (2.30)$$

$$\mathbf{B} = \mathbf{H}^T \mathbf{H}, \quad (2.31)$$

where $\mathbf{Q} = \text{diag}\{[(0 - \bar{n})^2, \dots, (L_w + L_h - \bar{n})^2]\}$ is a diagonal weighting matrix.

Similar to the above minimum delay spread (MDS) method, Celebi [32] proposes to use a different diagonal weighting matrix to minimize interblock interference (Min-IBI). Let Δ denote the start index of $\nu + 1$ window as in MSSNR, then $\mathbf{Q} = \text{diag}\{[|(0 - \Delta)|, |(1 - \Delta)|, \dots, \Delta - \Delta + 1, \nu \text{ 1s}, 1, 2, \dots, |L_w + L_h - \Delta|]\}$.

MDS and Min-IBI TEQ designs are quite similar to MSSNR TEQ design, except for a different weighting window [23]. Noise is clearly ignored in both cases as in MSSNR's. Tkancenko and Vaidyanathan [58, 59] fix this problem by constructing a cost function that combines both shortening and noise mitigating objectives.

2.3.2 Multiple Filters

This part focuses on alternative equalizer designs that maximize the DMT system bit rate. DMT is intrinsically a divide-and-conquer approach. The broadband transmission is divided into a set of narrow bands and transmission is taken care of individually on each subchannel. This idea can be naturally extended to equalization: each data-carrying subchannel receives an equalizer, which is designed to maximize the bit rate on that subchannel. The logic behind this is that when every subchannel achieves the maximum number of bits, the sum of them is also maximized. In terms of the common formulation given by (2.5), this means that a single generalized Rayleigh quotient ($M = 1$) is maximized per subchannel, which results in a separate solution for each subcarrier. This idea was originally presented in [34] as a “per-tone equalization” (PTEQ) architecture. An alternative formulation, called the “Time-Domain Equalizer Filter Bank” (TEQFB), is given in [27], [60].

Per Tone Equalizers

The linearity of TEQ filtering and DFT demodulation enables PTEQ scheme of [34] to interchange them resulting in a bank of post-FFT equalizers in the frequency domain. The idea behind the PTEQ scheme can be summarized compactly by noting that for a TEQ, the equalized i -th DFT output can be obtained in two ways:

$$\hat{X}_{t,i} = \phi_i \mathbf{q}_i^H (\mathbf{Y}_t \mathbf{w}) = (\mathbf{q}_i^H \mathbf{Y}_t) (\phi_i \mathbf{w}) \quad (2.32)$$

Here, \mathbf{Y}_t is an $N \times L_w$ Toeplitz matrix of received samples of the current symbol t as defined in (2.2). The middle part of (2.32) represents the classical convolution

of the received signal y with the TEQ, $\mathbf{Y}_t \mathbf{w}$, followed by the DFT (Fig. 5.1). The right-hand side of (2.32) implies that the equalized i -th DFT output $\hat{X}_{t,i}$ (tone i , symbol t) can also be seen as a linear combination by \mathbf{w} of L_w consecutive outputs of a sliding FFT on the i -th tone, applied to the received signal $y_t(n)$.

A symbol estimate $\hat{X}_{t,i}$ is then obtained as

$$\hat{X}_{t,i} = (\mathbf{q}_i^H \mathbf{Y}_t) \underbrace{\phi_i \mathbf{w}}_{\mathbf{w}_i}, \quad (2.33)$$

where now a tone-dependent and complex multi-tap linear combiner \mathbf{w}_i has been introduced by combining the TEQ \mathbf{w} and the FEQ ϕ_i . The PTEQ scheme uses a clever implementation of L_w consecutive FFT operations per symbol $\mathbf{q}_i^H \mathbf{Y}_t$ in (2.33). The Toeplitz structure of \mathbf{Y}_t is exploited in a sliding DFT:

$$\begin{aligned} \mathbf{q}_i^H \mathbf{Y}_t[:, l+1] &= \exp(-j2\pi(i-1)/N) \mathbf{q}_i^H \mathbf{Y}_t[:, l] \\ &\quad + \underbrace{(y_t(\nu-l) - y_t(\nu-l+N))}_{\Delta y_t(l)}, \quad l = 1, \dots, L_w - 1. \end{aligned} \quad (2.34)$$

Here $\mathbf{Y}_t[:, l]$ denotes the l -th column of \mathbf{Y}_t . An efficient implementation of (2.33) then only needs one DFT per symbol. The symbol estimate $\hat{X}_{t,i}$ is obtained by linearly combining the i -th DFT output $\mathbf{Y}_{t,i}$ with $L_w - 1$ real difference terms $\Delta y_t(l), l = 1, \dots, L_w - 1$, as defined in (2.34):

$$\hat{X}_{t,i} = \underbrace{\left[Y_{t,i}, \Delta y_t(1), \dots, \Delta y_t(L_w - 1) \right]}_{\Psi_{t,i}} \mathbf{v}_i. \quad (2.35)$$

Here, \mathbf{v}_i are the complex PTEQ coefficients, related to \mathbf{w}_i in (2.33), by

$$\mathbf{v}_i(l) = e^{-j2\pi(i-1)l/N} \mathbf{v}_i(l+1) + \mathbf{w}_i(l), \quad l = 0, \dots, L_w - 2 \quad (2.36)$$

$$\mathbf{v}_i(L_w - 1) = \mathbf{w}_i(L_w - 1). \quad (2.37)$$

Fig. 2.3 depicts the PTEQ scheme with this efficient implementation, which has comparable complexity with a conventional TEQ-FEQ structure.

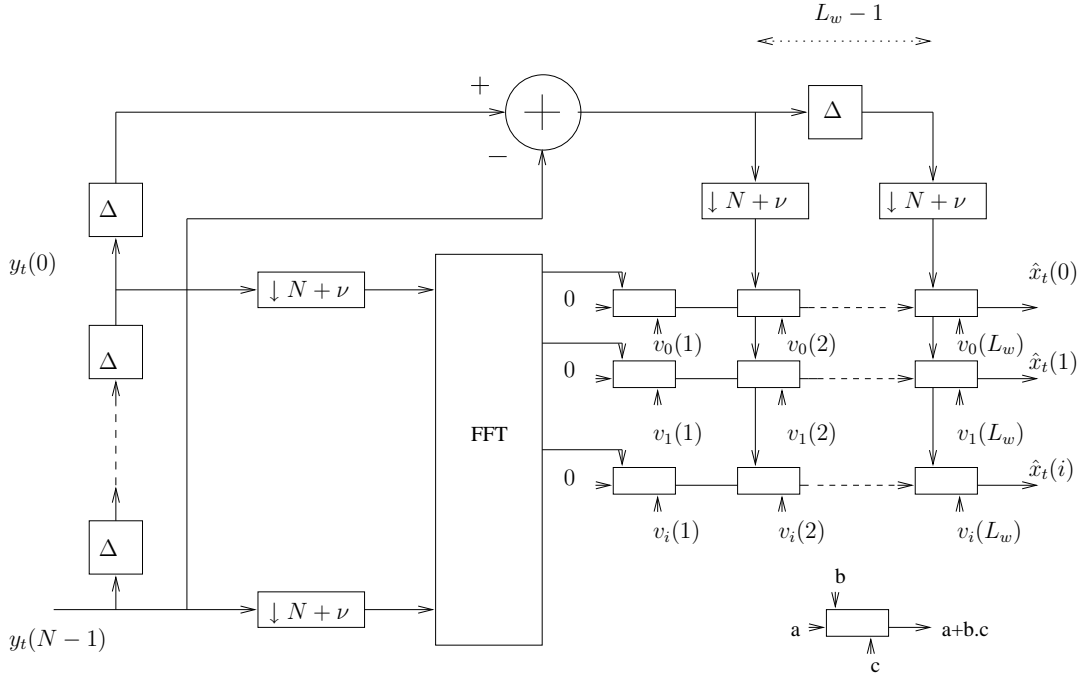


Figure 2.3: PTEQ architecture: channel equalization block diagram at the receiver

To determine a bit rate maximizing set of PTEQ coefficients a generalized eigenvalue problem (2.7) could be solved for each tone i with [61]

$$\mathbf{A}_i = E[(\Psi_{t,i})^H \Psi_{t,i}] \quad (2.38)$$

$$\mathbf{B}_i = E[(\Psi_{t,i})^H (X_{t,i})] E[\Psi_{t,i} (X_{t,i})^*], \quad (2.39)$$

which is equivalent to the MMSE solution.

Acker *et al.* describe an adaptive initialization of PTEQ based on recursive least squares (RLS) method in [62]. Ysebaert *et al.* present a combined RLS-LMS algorithm in [63], which reduces complexity cost and memory usage considerably while only showing slightly slower convergence than RLS method. Blind adaptive methods using constant modulus algorithm (CMA) and decision-directed LMS are provided for PTEQ scheme by Martin and Johnson [64].

Time Domain Equalizer Bank

An alternative scheme with an equalizer for each subchannel is the TEQ Filter Bank (TEQFB) [27]. The derivation writes the subchannel SNR as a single generalized Rayleigh quotient

$$\text{SNR}_i = \frac{\mathbf{w}^T \tilde{\mathbf{B}}_i \mathbf{w}}{\mathbf{w}^T \tilde{\mathbf{A}}_i \mathbf{w}}, \quad (2.40)$$

where

$$\begin{aligned} \tilde{\mathbf{A}}_i &= 2S_{x,i} (\mathbf{H}_{wall,1}^T \boldsymbol{\Omega}_i \boldsymbol{\Omega}_i^H \mathbf{H}_{wall,1} + \mathbf{H}_{wall,2}^T \boldsymbol{\Theta}_i \boldsymbol{\Theta}_i^H \mathbf{H}_{wall,2}) \\ &\quad + \mathbf{Q}_i^{\text{noise}} \mathbf{R}_n [\mathbf{Q}_i^{\text{noise}}]^H + \frac{\sigma_{\text{DNF}}^2}{\mathbf{w}^T \mathbf{w}} \mathbf{I}_{L_w+1}, \end{aligned} \quad (2.41)$$

$$\tilde{\mathbf{B}}_i = S_{x,i} \mathbf{H}^T \mathbf{Q}_i^{\text{circ}} [\mathbf{Q}_i^{\text{circ}}]^H \mathbf{H}. \quad (2.42)$$

$\mathbf{H}_{wall,1} = [\mathbf{D}[:, 0 : \Delta - 1] \quad \mathbf{0}_{N \times (N - \Delta)}]$ and $\mathbf{H}_{wall,2} = [\mathbf{0}_{N \times (\Delta + \nu)} \quad \mathbf{D}[:, \Delta + \nu + 1 : N]]$; $\boldsymbol{\Omega}_i$ and $\boldsymbol{\Theta}_i$ are upper and lower triangular Hankel matrices made from the i th row of the DFT matrix, \mathbf{q}_i ; $\mathbf{Q}_i^{\text{noise}}$ and $\mathbf{Q}_i^{\text{circ}}$ are Hankel matrices made from \mathbf{q}_i ; \mathbf{R}_n is the noise (AWGN and crosstalk) covariance matrix; and σ_{DNF}^2 is the power of the noise due to the digital noise floor. See [27] for full definitions. The dependence of the number of bits per symbol on the TEQ is then established using (2.40):

$$\begin{aligned} b_{\text{DMT}}^{\text{int}}(\mathbf{w}) &= \sum_{i \in \mathcal{S}} \left[\log_2 \left(1 + \frac{\text{SNR}_i}{\Gamma_i} \right) \right] \\ &= \sum_{i \in \mathcal{S}} \left[\log_2 \frac{\mathbf{w}^T (\Gamma_i \tilde{\mathbf{A}}_i + \tilde{\mathbf{B}}_i) \mathbf{w}}{\mathbf{w}^T (\Gamma_i \tilde{\mathbf{A}}_i) \mathbf{w}} \right] \\ &= \sum_{i \in \mathcal{S}} \underbrace{\left[\log_2 \left(\frac{\mathbf{w}^T \mathbf{B}_i \mathbf{w}}{\mathbf{w}^T \mathbf{A}_i \mathbf{w}} \right) \right]}_{b_i^{\text{int}}(\mathbf{w})} \end{aligned} \quad (2.43)$$

Here, $\mathbf{B}_i = \Gamma_i \tilde{\mathbf{A}}_i + \tilde{\mathbf{B}}_i$; $\mathbf{A}_i = \Gamma_i \tilde{\mathbf{A}}_i$; $[\cdot]$ is the flooring operation; Γ_i is the SNR gap, which is a function of the desired error probability, coding gain and system margin [65]; and \mathcal{S} is the set of subchannels that carry data. The constraint $\mathbf{w}^T \mathbf{w} = 1$ is used in [27] to remove the dependence of the last term of $\tilde{\mathbf{A}}$ on \mathbf{w} , turning the argument of (2.43) into a generalized Rayleigh quotient.

The TEQFB then follows from (2.43) by maximizing each term b_i^{int} of the summation separately, as this maximizes the sum. For each subchannel i , a TEQ \mathbf{w}_i is designed by solving

$$\mathbf{w}_i^{\text{opt}} = \arg \max_{\mathbf{w}_i: \|\mathbf{w}_i\|^2=1} \left(\frac{\mathbf{w}_i^T \mathbf{B}_i^r \mathbf{w}_i}{\mathbf{w}_i^T \mathbf{A}_i^r \mathbf{w}_i} \right), \quad (2.44)$$

where $(\cdot)^r$, denoting the real part, follows from the assumption that the TEQs \mathbf{w}_i are real; and the flooring operation and the \log_2 function have both been dropped as they do not change the solution $\mathbf{w}_i^{\text{opt}}$. The optimum bit allocation is then given by

$$[b^{\text{int}}]^{\text{opt}} = \sum_{i \in \mathcal{S}} \left\lceil \log_2 \lambda_i^{\text{opt}} \right\rceil, \quad (2.45)$$

where λ_i^{opt} is the largest generalized eigenvalue:

$$\lambda_i^{\text{opt}} = \frac{\left(\mathbf{w}_i^{\text{opt}} \right)^T \mathbf{B}_i^r \mathbf{w}_i^{\text{opt}}}{\left(\mathbf{w}_i^{\text{opt}} \right)^T \mathbf{A}_i^r \mathbf{w}_i^{\text{opt}}} = \frac{\left(\mathbf{w}_i^{\text{opt}} \right)^T \mathbf{B}_i \mathbf{w}_i^{\text{opt}}}{\left(\mathbf{w}_i^{\text{opt}} \right)^T \mathbf{A}_i \mathbf{w}_i^{\text{opt}}}. \quad (2.46)$$

Matrices with special structures such as symmetric, Hermitian and Toeplitz have been exploited in [66] to reduce overall computations of TEQFB training.

2.4 Products of Quotients Cases

This section discusses TEQ designs that attempt to optimize the bit rate by modelling it as a sum of logs of generalized Rayleigh quotients. This is equivalent to maximizing a product of generalized Rayleigh quotients, as in (2.5). The methods that fall into this category are all targeted at directly maximizing bit rate function:

$$b(\mathbf{w}) = \sum_{i \in \mathcal{S}} \log_2 \left(1 + \frac{\text{SNR}_i}{\Gamma} \right). \quad (2.47)$$

where Γ is the SNR gap in dB, namely, the excessive SNR needed to achieve Shannon capacity and \mathcal{S} is the set of data carrying subchannels. The main distinctions

between these designs are the approximations that are made and the progressively more rigorous models of the subchannel SNRs. Whereas the methods in the previous section optimized the bit rate separately on each tone, the methods in this section use a *single TEQ* to optimize the bit rate of the entire system, thereby leading to more complicated mathematical problems with no closed-form solutions usually.

2.4.1 Maximum Geometric Signal-to-noise Ratio Method

Al-Dhahir and Cioffi [25], [67], [68], [69] notice that MMSE does not directly maximize the bit rate. Their approach is the first to work directly on subchannel SNR. Let B_i , W_i , and H_i denote the complex valued DFT domain components of the TIR \mathbf{b} , the TEQ \mathbf{w} , and the transmission channel \mathbf{h} in subchannel i , respectively. Assuming a flat energy distribution in all subchannels, the SNR in subchannel i is

$$\begin{aligned} \text{SNR}_i &= \frac{S_x |H_i|^2}{S_{n,i}} = \frac{S_x |H_i|^2 |W_i|^2}{S_{n,i} |W_i|^2} \\ &\cong \frac{S_x |B_i|^2}{S_{n,i} |W_i|^2} \end{aligned} \quad (2.48)$$

where $S_{n,i}$ and S_x are the noise and signal powers in subchannel i , respectively. The geometric SNR is then defined as

$$\text{SNR}_{geom} \approx S_x \left[\prod_{i \in \mathcal{S}} \left(\frac{|B_i|^2}{S_{n,i} |W_i|^2} \right) \right]^{\frac{1}{N_u}} \quad (2.49)$$

Here, N_u is the size of the set of used carriers, \mathcal{S} . Several simplifying assumptions are made. It is assumed that $\text{SNR}_i \gg \Gamma$ for all i . Also, the subchannel SNR definition does not include the effects of the ISI, ICI, and FFT leakage in the denominator besides the power of the noise after the equalizer. The definition of the geometric SNR (2.48) also assumes that

$$\mathbf{q}_i^H (\mathbf{w} \star \mathbf{h}) = \mathbf{q}_i^H \mathbf{w} \mathbf{q}_i^H \mathbf{h} = W_i H_i \quad \text{and} \quad B_i = W_i H_i, \quad (2.50)$$

where \star denotes linear convolution and \mathbf{q}_i^H is the i -th row of DFT matrix (assumed to be truncated to the length of \mathbf{w} or \mathbf{h}). However, linear convolution of \mathbf{h} and

\mathbf{w} may not be equal to their product in the frequency domain and the difference consists of ICI.

Under these assumptions, using (2.43) and (2.49), the DMT bit rate is approximately given by

$$b(\mathbf{w}) = N_u \log_2 \left(1 + \frac{\text{SNR}_{geom}}{\Gamma} \right). \quad (2.51)$$

Maximizing (2.49) maximizes (2.51) as the logarithmic function is monotonically increasing. Maximizing (2.49) is *approximately* equivalent to maximizing the log of its numerator [25],

$$\begin{aligned} L(\mathbf{b}) &= \frac{1}{N_u} \sum_{i \in \mathcal{S}} \ln |B_i|^2 \\ &= \frac{1}{N_u} \sum_{i \in \mathcal{S}} \ln (\mathbf{b}^T \mathbf{G}_i \mathbf{b}), \end{aligned} \quad (2.52)$$

where $\mathbf{G}_i = \mathbf{g}_i \mathbf{g}_i^H$, and \mathbf{g}_i^H consists of the first $\nu + 1$ elements of \mathbf{q}_i^H . An assumption is made in (2.52) that the noise and the time domain equalizer \mathbf{w} are independent of \mathbf{b} , which is not correct as \mathbf{w} is a function of \mathbf{b} from (2.12).

The optimal TIR \mathbf{b} in terms of the maximum geometric SNR algorithm is then found by

$$\begin{aligned} \mathbf{b}_{\text{GSNR}}^{\text{opt}} &= \arg \max_{\mathbf{b}} L(\mathbf{b}) = \arg \max_{\mathbf{b}} \prod_{i \in \mathcal{S}} \mathbf{b}^T \mathbf{G}_i \mathbf{b} \\ \text{s. t. } \mathbf{b}^T \mathbf{b} &= 1, \text{ and } \mathbf{b}^T \mathbf{R}_{\Delta} \mathbf{b} < \text{MSE}_{\text{max}}, \end{aligned} \quad (2.53)$$

where $\mathbf{R}_{\Delta} = \mathbf{A}$ from in (2.15). Note that (2.53) is equivalent to (2.5) with $\mathbf{B}_i = \mathbf{G}_i$ and $\mathbf{A}_i = \mathcal{I}_{N\nu+1}$, but with an extra inequality constraint. This non-linear optimization problem can only be solved using numerical methods such as sequential programming methods. Al-Dhahir and Cioffi [68] change the subchannel SNR model in (2.48) to include partially the effects of the ISI when evaluating the TEQ designed using (2.48). An iterative method using projection on convex sets to maximize geometric SNR is presented by Lashkarian and Kiaei in [70].

2.4.2 Maximum Bit Rate method

Arslan, Evans, and Kiaei [3], [26], propose the maximum bit rate (MBR) TEQ design. The separation of channel impulse response into the ISI-free and the ISI-inducing parts in the development of MBR is obtained by the same rectangular windowing as MSSNR method. It defines a better model for the subchannel SNR. The subchannel SNR is modelled as in (2.19), which leads to

$$\tilde{\mathbf{A}} = S_{n,i} \mathbf{F}^T \mathbf{q}_i \mathbf{q}_i^H \mathbf{F} + S_x \mathbf{H}^T \mathbf{D}^T \mathbf{q}_i \mathbf{q}_i^H \mathbf{D} \mathbf{H} \quad (2.54)$$

$$\tilde{\mathbf{B}} = S_x \mathbf{H}^T \mathbf{G}^T \mathbf{q}_i \mathbf{q}_i^H \mathbf{G} \mathbf{H}. \quad (2.55)$$

where $\mathbf{F} = \begin{bmatrix} \mathbf{I}_{L_w \times L_w} \\ \mathbf{0}_{N-L_w \times L_w} \end{bmatrix}$. Again the bit rate is modelled as a sum of logs of generalized Rayleigh quotients. Proceeding as in (2.43), $\mathbf{A}_i = \Gamma_i \tilde{\mathbf{A}}_i$ and $\mathbf{B}_i = \Gamma_i \tilde{\mathbf{A}}_i + \tilde{\mathbf{B}}_i$.

In the SNR definition of (2.19), the signal part contains only the portion of the resulting equalized channel that contributes no ISI as opposed to (2.48) where the signal part contains the contribution of the entire channel. In (2.19), the noise part limits the contribution of the ISI noise to the shortened channel impulse response outside of the desired window, as opposed to the MGSNR model of (2.48), which ignores ISI-induced noise. The improvement over the MSSNR method [21] is that the subchannel SNR is defined in the frequency domain, thus enabling the design of a TEQ for a particular frequency band as opposed to MSSNR which cannot discriminate between subchannels. The subchannel SNR model in (2.19) includes ISI and additive Gaussian noise and is substituted into (2.43) to determine the bit rate.

The MBR method uses the computationally intensive Broyden-Fletcher-Goldfarb-Shanno quasi-Newton algorithm to find the optimum solution. It does not have any less computation intensive algorithm to support real-time implementations.

2.4.3 Maximum Data Rate TEQ

Milosevic *et al.* [27] improve on the MBR method by forming a more rigorous model of the subchannel SNR. This model was presented in Section 2.3.2 in the context of the TEQFB. The model includes near-end crosstalk, AWGN, analog-to-digital converter quantization noise, and the digital noise floor due to finite precision arithmetic. They also redefine the subchannel SNR model so that the desired signal is formed as the circular convolution of the data symbol with the channel impulse response at the input of the FFT (based on the minor approximation of a perfectly shortened channel), and the noise is the difference between the received and the desired signal. For a single TEQ, Milosevic *et al.* [27] simplify (2.43) by removing the flooring function, as in [3] [26]. The simplified function is the fractional number of bits per symbol,

$$b(\mathbf{w}, \mathcal{S}) = \sum_{i \in \mathcal{S}} \log_2 \left(\frac{\mathbf{w}^T \mathbf{B}_i \mathbf{w}}{\mathbf{w}^T \mathbf{A}_i \mathbf{w}} \right), \quad (2.56)$$

with \mathbf{A}_i and \mathbf{B}_i as in (2.41), (2.42), and (2.43). Empirical evidence suggests that the TEQs that maximize (2.43) and (2.56) may often be identical [27]; however, there is no guarantee that that is the case in general.

Equation (2.56) is again a sum of logarithms of ratios. Sum-of-ratios maximization is an active research topic in the fractional programming community for which no definitive solution exists yet (see e.g. [71], [72]). Milosevic *et al.* [27] use modifications of Almgly and Levin's approach to the sum-of-ratios problem [73] to optimize (2.56).

2.4.4 Bitrate Maximizing TEQ

Whereas the previous TEQ designs formulate a subchannel SNR model at the FFT output, Vanbleu *et al.* [74], [28] propose an improved/exact subchannel SNR. It is defined at the FEQ output by exploiting the dependence of the FEQs on the TEQ

coefficients. The resulting SNR model is a nonlinear function of the TEQ coefficients which now accounts for the function of the FEQ, as well. The output of the FEQ is modelled as

$$\phi_i \underbrace{\mathbf{q}_i^H \mathbf{Y}_t \mathbf{w}}_{\varrho_{t,i}} = \alpha_i X_{t,i} + \epsilon_{t,i} \quad (2.57)$$

where α_i is a bias, due to the equalizer, $\varrho_{t,i}$ is i th FFT output and $\epsilon_{t,i}$ is the noise remaining on tone i of symbol t . Assuming that unbiased MMSE FEQs are adopted,

$$\phi_i = \frac{E[|X_{t,i}|^2]}{E[(X_{t,i})^* \varrho_{t,i}]} \quad (2.58)$$

Hence α_i is 1 and $\epsilon_{t,i}$ contains all noise sources, including residual ISI/ICI and crosstalk. The dependence of the FEQs on the TEQ leads to the subchannel SNR model

$$SNR_i = \frac{E[|X_{t,i}|^2]}{E[|\phi_i \varrho_{t,i} - X_{t,i}|^2]} = \frac{1}{\rho_i^{-2} - 1} \quad (2.59)$$

where

$$\rho_i^2 = \frac{|E[(X_{t,i})^* \varrho_{t,i}]|^2}{E[|X_{t,i}|^2]E[|\varrho_{t,i}|^2]} \quad (2.60)$$

Substituting (2.59) into the bit rate equation (2.43) and exploiting (2.32), a bit rate is then formed as a nonlinear function of the TEQ coefficients, with

$$\mathbf{A}_i = \Gamma_i \left(E[|X_{t,i}|^2] E[(\mathbf{Y}_t)^H \mathbf{q}_i \mathbf{q}_i^H \mathbf{Y}_t] - E[(\mathbf{Y}_t)^H \mathbf{q}_i X_{t,i}] E[(X_{t,i})^H \mathbf{q}_i^H \mathbf{Y}_t] \right) \quad (2.61)$$

$$\begin{aligned} \mathbf{B}_i &= \Gamma_i E[|X_{t,i}|^2] E[(\mathbf{Y}_t)^H \mathbf{q}_i \mathbf{q}_i^H \mathbf{Y}_t] \\ &\quad + (1 - \Gamma_i) E[(\mathbf{Y}_t)^H \mathbf{q}_i X_{t,i}] E[(X_{t,i})^H \mathbf{q}_i^H \mathbf{Y}_t] \end{aligned} \quad (2.62)$$

where \mathbf{Y}_t is as in (2.2). The authors observe that the different local minima of BM-TEQ cost function yield nearly optimal performance. Therefore, a rapidly converging recursive TEQ update based on a Gauss-Newton like search direction is proposed to solve the bit rate maximizing problem [28].

2.5 Conclusion

This chapter presents an overview of existing design methods to tackle the equalization problem in multicarrier systems where the channel memory is longer than the cyclic prefix duration. Since most of these techniques share a common formulation based on a maximization of a product of generalized Rayleigh quotients, a unified notational framework is defined and common optimization techniques are provided. The subtle differences between these methods have been addressed in this literature survey as well.

Based on this common formulation, design methods are classified into several categories, each leading to a different design strategy. A single TEQ design with a single generalized Rayleigh quotient led to a closed-form solution, which is sub-optimal in terms of bit rate maximization. On the other hand, optimizing a single generalized Rayleigh quotient for each tone separately resulted in a bank of TEQ filters, which is a generalization of the single TEQ case and can achieve better performance. The more difficult case with a product of multiple generalized Rayleigh quotients is required for optimal single TEQ design. Usually, one resorts to non-linear search methods to find a local optimum. To obtain a practical solution to achieve high bit rates, an entire class of intermediate designs could be devised based on multiple TEQ designs for grouping of tones.

Chapter 3

Symmetric Equalizer Design

3.1 Introduction

This chapter studies magnitude and phase responses of infinite length MMSE and MSSNR TEQs. These two families of TEQ designs are widely adopted for cost-effective real-time implementations. For infinite length MMSE TEQ designs, I show that a target impulse response (TIR) of length $\nu + 1$ samples is symmetric and has all ν of its zeros on the unit circle. Also an infinite length MSSNR TEQ has its ν dominant zeros on the unit circle and a linear phase response if the unit norm constraint on the TEQ taps is applied. These infinite length results suggest that (1) increasing TEQ length may result in bit rate loss for finite length MMSE and MSSNR TEQs and (2) finite length symmetric design could be used to reduce implementation complexity. Results in this chapter are from a joint research project with the Broadband Adaptive Receiver Design group at Cornell University. Most of the content of this chapter has been published in [20, 56, 75, 76].

3.2 Infinite Length Results

This section considers infinite length MMSE and MSSNR TEQ designs. Under the unified framework in Chapter 2, optimal MMSE TIR and MSSNR TEQ are generalized eigenvectors of a matrix pair (\mathbf{A}, \mathbf{B}) with

$$\begin{aligned}\mathbf{A}_{MMSE} &= \mathbf{R}_x - \mathbf{R}_{xr}\mathbf{R}_r^{-1}\mathbf{R}_{rx} \\ \mathbf{B}_{MMSE} &= \mathbf{I}_{\nu+1}\end{aligned}\tag{3.1}$$

for the MMSE TIR and

$$\begin{aligned}\mathbf{A}_{MSSNR} &= \mathbf{H}_{wall}^T \mathbf{H}_{wall} \\ \mathbf{B}_{MSSNR} &= \mathbf{H}_{win}^T \mathbf{H}_{win}\end{aligned}\tag{3.2}$$

for the MSSNR TEQ, where \mathbf{R}_{xr} , \mathbf{R}_x , and \mathbf{R}_r are the channel input-output cross-correlation, input correlation, and channel output correlation matrices, respectively [16], [18], [19]. \mathbf{H}_{win} and \mathbf{H}_{wall} are windowed channel convolution matrices defined in (2.9). When the input signal is white and there is no noise, the MMSE design produces the same TEQ as the MSSNR design [51]. This can be extended to the noisy case to show that the TEQ for the MMSE design must satisfy [76]

$$\mathbf{B}\mathbf{w} = \lambda(\mathbf{A} + \mathbf{R}_n)\mathbf{w},\tag{3.3}$$

where λ is the largest generalized eigenvalue of the matrix pair $(\mathbf{B}, (\mathbf{A} + \mathbf{R}_n))$.

3.2.1 Magnitude Response

In this section, I show why the MMSE TEQ has nulls in its magnitude response.

Theorem 1 *If the input signal is white, the TEQ \mathbf{w} is allowed to be any infinite length discrete-time filter, and the minimum eigenvalue of \mathbf{A}_{MMSE} has multiplicity 1, then the finite length MMSE TIR \mathbf{b} will have all ν of its zeros on the unit circle.*

Proof: The MMSE solution requires that $\mathbf{R}_{rr}\mathbf{w} = \mathbf{R}_{rx}\mathbf{b}$ [18], which can be simplified to

$$\mathbf{R}_n\mathbf{w} = \mathbf{H}_{win}^T\mathbf{b} - \mathbf{H}^T\mathbf{H}\mathbf{w}. \quad (3.4)$$

Allowing $-\infty < i < \infty$, the i^{th} component becomes

$$\begin{aligned} \sum_j R_n(i, j)w(j) &= \sum_{j=0}^{\nu} h(\Delta + j - i)b(j) - \sum_j \sum_l h(l - i)h(l - j)w(j) \\ &= \sum_{j=0}^{\nu} h(\Delta + j - i)b(j) - \sum_j \phi(i - j)w(j), \end{aligned} \quad (3.5)$$

where $\phi(m) = \sum_l h(l)h(l + m)$ is the channel covariance function. In convolution notation,

$$w(i) \star R_n(i) = b(i) \star h(\Delta - i) - w(i) \star \phi(i), \quad (3.6)$$

where $R_n(m)$ is the noise autocorrelation function with z-transform $S_n(z)$. Taking z-transforms,

$$W(z)S_n(z) = B(z)z^{-\Delta}H(z^{-1}) - W(z)\Phi(z). \quad (3.7)$$

Solving for $W(z)$,

$$\boxed{W(z) = \frac{z^{-\Delta}B(z)H(z^{-1})}{S_n(z) + \Phi(z)}}. \quad (3.8)$$

The error sequence is

$$e(k) = \sum_l b(l)x(k - \Delta - l) - \sum_l w(l)r(k - l). \quad (3.9)$$

Assuming $x(k)$ is white with unit variance, the error covariance is

$$\begin{aligned} E_m &\triangleq \mathbb{E}[e(k)e(k + m)] = \sum_l b(l)b(m + l) \\ &\quad - \sum_{l_1, l_2} w(l_1)b(l_2)h(\Delta - m + l_2 - l_1) - \sum_{l_1, l_2} w(l_1)b(l_2)h(\Delta + m + l_2 - l_1) \\ &\quad + \sum_{l_1, l_2} w(l_1)w(l_2) [\phi(m + l_1 - l_2) + R_n(m + l_1 - l_2)]. \end{aligned} \quad (3.10)$$

In convolution notation,

$$\begin{aligned}
E_m &= b(m) \star b(-m) - b(m - \Delta) \star w(\Delta - m) \star h(\Delta - m) \\
&\quad - b(-m - \Delta) \star w(\Delta + m) \star h(\Delta + m) + w(m) \star w(-m) \star [\phi(m) + R_n(m)].
\end{aligned} \tag{3.11}$$

Taking z-transforms,

$$\begin{aligned}
E(z) &= B(z)B(z^{-1}) - z^{-3\Delta}B(z)W(z^{-1})H(z^{-1}) \\
&\quad - z^{3\Delta}B(z^{-1})W(z)H(z) + W(z)W(z^{-1})[\Phi(z) + S_n(z)].
\end{aligned} \tag{3.12}$$

Now insert (3.8) into (3.12). Noting that $\Phi(z) = H(z)H(z^{-1})$, and simplifying considerably,

$$E(z) = B(z)B(z^{-1}) \underbrace{\left[\frac{S_n(z) - \Phi(z)(z^\Delta - z^{-\Delta})^2}{S_n(z) + \Phi(z)} \right]}_{G(z)}. \tag{3.13}$$

Minimizing the MSE attempts to minimize E_0 . By setting $z = e^{j\omega}$, taking the inverse Fourier transform, and setting $m = 0$, one obtains

$$\begin{aligned}
E_0 &= \frac{1}{2\pi} \int_{-\pi}^{\pi} E(e^{j\omega}) d\omega \\
&= \frac{1}{2\pi} \int_{-\pi}^{\pi} \|b(e^{j\omega})\|^2 G(e^{j\omega}) d\omega,
\end{aligned} \tag{3.14}$$

where $b(e^{j\omega}) = \mathbf{b}^T [1, e^{j\omega}, \dots, e^{j\omega\nu}]^T$. This can be rewritten as

$$E_0 = \mathbf{b}^T \mathbf{A}_{MMSE} \mathbf{b}, \quad [\mathbf{A}_{MMSE}]_{m,n} = \frac{1}{2\pi} \int_{-\pi}^{\pi} e^{j\omega(m-n)} G(e^{j\omega}) d\omega = g(m-n). \tag{3.15}$$

Since $S_n(e^{j\omega})$ and $\Phi(e^{j\omega})$ are even functions in ω , $G(e^{j\omega})$ is as well. Thus, $[\mathbf{A}_{MMSE}]_{m,n} = [\mathbf{A}_{MMSE}]_{n,m}$, so \mathbf{A}_{MMSE} is a symmetric Toeplitz matrix. Robinson [77] and Makhoul [78] have shown that any eigenvector of a symmetric Toeplitz matrix has all of its zeros on the unit circle as long as the corresponding eigenvalue has multiplicity 1. This implies that the TIR (an eigenvector of \mathbf{A}_{MMSE}) has ν zeros on the unit circle.

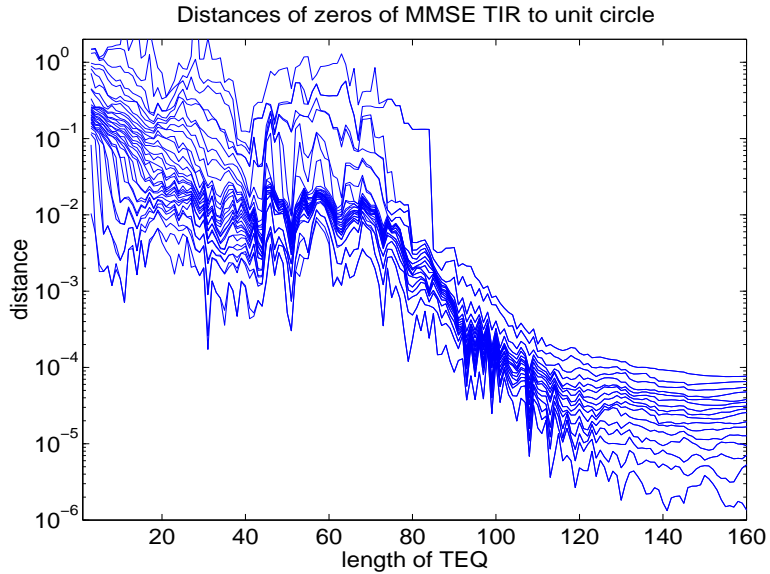


Figure 3.1: Distance of the ν zeros of the MMSE TIR to the unit circle for the case $\nu + 1 = 33$. The values are averaged over CSA loops 1 through 8. Each curve represents the distance for single zero.

■

Remarks: First, a similar result was observed in a footnote in [79], under the three restrictive assumptions noted in the “remarks” after Theorem 1. Second, in the noiseless case with a white input, the MMSE and MSSNR designs produce identical TEQs [51]. The proof of Theorem 1 is still valid in the absence of noise, so long as $\Delta \neq 0$. Thus, an infinite length MSSNR TEQ will have ν zeros on the unit circle. 3: If a null lies at one of the subchannel carrier frequencies, then no data can be transmitted in that subchannel [19]. This helps explain why the MMSE TEQ exhibits poor performance for long TEQ lengths [26].

For a finite length TEQ, \mathbf{A}_{MMSE} is not quite Toeplitz. Thus, the zeros of its eigenvector \mathbf{b} will not be precisely on the unit circle. Fig. 3.1 plots the distance of the zeros of the TIR to the unit circle for increasing TEQ length. There are 32

curves, one for each zero. For a length 32 TEQ, the zeros are clustered around a distance of 0.01 from the unit circle, and the asymptotic results agree with Theorem 1.

3.2.2 Symmetry in Eigenvectors

Symmetric centrosymmetric matrices are matrices in the set

$$V_N = \{\mathbf{C} : \mathbf{C}^T = \mathbf{C}, \quad \mathbf{J}\mathbf{C}\mathbf{J} = \mathbf{C}\}, \quad (3.16)$$

where \mathbf{J} is the square matrix with ones on the cross diagonal, and zeros elsewhere. $N \times N$ symmetric centrosymmetric matrices have $\lceil N/2 \rceil$ symmetric eigenvectors and $\lfloor N/2 \rfloor$ skew-symmetric eigenvectors [80]. This property can be loosely extended to the generalized eigenvector case.

The effects of an infinite length MMSE TEQ are considered next.

Theorem 2 *If the input signal is white and the TEQ \mathbf{w} is an infinite length discrete-time filter, then the finite length TIR \mathbf{b} will be symmetric or skew-symmetric.*

Proof: Proof given for Theorem 1 shows \mathbf{A}_{MMSE} is a symmetric Toeplitz matrix. Thus $\mathbf{A}_{MMSE} \in V_N$, and the optimal \mathbf{b} is the eigenvector corresponding to the minimum eigenvalue of \mathbf{A}_{MMSE} . By the results in [80], \mathbf{b} will be symmetric or skew-symmetric. ■

For an infinite length MSSNR TEQ, $\mathbf{A} = \mathbf{H}_{wall}^T \mathbf{H}_{wall}$ and $\mathbf{B} = \mathbf{H}_{win}^T \mathbf{H}_{win}$. Though the channel convolution matrix \mathbf{H} satisfies $\mathbf{H}^T \mathbf{H} \in V_N$, \mathbf{A} and \mathbf{B} are not perfectly centrosymmetric. But in the limit, the eigenvectors of \mathbf{A} converges to eigenvectors of $\mathbf{H}^T \mathbf{H}$, which is suggest by the following theorem:

Theorem 3 *For a channel convolution matrix \mathbf{H} and \mathbf{A} in a MSSNR-UNT design,*

$$\lim_{L_w \rightarrow \infty} \frac{\|\mathbf{H}^T \mathbf{H} - \mathbf{A}\|_F}{\|\mathbf{A}\|_F} = 0, \quad (3.17)$$

where $\|\cdot\|_F$ denotes the Frobenius norm.

Sketch of proof: Under the assumptions

$$\text{A1: } \Delta > L_h > \nu,$$

$$\text{A2: } L_w > \Delta + \nu,$$

I can partition \mathbf{H} as

$$\mathbf{H} = \begin{bmatrix} \mathbf{H}_1 & \mathbf{H}_{L2} & \mathbf{H}_{L1} & \mathbf{0} & \mathbf{0} \\ \mathbf{0} & \mathbf{H}_{U3} & \mathbf{H}_M & \mathbf{H}_{L3} & \mathbf{0} \\ \mathbf{0} & \mathbf{0} & \mathbf{H}_{U1} & \mathbf{H}_{U2} & \mathbf{H}_2 \end{bmatrix} \quad (3.18)$$

The row blocks have heights of Δ , $(\nu + 1)$, and $(L_h + L_w - \nu - \Delta)$; and the column blocks have widths $(\Delta - L_h)$, ν , $(L_h - \nu)$, ν , and $(L_w - \nu - \Delta)$. The sections $[\mathbf{H}_{L2}, \mathbf{H}_{L1}]$ and \mathbf{H}_{L3} are both lower triangular and contain the “head” of the channel, $[\mathbf{H}_{U1}, \mathbf{H}_{U2}]$ and \mathbf{H}_{U3} are both upper triangular and contain the “tail” of the channel, \mathbf{H}_1 and \mathbf{H}_2 are tall channel convolution matrices, and \mathbf{H}_M is Toeplitz. Then \mathbf{H}_{win} is simply the middle row (of blocks) of \mathbf{H} , and \mathbf{H}_{wall} is the concatenation of the top and bottom rows.

The limiting behavior for $\mathbf{B} = \mathbf{H}_{win}^T \mathbf{H}_{win}$ is

$$\begin{aligned} \mathbf{B} &= [\mathbf{0}, \mathbf{H}_{U3}, \mathbf{H}_M, \mathbf{H}_{L3}, \mathbf{0}]^T [\mathbf{0}, \mathbf{H}_{U3}, \mathbf{H}_M, \mathbf{H}_{L3}, \mathbf{0}] \\ &\triangleq [\mathbf{0}, \overline{\mathbf{H}}_3^T, \mathbf{0}]^T [\mathbf{0}, \overline{\mathbf{H}}_3, \mathbf{0}]. \end{aligned} \quad (3.19)$$

As L_w and Δ increase, the only change to \mathbf{B} is the size of the zero matrices. It can be shown that

$$\|\mathbf{B}\|_F^2 = \|\overline{\mathbf{H}}_3 \overline{\mathbf{H}}_3^T\|_F^2 \leq \|\mathbf{h}\|_2^4 \cdot (\nu + L_h)^2, \quad (3.20)$$

where L_h is the channel length.

Since $\mathbf{A} = \mathbf{H}_{wall}^T \mathbf{H}_{wall}$, it becomes a 5×5 block matrix, with $\mathbf{A}_{1,1} = \mathbf{H}_1^T \mathbf{H}_1$ and $\mathbf{A}_{5,5} = \mathbf{H}_2^T \mathbf{H}_2$. Thus,

$$\begin{aligned} \|\mathbf{A}\|_F^2 &\geq \|\mathbf{H}_1^T \mathbf{H}_1\|_F^2 + \|\mathbf{H}_2^T \mathbf{H}_2\|_F^2 \\ &\geq \|\mathbf{h}\|_2^4 \cdot (L_w - L_h - \nu). \end{aligned} \quad (3.21)$$

Noting that $\mathbf{B} = \mathbf{H}^T \mathbf{H} - \mathbf{A}$, taking the ratio of (3.20) to (3.21) and taking the limit completes the proof. ■

I have shown eigenvectors of \mathbf{A} in an MSSNR setup are symmetric or skew-symmetric asymptotically. It suggests that MSSNR TEQs are also symmetric or skew-symmetric if I force \mathbf{B} to be an identity matrix. This constraint leads to a MSSNR unit norm (MSSNR-UNT) TEQ.

3.3 Design Implication for Finite Length Cases

Observations on infinite length MMSE and MSSNR TEQ design make it clear that in the limit, these TEQs look symmetric. It implies that long finite length TEQ might display symmetry to some extent.

3.3.1 Exploiting Symmetry

In the case of MSSNR design, $\mathbf{A} = \mathbf{H}_{wall}^T \mathbf{H}_{wall}$ and $\mathbf{B} = \mathbf{H}_{win}^T \mathbf{H}_{win}$. \mathbf{A} and \mathbf{B} are not perfectly centrosymmetric, but they are nearly so.

MSSNR solution is to find a proper generalized eigenvector of (\mathbf{B}, \mathbf{A}) , and for the MMSE solution, generalized eigenvectors of $(\mathbf{B}, (\mathbf{A} + \mathbf{R}_n))$ are considered. However, if \mathbf{A} (or $(\mathbf{A} + \mathbf{R}_n)$ for the MMSE case) or \mathbf{B} is invertible, then the generalized eigenvalue problem can be reduced to a traditional eigenvalue problem [42]. When $L_w > \nu$, \mathbf{H}_{win} cannot have full column rank, so \mathbf{B} will not be invertible [43]. However, \mathbf{A} and $(\mathbf{A} + \mathbf{R}_n)$ are invertible for all channels longer than the CP.

Recall the generalized eigenvalue problem in (2.11). Since \mathbf{A} is invertible, \mathbf{w} must satisfy

$$(\mathbf{A}^{-1} \mathbf{B}) \mathbf{w} = \lambda \mathbf{w}. \quad (3.22)$$

The inverse of a centrosymmetric matrix is also centrosymmetric [78], and the product of centrosymmetric matrices is centrosymmetric, so $(\mathbf{A}^{-1} \mathbf{B})$ is approximately

centrosymmetric. Although \mathbf{A}^{-1} and \mathbf{B} are symmetric, $(\mathbf{A}^{-1}\mathbf{B})$ may not be, so the full range of results in [80] cannot be immediately applied. One result that still holds is that the eigenvectors are still symmetric or skew-symmetric, although there may not be exactly $\lfloor \frac{\tilde{L}_w}{2} \rfloor$ symmetric eigenvectors.

Since \mathbf{A} and \mathbf{B} are only approximately in V_N , the eigenvectors of $\mathbf{A}^{-1}\mathbf{B}$ will only be *approximately* symmetric or skew-symmetric. For the MMSE case, \mathbf{A} can be replaced by $(\mathbf{A} + \mathbf{R}_n)$ to obtain similar results. From the observed data in simulations, the MSSNR TEQs usually seem to be nearly symmetric rather than nearly skew-symmetric, at least for the carrier serving area (CSA) test loops [26], which are standard test channels for DSL.

To quantify the symmetry, an experiment is performed to compute the TEQ coefficients for $3 \leq \tilde{L}_w \leq 40$ for CSA test loops 1 through 8. Each TEQ \mathbf{w} is decomposed into \mathbf{w}_{sym} and \mathbf{w}_{skew} , and then computed $\|\mathbf{w}_{skew}\|^2/\|\mathbf{w}_{sym}\|^2$. A plot of this ratio is shown in Fig. 3.2. The value of Δ was determined via a global search. The ratios were averaged over the eight CSA loops. The symmetric part was obtained by considering all possible points of symmetry, and choosing the one for which the norm of the symmetric part divided by the norm of the perturbation was maximized. More specifically, for each tap i , $1 \leq i \leq L_w$:

1. assuming a Type I FIR linear phase filter, the filter length is determined as $2 \min(L_w - i, i - 1) + 1 = 2\alpha + 1$ with i being the index of the center tap. $\mathbf{w}_{sym} = [w(i - \alpha : i + \alpha) + w(i + \alpha : i - \alpha)]/2$ and $\mathbf{w}_{skew} = \mathbf{w} - \mathbf{w}_{sym}$.
2. assuming a Type II FIR linear phase filter, the filter length is determined as $2 \min(L_w - i, i) = 2\alpha$ with $i + 0.5$ in the center position. $\mathbf{w}_{sym} = [w(i - \alpha + 1 : i + \alpha) + w(i + \alpha : i - \alpha + 1)]/2$ and $\mathbf{w}_{skew} = \mathbf{w} - \mathbf{w}_{sym}$.

For example, if the TEQ coefficients were $\mathbf{w} = [1, 2, 4, 2.2]$, then $\mathbf{w}_{sym} = [0, 2.1, 4, 2.1]$ and $\mathbf{w}_{skew} = [1, -0.1, 0, 0.1]$. The MSSNR TEQ becomes increasingly symmetric with increasing length.

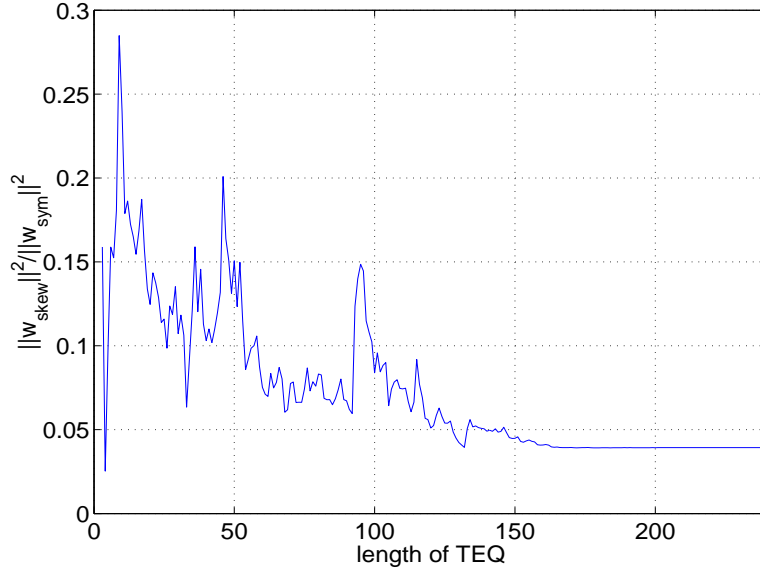


Figure 3.2: Energy in the skew-symmetric part of the TEQ over the energy in the symmetric part of the TEQ, for $\nu = 32$. The data was delay-optimized and averaged over CSA test loops 1 - 8.

Next I present a practical algorithm for enforcing symmetry in the TEQ. A similar approach was taken in [81], which presented simulations of linear phase equalizers for VDSL channel models. If the TEQ length \tilde{L}_w were even, then I could enforce the symmetry by

$$\mathbf{w}^T = \left[\mathbf{v}^T, (\mathbf{J}\mathbf{v})^T \right], \quad (3.23)$$

and if \tilde{L}_w were odd, I could enforce the symmetry by

$$\mathbf{w}^T = \left[\mathbf{v}^T, \gamma, (\mathbf{J}\mathbf{v})^T \right], \quad (3.24)$$

where in each case \mathbf{v} has dimensions $\lfloor \tilde{L}_w/2 \rfloor \times 1$. For the even-length case, the generalized eigenvalue problem of (2.10) can be simplified via

$$\begin{bmatrix} \mathbf{v}^T, \mathbf{v}^T \mathbf{J} \end{bmatrix} \begin{bmatrix} \mathbf{A}_{11} & \mathbf{A}_{12} \\ \mathbf{A}_{21} & \mathbf{A}_{22} \end{bmatrix} \begin{bmatrix} \mathbf{v} \\ \mathbf{J}\mathbf{v} \end{bmatrix} = \mathbf{v}^T \underbrace{[\mathbf{A}_{11} + \mathbf{J}\mathbf{A}_{21} + \mathbf{A}_{12}\mathbf{J} + \mathbf{J}\mathbf{A}_{22}\mathbf{J}]}_{\hat{\mathbf{A}}} \mathbf{v}, \quad (3.25)$$

with an analogous definition of $\hat{\mathbf{B}}$ (replace each \mathbf{A}_{ij} with \mathbf{B}_{ij}). Then the problem becomes

$$\min_{\mathbf{v}} \left(\mathbf{v}^T \hat{\mathbf{A}} \mathbf{v} \right) \quad \text{subject to} \quad \mathbf{v}^T \hat{\mathbf{B}} \mathbf{v} = 1. \quad (3.26)$$

The solution for \mathbf{v} is the generalized eigenvector of $(\hat{\mathbf{A}}, \hat{\mathbf{B}})$ corresponding to the minimum eigenvalue. This requires a generalized eigendecomposition of symmetric matrices of size $\tilde{L}_w/2 \times \tilde{L}_w/2$ rather than of size $\tilde{L}_w \times \tilde{L}_w$, thereby reducing the number of multiply-adds by a factor of 4. Similar results hold for the odd TEQ length case of (3.24), even though the partitioning of \mathbf{A} and \mathbf{B} is slightly different:

$$\begin{aligned} & [\mathbf{v}^T, \beta, \mathbf{v}^T \mathbf{J}] \begin{bmatrix} \mathbf{A}_{11} & \mathbf{A}_{12} & \mathbf{A}_{13} \\ \mathbf{A}_{21} & \mathbf{A}_{22} & \mathbf{A}_{23} \\ \mathbf{A}_{31} & \mathbf{A}_{32} & \mathbf{A}_{33} \end{bmatrix} \begin{bmatrix} \mathbf{v} \\ \beta \\ \mathbf{J}\mathbf{v} \end{bmatrix} \\ &= [\mathbf{v}^T, \beta] \underbrace{\begin{bmatrix} (\mathbf{A}_{11} + \mathbf{A}_{13}\mathbf{J} + \mathbf{J}\mathbf{A}_{31} + \mathbf{J}\mathbf{A}_{33}\mathbf{J}) & (\mathbf{A}_{12} + \mathbf{J}\mathbf{A}_{32}) \\ (\mathbf{A}_{21} + \mathbf{A}_{23}\mathbf{J}) & \mathbf{A}_{22} \end{bmatrix}}_{\hat{\mathbf{A}}} \begin{bmatrix} \mathbf{v} \\ \beta \end{bmatrix} \end{aligned} \quad (3.27)$$

In either case, I have reduced \mathbf{A} (size $\tilde{L}_w \times \tilde{L}_w$) to $\hat{\mathbf{A}}$ (size $\lceil \tilde{L}_w/2 \rceil \times \lceil \tilde{L}_w/2 \rceil$).

Matrices \mathbf{A} and \mathbf{B} can be calculated efficiently. It can be shown that [55]

$$\begin{aligned} \mathbf{A}_{m+1,n+1} &= \mathbf{A}_{m,n} - h(\Delta - n) h(\Delta - m) + h(\Delta + \nu - n + 1) h(\Delta + \nu - m + 1), \\ \mathbf{B}_{m+1,n+1} &= \mathbf{B}_{m,n} - h(\Delta + \nu + 1 - m) h(\Delta + \nu + 1 - n) + h(\Delta - m) h(\Delta - n). \end{aligned} \quad (3.28)$$

Fig 3.3 shows a computationally efficient method of implementing the proposed method. I have implemented it in the UT Austin DMT TEQ Matlab design toolbox [82].

Consider exploiting symmetry in the MMSE target impulse response. The length of \mathbf{b} is a fixed odd number $\nu + 1$. For instance, it is 33 for ADSL. The unit

1. Compute \mathbf{A} and \mathbf{B} using (3.28), then partition them as in (3.25) to form $\hat{\mathbf{A}}$ and $\hat{\mathbf{B}}$.
2. Solve for \mathbf{v} using a generalized eigendecomposition to find the maximum eigenvalue [83].
 - (a) Decompose $\hat{\mathbf{B}} = \mathbf{QR}$, where \mathbf{Q} is orthogonal and \mathbf{R} is upper triangular. Overwrite $\hat{\mathbf{B}}$ with \mathbf{R} .
 - (b) Overwrite $\hat{\mathbf{A}} = \mathbf{Q}^T \hat{\mathbf{A}}$.
 - (c) Hessenberg-Triangular Reduction ([42], p. 380): overwrite $\hat{\mathbf{A}}$ with an upper Hessenberg matrix and $\hat{\mathbf{B}}$ with an upper triangular matrix.
 - (d) Apply the “QZ” process to matrix pencil $\hat{\mathbf{A}} - \lambda \hat{\mathbf{B}}$ ([42] p. 385). It reduces $\hat{\mathbf{A}}$ to upper-quasi triangular form and $\hat{\mathbf{B}}$ to upper triangular form.
 - (e) Calculate the generalized eigenvalues by dividing each diagonal element of $\hat{\mathbf{A}}$ by the corresponding diagonal element of $\hat{\mathbf{B}}$.
 - (f) Choose the minimum generalized eigenvalue λ_{min} , then iteratively solve $(\hat{\mathbf{A}} - \lambda_{min} \hat{\mathbf{B}}) \hat{\mathbf{q}}^{new} = \hat{\mathbf{B}} \hat{\mathbf{q}}^{old}$, normalize $\hat{\mathbf{q}}^{new} = \hat{\mathbf{q}}^{new} / \|\hat{\mathbf{q}}^{new}\|_2$; using an initial guess of $\hat{\mathbf{q}}^0 = \mathbf{1}_{\lceil \tilde{L}_w/2 \rceil \times 1}$. Then $\mathbf{v} = \hat{\mathbf{q}}^{final}$.
3. $\mathbf{w} = \left[\mathbf{v}^T, (\mathbf{J}\mathbf{v})^T \right]^T$.

Figure 3.3: Fast symmetric MSSNR TEQ design method.

norm constraint forces $\mathbf{b}^T \mathbf{b} = 1$, which can be written as

$$\underbrace{[\mathbf{v}^T, \beta, (\mathbf{J}\mathbf{v})^T]}_{\mathbf{b}} \begin{bmatrix} \mathbf{v} \\ \beta \\ \mathbf{J}\mathbf{v} \end{bmatrix} = 1. \quad (3.29)$$

Setting $\hat{\mathbf{v}}^T = [\sqrt{2}\mathbf{v}^T, \beta]$ places the unit norm constraint $\hat{\mathbf{v}}^T \hat{\mathbf{v}} = 1$ on the symmetric design. Accordingly, the optimization is performed on

$$\mathbf{b}^T \mathbf{A}_{MMSE} \mathbf{b} = \hat{\mathbf{v}}^T \hat{\mathbf{A}}_{MMSE} \hat{\mathbf{v}} \quad (3.30)$$

where

$$\hat{\mathbf{A}}_{MMSE} = \begin{bmatrix} \frac{1}{2}(\mathbf{A}_{11} + \mathbf{A}_{13}\mathbf{J} + \mathbf{J}\mathbf{A}_{31} + \mathbf{J}\mathbf{A}_{33}\mathbf{J}) & \frac{1}{\sqrt{2}}(\mathbf{A}_{12} + \mathbf{J}\mathbf{A}_{32}) \\ \frac{1}{\sqrt{2}}(\mathbf{A}_{21} + \mathbf{A}_{23}\mathbf{J}) & \mathbf{A}_{22} \end{bmatrix} \quad (3.31)$$

Now consider the possibility of exploiting symmetry in a Min-ISI design. By inspecting (4.1), \mathbf{A} is generally Hermitian instead of symmetric because the set \mathcal{S} contains only positive frequencies for a real one-side baseband transmission. But if I force the mirrored subchannels $i = N - j$, $j = 0, 1, \dots, N/2 - 1$ to be added into the weighting function, and set the imaginary SNR_i on those mirrored subchannels equal to their positive counterpart, namely $\text{SNR}_i = \text{SNR}_{N-i}$, I actually end up at the same optimum due to the symmetry. I also notice that actually MSSNR is a special case of Min-ISI where all mirror subchannels are added into consideration and all $\text{SNR}_i = 1$. So adding the mirrored subchannels seems also a natural extension for Min-ISI. The good news here is that \mathbf{A} is symmetric instead of Hermitian. By following the analysis of MSSNR, I have laid the groundwork for symmetric Min-ISI design methods.

3.3.2 Exploiting Linear Phase Property

Another advantage of symmetric FIR filter designs is that symmetric TEQs have linear phase responses. A causal generalized linear phase TEQ with L_w taps satisfies

$$w(n) = \begin{cases} w(L_w - 1 - n), & 0 \leq n \leq L_w - 1 \\ 0, & \text{otherwise} \end{cases} \quad (3.32)$$

The transfer function of TEQ has the form

$$\mathbf{W}(e^{j\omega}) = \mathbf{W}_e(e^{j\omega})e^{-j\omega(L_w-1)/2} \quad (3.33)$$

where $\mathbf{W}_e(e^{j\omega})$ is a real, even, periodic function of ω . The result shows that given the TEQ length L_w , the phase response of a symmetric TEQ is known. The phases of the FEQs are then determined entirely by the the channel phase response. Thus,

if a channel estimate is available, which is usually true because many TEQ training methods are based on channel estimation, the FEQ phases can be determined in parallel with the TEQ design. If 4-QAM signaling is used on a subcarrier, the magnitude of the FEQ does not matter, and the entire FEQ for that tone is can be designed without the knowledge of TEQ.

During ADSL initialization, 4-QAM signaling is used across various special training sequences. FEQ can be partially trained along with the TEQ training by setting its phase response once channel estimation is made. The magnitude response can be set after the TEQ is designed. The benefit here is that if the FEQ is designed all at once, the design procedure involves all complex-valued operations. But if the phase response is already known, then determining the FEQ magnitude only requires real operations usually resulting in lower computational complexity.

3.4 Conclusion

Two commonly used channel shortening methods, the MMSE and the MSSNR designs, have been characterized in terms of their impulse, phase and magnitude responses. When TEQ length goes to infinity, the limiting behavior of matrices used in TEQ training lead to perfect symmetric filters. This observation motivated new algorithms resulting in causal linear phase TEQ designs for MMSE and MSSNR (extended to Min-ISI), which provide a dramatic decrease in implementation complexity.

Chapter 4

Improving Minimum Intersymbol Interference Methods

4.1 Introduction

Arslan, Kiaei, and Evans report a minimum intersymbol interference (Min-ISI) method for TEQ design. Min-ISI TEQs generalize MSSNR TEQs by weighting the ISI in the frequency domain [26]. Frequency-weighted ISI is an approximation of achievable bit rate. Min-ISI is amenable to real-time implementation on programmable fixed-point Digital Signal Processors (DSPs). The Min-ISI method, however, has several disadvantages: (1) sensitivity to transmission delay, (2) inability to design TEQs longer than $\nu + 1$ taps, where ν is the cyclic prefix length, and (3) sensitivity to the fixed-point computation in the Cholesky decomposition to solve the generalized eigen-problem described in Section 2.2.2. On fixed-point DSPs with 16-bit multipliers, e.g. TI TMS320C6200 and Motorola 56300, the Cholesky decomposition may become unstable for TEQs longer than 15 taps.

In this chapter, I reformulate the Min-ISI cost function to enable it to be applied to the design of TEQs longer than $\nu + 1$ taps. The new cost function significantly reduces computational complexity in searching for the optimal transmission delay. To reduce the number of multiplications further, I introduce quantized frequency-domain ISI weighting functions. I derive an iterative version of the Min-ISI method, based on the new cost function. The iterative method does not require any matrix decompositions, is free of any division calculations, and is well suited for fixed-point implementation.

4.2 Original Methods

4.2.1 Review

Chapter 2 shows that the Min-ISI method is a suboptimal solution of MBR method [26]. While optimum MBR leads to a non-linear maximization problem with no closed-form solution, Min-ISI ends up at a mathematically tractable generalized eigenvalue problem.

The Min-ISI cost function can be written as [26]

$$\begin{aligned} J(\mathbf{w}) &= \frac{\mathbf{w}^T \mathbf{H}^T \mathbf{D}^T \sum_{i \in \mathcal{S}} \left(\mathbf{q}_i \frac{S_{x,i}}{S_{n,i}} \mathbf{q}_i^H \right) \mathbf{D} \mathbf{H} \mathbf{w}}{\mathbf{w}^T \mathbf{H}^T \mathbf{G}^T \mathbf{G} \mathbf{H} \mathbf{w}} \\ &= \frac{\mathbf{w}^T \mathbf{A} \mathbf{w}}{\mathbf{w}^T \mathbf{B} \mathbf{w}} \end{aligned} \quad (4.1)$$

where $S_{x,i}$ and $S_{n,i}$ are the transmitted signal power and channel noise power for i th tone, respectively.

In the original proposal, one can convert the Min-ISI TEQ design problem to a constrained minimization problem by setting $\mathbf{w}^T \mathbf{B} \mathbf{w} = 1$:

$$\min_{\mathbf{w}} (\mathbf{w}^T \mathbf{A} \mathbf{w}) \quad \text{subject to} \quad \mathbf{w}^T \mathbf{B} \mathbf{w} = 1 \quad (4.2)$$

The solution is obtained by solving the generalized eigenvector problem

$$\mathbf{A}\mathbf{w} = \tilde{\lambda}\mathbf{B}\mathbf{w} \quad (4.3)$$

where $\tilde{\lambda}$ is the smallest generalized eigenvalue of the matrix pencil (\mathbf{A}, \mathbf{B}) .

Actually MSSNR is a special case of Min-ISI with $\frac{S_{x,i}}{S_{n,i}} = 1$ for each subchannel i and \mathcal{S} contains all subchannels allocated to the full bandwidth, namely, $i = 0, 1, \dots, N - 1$. MSSNR tries to maximize the sum of channel energy in a length $\nu + 1$ rectangular window, but it does not care how the ISI reduction is distributed in the frequency domain. As pointed out in [3], both the signal (ISI-free part) and channel noise are filtered by the equalizer, and hence the change in SNR before and after equalization is due to the effect on ISI and not on the signal or the noise.¹ In other words, SNR_i after the TEQ has an upper bound as $\frac{S_{x,i}|H_i|^2}{S_{n,i}}$, where $|H_i|^2$ is the channel gain in the i th subchannel and this upper bound is approximately the matched filter bound for the i th subchannel. There exists a lower bound on SNR, which supports minimum number of bits defined in standards (2 bits in first generation ADSL). If $\frac{S_{x,i}|H_i|^2}{S_{n,i}}$ terms are already below the lower bound because of severe channel noise on some subchannels, then it does not matter whether or not more ISI is injected into these subchannels because these subchannels will be turned off. So what Min-ISI does is to have the residual ISI primarily residing in the subchannels with low SNR. The more residual ISI resides in the bands that can carry nothing before the TEQ, the less loss is introduced in the bit rate. It seems natural to have $\frac{S_{x,i}}{S_{n,i}}$ as the weighting function because it successfully places the residual ISI into those subchannels with higher noise power.

¹This claim is not 100% true because noise is not periodic thus shaped noise does contribute to the change of SNR. I assume it is true to simplify the analysis and highlight the basic idea.

4.2.2 Evaluation

Solvability

When $L_w > \nu + 1$, a case mostly happens in an upstream transmission, \mathbf{GH} is rank deficient and \mathbf{B} will not be invertible. One cannot apply the method in [21] to solve the problem. Thus, the original formulation of Min-ISI is not suitable for design of arbitrary length TEQs.

As reported in [3], one can follow the approach in [43], which solves

$$\mathbf{B}\mathbf{w} = \lambda\mathbf{A}\mathbf{w} \quad (4.4)$$

where $\lambda = 1/\tilde{\lambda}$ is the largest eigenvalue of the matrix pencil (\mathbf{A}, \mathbf{B}) . Authors of [3] claim that in practice \mathbf{B} is always invertible for all channel impulse responses longer than the CP length, but do not offer a proof. A more rigorous argument is presented here with proof:

Theorem 4 *For an FIR channel \mathbf{h} , if channel length $L_h > \nu$, then the matrix \mathbf{A} in (4.1) will be invertible if and only if all subchannels have been used.*

Proof: I denote $\mathbf{Z} = \sum_{i \in \mathcal{S}} \left(\mathbf{q}_i \frac{S_{x,i}}{S_{n,i}} \mathbf{q}_i^H \right) = \sum_i \mathbf{Z}_i$. It is obviously that $\mathbf{Z}_i = \left(\mathbf{q}_i \frac{S_{x,i}}{S_{n,i}} \mathbf{q}_i^H \right)$ is Hermitian. Thus I have \mathbf{Z} , the sum of Hermitian matrices is also Hermitian. A Hermitian matrix can be decomposed into [5]

$$\mathbf{Z} = \mathbf{U}\mathbf{\Lambda}\mathbf{U}^H \quad (4.5)$$

where \mathbf{U} is a unitary matrix and $\mathbf{\Lambda}$ is a diagonal matrix with all the diagonal entries being eigenvalues of \mathbf{Z} . Let $\mathbf{V} = \mathbf{U}^H$, and form another matrix $\mathbf{\Lambda}_s$ whose diagonal entries are the square roots of the corresponding entries in $\mathbf{\Lambda}$. It can be done because all the eigenvalues of a Hermitian matrix are real [5]. Since each \mathbf{Z}_i is a rank one matrix, \mathbf{Z} will be full rank only if all $\mathbf{Z}_i, i = 0, 1, \dots, N$ are added in the formulation of \mathbf{Z} . The matrix \mathbf{A} can be written as

$$\mathbf{A} = \mathbf{H}^T \mathbf{D}^T \mathbf{V}^H \mathbf{\Lambda}_s^H \mathbf{\Lambda}_s \mathbf{V} \mathbf{D} \mathbf{H} = \mathbf{S}^H \mathbf{S} \quad (4.6)$$

If I denote rank of a matrix \mathbf{X} as $R(\mathbf{X})$, it is well-known that [5]

$$R(\mathbf{S}) = R(\mathbf{\Lambda}_s \mathbf{V} \mathbf{D} \mathbf{H}) \leq R(\mathbf{D} \mathbf{H}) \quad (4.7)$$

where equality holds only when $\mathbf{\Lambda}_s \mathbf{V}$ is a invertible square matrix; namely, all diagonal entries of $\mathbf{\Lambda}_s$ are non-zero, which is true only when all subchannels used in the formulation of \mathbf{Z} . Thus I have [5]

$$R(\mathbf{S}) = R(\mathbf{D} \mathbf{H}). \quad (4.8)$$

It has been proven that $\mathbf{D} \mathbf{H}$ has full column rank in [20]. Hence \mathbf{S} has full column rank. By the theory of singular value decomposition [6], $\mathbf{A} = \mathbf{S}^H \mathbf{S}$ has the same number of singular values as \mathbf{S} ; i.e., it has full column rank. It is invertible. However, in the case that not all subchannels are used in the formulation of \mathbf{A} , $R(\mathbf{S}) < R(\mathbf{D} \mathbf{H})$, and \mathbf{A} is singular. ■

In the worst case, when both \mathbf{A} and \mathbf{B} are not invertible, I still can apply a generalized power method to solve the Min-ISI optimization problem. But numerical instability usually prevents a practical fixed-point implementation.

When either \mathbf{A} or \mathbf{B} is invertible, (4.3) or (4.4) respectively is used to train the TEQ. However, the dependence between \mathbf{A} , \mathbf{B} , and the windowing matrix \mathbf{G} introduces additional computations.

Non-optimality of Weighting function

In [3], the inventors of the Min-ISI method propose another weighting $\frac{S_{x,i}|H_i|^2}{S_{n,i}}$ instead of $\frac{S_{x,i}}{S_{n,i}}$ after observing possible bit rate improvement when new weighting is used. I agree that the original weighting is not optimum. $\frac{S_{x,i}}{S_{n,i}}$ places ISI into subchannels with higher noise power because $S_{x,i}$ is a constant in a standard flat energy distribution for DSL applications. But a subchannel with higher noise power does not necessarily have lower SNR because channel gain also plays a role here. This

weighting may not actually push ISI into those bands below the lower bound of pre-TEQ SNR.

But the weighting $\frac{S_{x,i}|H_i|^2}{S_{n,i}}$ has its own problems. Since bit rate is a logarithm function of SNR, the same SNR increment seems to gain more bits on these subchannels with low $\frac{S_{x,i}|H_i|^2}{S_{n,i}}$ as long as the SNR is still above the lower bound. $\frac{S_{x,i}|H_i|^2}{S_{n,i}}$ misplaces ISI reduction in this sense. Sometimes the original weighting will also misplace ISI reduction in this sense, although not always. Second, additive noise is not periodic. The TEQ does change $\frac{S_{x,i}|H_i|^2}{S_{n,i}}$. Some subchannels, which have a pre-TEQ SNR below the lower SNR bound, could pass the bound after TEQ. For those subchannels, the assumption, which says $\frac{S_{x,i}|H_i|^2}{S_{n,i}}$ is an upper bound and ISI has no effect on the bit rate performance in those subchannels, is not valid.

The weighting $\frac{S_{x,i}}{S_{n,i}}$ seems to be a more favorable choice over $\frac{S_{x,i}|H_i|^2}{S_{n,i}}$ for the above reasons. But it is not able to completely avoid the issue resulting from $\frac{S_{x,i}|H_i|^2}{S_{n,i}}$ weighting. Simulations confirm these concerns. Sometimes the MSSNR method outperforms the Min-ISI method because non-optimal weighting either shuts down some subchannels that could carry 2 bits or results in less bit rate improvement due to misplacement of ISI reduction. Min-ISI seems to have a better bit rate performance on more occasions than MSSNR.

Sensibility to fixed point implementation

In practice, Cholesky decomposition is usually used to convert a generalized eigenvalue problem to a normal eigenvalue problem. If we define

$$\begin{aligned}
 \mathbf{B} &= \mathbf{Q}\mathbf{\Lambda}\mathbf{Q}^T = (\mathbf{Q}\sqrt{\mathbf{\Lambda}})(\sqrt{\mathbf{\Lambda}}\mathbf{Q}^T) \\
 &= \sqrt{\mathbf{B}}\sqrt{\mathbf{B}}^T \\
 \mathbf{C} &= \sqrt{\mathbf{B}}^{-1}\mathbf{A}(\sqrt{\mathbf{B}}^T)^{-1} \\
 \mathbf{v} &= \sqrt{\mathbf{B}}^T\mathbf{w},
 \end{aligned} \tag{4.9}$$

the original problem is equivalent to solve

$$\min_{\mathbf{v}} (\mathbf{v}^T \mathbf{C} \mathbf{v}) \quad \text{subject to} \quad \mathbf{v}^T \mathbf{v} = 1 \quad (4.10)$$

Cholesky decomposition is a favorable choice over matrix inversion in fixed-point implementation due to its better numerical stability. However, when the matrix dimension keeps increasing, Cholesky decomposition will experience more and more numerical errors. At some point, it generates unacceptable results that can significantly degrade TEQ performance.

In the rest of this chapter, I propose several modifications to the original Min-ISI design to address above concerns.

4.3 Reformulation of the Cost Function

The original formulation minimizes the ratio of a weighted sum of the ISI power over the sum of the desired signal power within a target window. The target window starts from a given delay Δ and ends at $\Delta + \nu$. To find the optimum Δ , it is necessary to search over all possible Δ values. For each delay, a generalized eigenvector is found to be the TEQ to minimize the cost function. Because \mathbf{B} is a function of Δ , Cholesky decompositions have to be performed as many times as the number of searched Δ values. The alternative approach in (4.4) faces the same problem because \mathbf{A} is also a function of delay Δ .

To reach a more efficient implementation of the Min-ISI method, authors of [55] first proposed a complexity-reduced design (also applies to MSSNR) to take advantage of the tremendous amount of redundancy involved in the brute force calculation of \mathbf{A} and \mathbf{B} . Later, authors of [56] discussed methods of reusing even more of the computations to dramatically decrease the required complexity. Specifically, for a given delay Δ ,

- $\mathbf{A}(\Delta)$ can be computed from $\mathbf{B}(\Delta)$ almost for free

- $\mathbf{B}(\Delta + 1)$ can be computed from $\mathbf{B}(\Delta)$ almost for free
- A shifted version of the optimal solution for delay Δ can be used to initialize the optimal solution for delay $\Delta + 1$

However, an even simpler approach is presented in this section. I reformulate the Min-ISI cost function not only to make it suitable for designing TEQ longer than CP length, but also to avoid the need of multiple Cholesky decompositions. In a similar fashion to recently proposed minimum delay spread equalizers [22, 23], I change the definition of matrix \mathbf{B} in (4.1) from $\mathbf{H}^T \mathbf{G}^T \mathbf{G} \mathbf{H}$ to $\mathbf{H}^T \mathbf{H}$. With this change, I aim at minimizing the ratio of the weighted sum of ISI power over the total signal power instead of the windowed signal power. Mathematically the optimum TEQ of the original one will also be the one optimizing the new cost function. However, many fewer computations are involved when searching for an optimal delay. The new \mathbf{B} is a positive definite matrix [20] and a Cholesky decomposition $\mathbf{B} = \mathbf{L}\mathbf{L}^T$ can be pre-calculated. The matrix \mathbf{L} is an upper triangular matrix. The modified min-ISI has a cost function as

$$J(\mathbf{w}) = \frac{\mathbf{w}^T \mathbf{A} \mathbf{w}}{\mathbf{w}^T \mathbf{L}\mathbf{L}^T \mathbf{w}} \quad (4.11)$$

Since \mathbf{L} here does not depend on Δ , only one Cholesky decomposition is needed for the modified Min-ISI method. Once \mathbf{L} is available, it can be used for any delay value. \mathbf{B} is always invertible when $L_w \leq N$ where N is the symbol length; hence, this new formulation can be applied to the design of a TEQ with the number of taps up to N .

The formulation of \mathbf{B} takes more computation than the original one, but it is negligible because (1) the additional computations are far less than the reductions of multiple Cholesky decompositions involved in searching for the optimum delay, and (2) it only requires the calculation of \mathbf{B} once whereas the original method requires to update \mathbf{B} for each delay.

L_w	Proposed cost function	Original cost function	Savings
5	42	20042	20000
17	1638	787718	786080
32	10923	5253803	5242880

Table 4.1: Comparison of total number of flops associated with Cholesky decomposition between original Min-ISI design and proposed one

An analysis of computational complexity of the modified Min-ISI method follows. All possible transmission delays range from 0 to $N - \nu$, which is 481 possible delay values in an ADSL system. For a *non-Toeplitz* $L_w \times L_w$ matrix \mathbf{B} , the Cholesky decomposition can be computed in $(L_w)^3/3$ floating operations [84]. Table 4.3 compares the number of floating point operations needed to perform a Cholesky decomposition of a 5-tap, a 17-tap and a 32-tap TEQ, respectively, between the original Min-ISI method and the proposed Min-ISI method.

It has been shown in [3] that for the original design, calculating \mathbf{B} for each delay needs $2L_w(\nu + Lw)$ floating point operations (by exploiting symmetry of \mathbf{GH}). After including the floating point operations for updating of \mathbf{GH} in each delay, the computations are far more than those of the proposed method, which only needs $2L_w(N + Lw)$ floating point operations regardless of the number of delay values searched.

4.4 Quantized Weighting Function

In the original Min-ISI cost function (4.1), the weighting $\sum_i \left(\mathbf{q}_i \frac{S_{x,i}}{S_{n,i}} \mathbf{q}_i^H \right)$ pushes the ISI power into the subchannels with higher noise power (hopefully lower SNR). The MSSNR method, however, treats ISI in low and high SNR subchannels equally. Hence, Min-ISI has the potential to outperform MSSNR in terms of achievable bit rate.

As analyzed in previous section, the major improvement of Min-ISI over MSSNR comes from the placement of ISI to the bands have a pre-TEQ SNR lower than a bound which can support 2-bit constellation. I propose an “on-off” weighting to achieve this goal. I could compare the $\frac{S_{x,i}|H_i|^2}{S_{n,i}}$ to a preset threshold T_i , and set the weighting to 1 if the condition is true and 0 otherwise. That is, an “off” weighting of 0 means that the noise power is too strong in that subcarrier, and I do not care whether or not ISI is minimized there. This is correct in theory but in practice $\frac{S_{x,i}}{S_{n,i}}$ is easier to obtain. Thus, I propose an on-off weighting with a threshold on $\frac{S_{x,i}}{S_{n,i}}$.

When the transmitted signal has a flat spectrum, as in the case of the transmission of the training sequences in the G.DMT ADSL standard, $S_{n,i}$ is estimated during initialization. Because training sequences are periodic, no ISI will corrupt the estimation of $S_{n,i}$. In my proposed method, the comparison would reduce to a simple subtraction operation, $S_{n,i} - S_{n,preset}$, where $S_{n,preset}$ is the threshold. For the on-off case, the preset value $S_{n,preset}$ may be calculated offline by

$$S_{n,preset} = \frac{S_x}{3 \times 10^{(\Gamma_{gap}/10)}} \quad (4.12)$$

where S_x is the common value of signal power for all subcarriers and Γ_{gap} is SNR gap for achieving Shannon channel capacity. In this case, $\frac{S_x}{S_{n,preset}}$ will support a 4-QAM constellation.

One additional advantage of this weighting is its ability to reduce the complexity of original method. To implement the original method, I need multiplication operations to form the weighting function. In the proposed method, I threshold the SNR calculation to compute “on-off” weighting. This digitized “on-off” weighting drops the subcarriers that are below the threshold and saves multiplication operations. In this way, the implementation complexity is reduced. MSSNR is a special case of this on-off weighting in the sense that MSSNR turns on all of the subcarriers.

The on-off weighting does not contradict the logarithm property of bit rate function as it treats all subchannels above the threshold equally. That might be the

reason that sometimes on-off Min-ISI achieves better performance than both the MSSNR and original Min-ISI.

The on-off weighting can be extended to multiple levels if I use multiple thresholds and assign different weighting values. For G.DMT ADSL, each subcarrier can support 0–15 bits. (There is a provision in the G.DMT ADSL standard to support one bit on a subcarrier, although this provision is rarely implemented.) I can put four thresholds and assign weighting values of 0, 1, 2^1 , or 2^2 . Quantization to 4 levels can be performed with two comparisons. The weighting can be implemented as shifting, which is still a computational savings over multiplication.

4.5 Iterative Implementation

Considering all the refinements mentioned in previous sections of this chapter, I propose an iterative algorithm in this section that can be easily applied once the channel estimates and the frequency weighting functions are available. Hereafter, I denote the weighting function for subcarrier i as α_i . In the original Min-ISI, $\alpha_i = \frac{Sx_i}{Sn_i}$, which can be estimated from a periodic sequence that is transmitted in the early stage of receiver initialization and that does not need a TEQ.

The cost function in (4.1) can be written as

$$\begin{aligned} J(\mathbf{w}_k) &= \mathbf{w}_k^T \mathbf{H}^T \mathbf{D}^T \sum_i (\mathbf{q}_i \alpha_i \mathbf{q}_i^H) \mathbf{D} \mathbf{H} \mathbf{w}_k \\ &= \mathbf{w}_k^T \mathbf{A} \mathbf{w}_k \end{aligned} \quad (4.13)$$

where \mathbf{A} only differs from the definition in (4.1) in the weights α_i .

The performance surface is quadratic and the method of steepest descent is readily implemented. The gradient ∇_k is obtained by

$$\begin{aligned} \nabla_k &= \left. \frac{\partial J}{\partial \mathbf{w}} \right|_{\mathbf{w}=\mathbf{w}_k} = \frac{\partial(\mathbf{w}_k^T \mathbf{A} \mathbf{w}_k)}{\partial \mathbf{w}_k} \\ &= (\mathbf{A} + \mathbf{A}^T) \mathbf{w}_k \end{aligned} \quad (4.14)$$

1. Obtain the weighting values $\alpha_i = \frac{Sx_i}{Sn_i}$.
2. Pre-compute $L_w \times L_w$ Hermitian matrix $\mathbf{A} = \mathbf{H}^T \mathbf{D}^T \sum_i (\mathbf{q}_i \alpha_i \mathbf{q}_i^H) \mathbf{D} \mathbf{H}$ and $\hat{\mathbf{A}} = \mathbf{A} + \mathbf{A}^T$, where \mathbf{H} , \mathbf{D} , and \mathbf{q}_i are defined in (2.20).
3. Start with non-zero initial guess \mathbf{w}_0
4. $\nabla_k = \hat{\mathbf{A}} \mathbf{w}_k$
5. $\hat{\mathbf{w}}_{k+1} = \mathbf{w}_k + \mu(-\nabla_k)$
6. $\mathbf{w}_{k+1} = \frac{\hat{\mathbf{w}}_{k+1}}{\sqrt{\hat{\mathbf{w}}_{k+1}^T \mathbf{B} \hat{\mathbf{w}}_{k+1}}}$

Figure 4.1: Proposed iterative Min-ISI TEQ design method with normalization.

The iterative update of TEQ is

$$\mathbf{w}_{k+1} = \mathbf{w}_k + \mu(-\nabla_k) \quad (4.15)$$

where μ is the step size which regulates the speed and stability of adaptation. The constraint $\mathbf{w}^T \mathbf{B} \mathbf{w}$ should also be included, which can be implemented by renormalizing \mathbf{w} after each iteration. Fig. 4.1 presents the full algorithm.

One problem with the iterative Min-ISI method in Fig. 4.1 is the step size parameter μ . It is difficult to bound the step size because of the normalization in the last step of each iteration. However, this problem has been nicely solved in the neural networks area. A self-organizing algorithm [85] to adaptively calculate the principal component (generalized eigenvector corresponding to the largest generalized eigenvalue) of $\mathbf{w}^T \mathbf{B} \mathbf{w}$ constrained to $\mathbf{w}^T \mathbf{A} \mathbf{w} = 1$. It suggests the extraction of the principal component according to the update equation

$$\mathbf{w}_{k+1} = \mathbf{w}_k + \mu[\mathbf{B} \mathbf{w}_k - \mathbf{A} \mathbf{w}_k (\mathbf{w}_k^T \mathbf{B} \mathbf{w}_k)] \quad (4.16)$$

where k is the iteration index and μ is the step size. The normalization step has been replaced by the second correction item in the solid parentheses. For the problem at hand, I formulate a Lagrange multiplier as

$$L(\mathbf{w}, \lambda) = \mathbf{w}^T \mathbf{A} \mathbf{w} - \lambda(\mathbf{w}^T \mathbf{B} \mathbf{w} - 1). \quad (4.17)$$

By calculating the gradient of $L(\mathbf{w}, \lambda)$, left multiplying by \mathbf{w}^T , and setting it to zero, optimum λ is determined as $\frac{1}{2} \mathbf{w}^T (\mathbf{A} + \mathbf{A}^T) \mathbf{w}$. Note \mathbf{A} is Hermitian instead of symmetric. Substituting optimum λ to (4.17) and calculating the gradient of $L(\mathbf{w}, \lambda)$ again, I obtain the update as

$$\mathbf{w}_{k+1} = \mathbf{w}_k + \mu[(\mathbf{A} + \mathbf{A}^T) \mathbf{w}_k - \mathbf{B} \mathbf{w}_k (\mathbf{w}_k^T (\mathbf{A} + \mathbf{A}^T) \mathbf{w}_k)] \quad (4.18)$$

The step size μ has an upper bound as shown in the Lemma 5 of [85]:

$$\mu < \frac{1}{\lambda_{max}(\mathbf{A} + \mathbf{A}^T)(\lambda_{max}(\mathbf{B}) - 1)^2} \quad (4.19)$$

where $\lambda_{max}(\mathbf{M})$ means the largest eigenvalue of matrix \mathbf{M} . Fig. 4.2 presents the algorithm based on the self-organizing update.

4.6 Conclusion

This chapter derives a new cost function that measures ISI at the FFT output. I use the new cost function to design Min-ISI TEQs longer than the cyclic prefix length. I also use the new cost function to reduce the number of Cholesky decompositions to one when searching for the optimal transmission delay. I introduce quantized ISI frequency weightings to reduce computational complexity. This weighting makes possible bit rate improvement as well.

Based on the new cost function, I derive an iterative Min-ISI method. The iterative Min-ISI method avoids Cholesky decomposition entirely, and achieves the bit rate performance of the original Min-ISI method. The iterative Min-ISI method is amenable to implementation on fixed-point programmable digital signal processors.

1. Obtain the weighting values $\alpha_i = \frac{Sx_i}{Sn_i}$.
2. Pre-compute $L_w \times L_w$ Hermitian matrix $\mathbf{A} = \mathbf{H}^T \mathbf{D}^T \sum_i (\mathbf{q}_i \alpha_i \mathbf{q}_i^H) \mathbf{D} \mathbf{H}$ and $\hat{\mathbf{A}} = \mathbf{A} + \mathbf{A}^T$, where \mathbf{H} , \mathbf{D} , and \mathbf{q}_i are defined in (2.20).
3. Start with non-zero initial guess \mathbf{w}_0
4. Choose a step size $\mu < \frac{1}{\lambda_{max}(\hat{\mathbf{A}})(\lambda_{max}(B)-1)^2}$
5. $\mathbf{w}_{k+1} = \mathbf{w}_k + \mu[\hat{\mathbf{A}}\mathbf{w}_k - \mathbf{B}\mathbf{w}_k(\mathbf{w}_k^T \hat{\mathbf{A}}\mathbf{w}_k)]$

Figure 4.2: Proposed iterative Min-ISI TEQ design method with self-organizing update. With the right pre-set value of the step size μ , this method is free of division operations.

Chapter 5

Filter Bank Equalization

5.1 Introduction

The traditional TEQ-FEQ structure equalizes all subchannels in a combined fashion, which may limit bit rate performance. In particular time domain equalizers have limited abilities to treat frequency discontinuities in the transmission bandwidth. The time domain approach appears contrary the original divide-and-conquer idea of DMT. At least three alternate equalizer structures have been proposed with improved performance as mentioned in Chapter 1. The dual-FIR TEQ [33] uses a standard single-FIR TEQ to achieve good bit rate over the entire transmission bandwidth, and uses a second FIR TEQ to improve the bit rate over a subset of subcarriers. The per-tone equalizer [34] essentially moves the single-FIR TEQ into the FEQ, which converts the FEQ into a linear combiner for each subcarrier. A third alternate structure is a TEQ filter bank [27], in which a different FIR TEQ is designed for each tone. The FFT becomes a bank of Goertzel filters and a single-tap FEQ is also used.

All three alternative approaches have the potential to achieve a higher bit rate than a single TEQ-FEQ design. The question is what is the best we can do

given a DMT setup. To study the bit rate performance upper bound in a DMT modulated system, I construct a new equalization structure motivated by the TEQ filter bank and per tone equalizer. In this model, I move all FEQ operations to the time domain and combine this with the TEQ to obtain a multi-tap complex-valued FIR for each tone. This structure provides time domain equalizer designers with the most freedom. The design freedom is equivalent to the per-tone structure for frequency domain equalizers. It can perform delay optimization on each individual path, which per-tone cannot do if either a sliding FFT or a modified single FFT structure is applied. This constructed complex-tap time domain equalizer filter bank is meant to provide an upper bound on achievable bit rate. However, it is also implementable on TI's TMS320C6000 digital signal processors (DSPs), which have clock speeds at 1 GHz. A design procedure, which depends on the second-order statistics of the input and output sequences, is provided. Particularly, in the proposed training algorithm, channel estimation is not required as it is in many other equalization schemes [17, 26, 86].

5.2 Complex Filter Bank Equalization: A Performance Bound

5.2.1 Structure

Fig. 5.1 depicts a traditional DMT system with a TEQ-FEQ equalization structure at the receiver. Information bearing bits are divided into a set of independent data transmission subchannels. Signals are modulated by QAM on each subchannel. An inverse FFT (IFFT) converts signal on each subchannel (which acts as one of the frequency components) into a time-domain signal. The input to the channel is made to appear circular by adding a cyclic prefix to the start of each data block. The cyclic prefix is a copy of the last ν samples of each block. I use the notation $x(n)$,

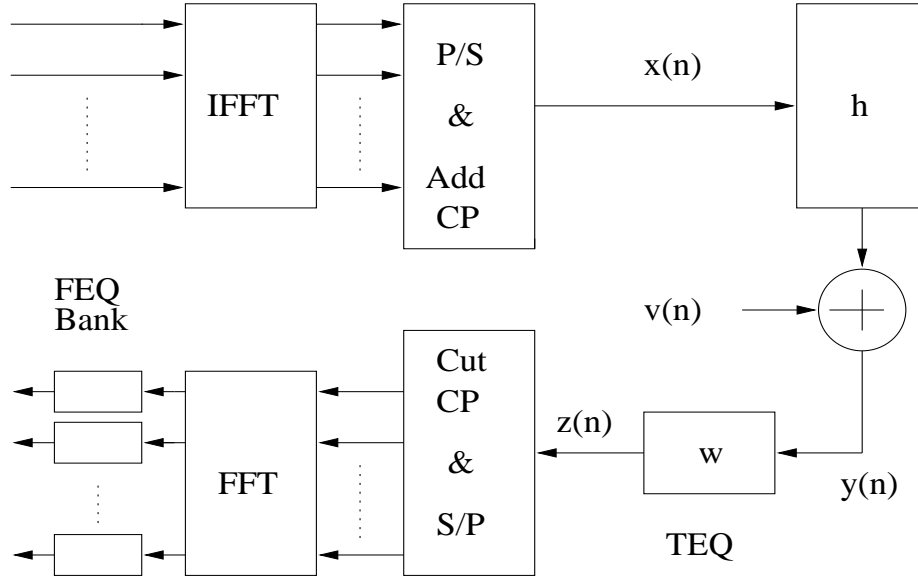


Figure 5.1: System model. (I)FFT: (inverse) fast Fourier transform, P/S: parallel to serial, S/P: serial to parallel.

$h(n)$, and $y(n) = \sum_{i=0}^{L_h-1} h(i) * x(n-i) + v(n)$ to denote the channel input, channel impulse response, and noise-added channel output, respectively, where L_h denotes the channel length.

If the CP is at least as long as the channel, then the CP-removed channel output is equivalent to a circular convolution of the channel impulse response and transmitted data. After the FFT converts the received data to the frequency domain, the signals can then be equalized by a bank of complex scalars, referred to as FEQs. If the channel is longer than $\nu + 1$ samples, then a TEQ is needed to shorten the channel. I have pointed out that a single-FIR TEQ is not optimum in terms of bit rate performance. I start from a TEQ filter bank structure to construct the bit rate maximizing structure.

At a DMT receiver with the TEQ filter bank (TEQFB) structure [27], the channel output goes through a bank of TEQs. The FFT block can be implemented

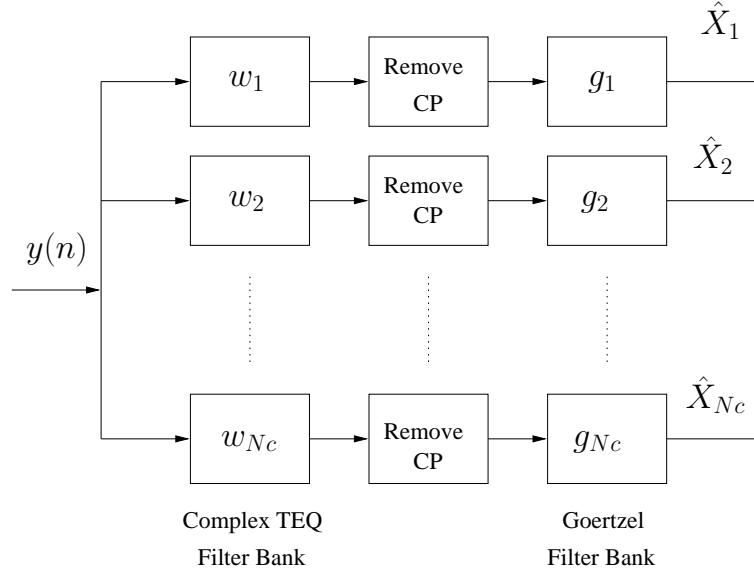


Figure 5.2: Proposed complex-tap time domain equalizer filter bank for multicarrier modulation with a cyclic prefix (CP).

as a bank of Goertzel filters with each one computing a single point DFT. There are $N_c = 256$ possible data carrying subchannels if FFT size N equals 512 as in an ADSL system.

Fig. 5.2 shows the proposed complex-tap time domain equalizer filter bank (CTEQFB) structure. Let t indicate the DMT symbol index, $n = 0, 1, \dots, N + \nu - 1$ indicate the samples within the given symbol, and Δ be transmission delay of the signal from the transmitter to receiver. The output of the i th TEQ is

$$z_{i,t}(n) = \sum_{\tau=0}^{L_w} \mathbf{w}_i(\tau) y_t(n - \tau) \quad (5.1)$$

where \mathbf{w}_i denotes the length $L_w + 1$ column vector of the the TEQ coefficients and $y_t(n) = y(n - \Delta)$ is the received sequence with delay reference. For each symbol, only N samples from $Z_t(\nu)$ to $Z_t(N + \nu - 1)$ are used for further processing. The other samples are discarded since they correspond to the heavily ISI-corrupted CP.

The i th TEQ operation in the receiver can be written as

$$\mathbf{z}_{i,t} = \begin{bmatrix} y_t(\nu) & y_t(\nu-1) & \dots & y_t(\nu-L_w) \\ y_t(\nu+1) & y_t(\nu) & \dots & y_t(\nu-L_w+1) \\ \vdots & \vdots & \ddots & \vdots \\ y_t(N+\nu-1) & \dots & \dots & y_t(N+\nu-1-L_w) \end{bmatrix} \times \begin{bmatrix} \mathbf{w}_i(0) \\ \mathbf{w}_i(1) \\ \vdots \\ \mathbf{w}_i(L_w) \end{bmatrix} = \mathbf{Y}_t \mathbf{w}_i \quad (5.2)$$

$$\quad (5.3)$$

where \mathbf{Y}_t is Toeplitz matrix which contains the received signal for detection of t th symbol. The output of i th Goertzel filter is

$$g_{t,i} = \begin{bmatrix} W_N^{i0} & W_N^{i1} & \dots & W_N^{i(N-1)} \end{bmatrix} z_{t,i} = \mathbf{q}_i^H \mathbf{Y}_t \mathbf{w}_i \quad (5.4)$$

where $W_N = e^{-j2\pi/N}$ is the DFT complex quantity and \mathbf{q}_i^H is the i th row of DFT matrix. The output of the i th one-tap FEQ (denoted as ϕ_i) is then

$$\hat{X}_{t,i} = \phi_i \times g_{t,i} = \phi_i \mathbf{q}_i^H \mathbf{Y}_t \mathbf{w}_i \quad (5.5)$$

I move all FEQ operations to the time domain and combine them with the TEQ to obtain a multi-tap complex valued FIR filter for each tone. Denote this filter for subchannel i as $\tilde{\mathbf{w}}_i$, the output of the i th Goertzel filter is

$$\hat{X}_{t,i} = \mathbf{q}_i^H \mathbf{Y}_t \tilde{\mathbf{w}}_i, \quad (5.6)$$

which is ready for decision making.

In terms of design freedom, I compare the existing four equalization structures. By inspecting (5.5), I conclude that the conventional TEQ-FEQ structure

has the least freedom. It uses only one TEQ \mathbf{w} for all subchannels. TEQFB lifts this restriction to have \mathbf{w}_i for each used subchannel, but it has a common frequency domain scalar ϕ_i for each tap of the TEQ. Per-tone equalizer moves the TEQ to the frequency domain and directly optimize on multi-tap FEQ. CTEQFB is moving the FEQ into the TEQ. Both of them could have a different scalar $\phi_{i,j}$ for the j th tap of the TEQ \mathbf{w}_i . Thus, the per-tone equalizer and CTEQFB have the most design freedom. The per-tone equalizer is trained in the DFT domain at the symbol rate (e.g. 4 kHz in ADSL). The CTEQFB is trained at the sampling rate (e.g. 2.208 MHz in ADSL). During data transmission, however, the implementation complexity of CTEQFB is much higher than that of a per-tone equalizer because the per-tone equalizer exploits the Toeplitz structure of $\mathbf{z}_{i,t}$. However, the per-tone equalizer with this efficient implementation relies on a single chosen delay parameter. I expect that the CTEQFB will reach a higher bit rate after delay optimization performed on each single logic path.

5.2.2 Design

In wireline MCM systems such as ADSL and VDSL, it is desirable that the optimization of each subsystem finally leads to bit rate maximization for a target bit error rate tolerance. The number of bits per symbol for the proposed CTEQFB is

$$b_{CTEQFB} = \sum_i \log_2 \left(1 + \frac{\text{SNR}(w_i)}{\Gamma} \right) \quad (5.7)$$

where Γ is the excessive SNR required to reach Shannon capacity. Various SNR models exist in current literature. Most of them reach an approximate modeling of noise. [25] only considers additional noise, [26] takes ISI into account, and [27] models noise as sum of ISI, additive white Gaussian noise (AWGN), near end Crosstalk (NEXT) and digital noise floor. The latter is very close to true configuration of impairments, but there are other possible noise sources such as radio frequency interference (RFI), clipping noise, FFT leakage and FEQ error left unattended.

To model noise as accurately as possible, I define the SNR at the i th Goertzel filter output as

$$\text{SNR}_i = \frac{E[|X_{t,i}|^2]}{E[|X_{t,i} - \hat{X}_{t,i}|^2]} \quad (5.8)$$

where E stands for expectation, and $X_{t,i}$ is the frequency domain input on the i th subchannel at t th symbol. In a wireline MCM system, the expected energy $E[|X_{t,i}|^2]$ is constant across all subchannels during training. Thus, I can write $E[|X_{t,i}|^2] = S_x$. A similar SNR definition can be found in [28]. With this definition, I implicitly include all possible noise sources up to the point before the slicer.

Maximizing the SNR in each single subchannel also maximizes the bit rate. It turns out the maximization of SNR_i is equivalent to the minimization of

$$\begin{aligned} J_i &= E[|X_{t,i} - \hat{X}_{t,i}|^2] \\ &= E[|X_{t,i} - \hat{X}_{t,i}| |X_{t,i} - \hat{X}_{t,i}|^*] \\ &= S_x - \tilde{\mathbf{w}}_i^H E[X_{t,i} \mathbf{Y}_t^H \mathbf{q}_i] - E[\mathbf{q}_i^H \mathbf{Y}_t X_{t,i}^*] \tilde{\mathbf{w}}_i \\ &\quad + \tilde{\mathbf{w}}_i^H E[\mathbf{Y}_t^H \mathbf{q}_i \mathbf{q}_i^H \mathbf{Y}_t] \tilde{\mathbf{w}}_i \end{aligned} \quad (5.9)$$

To minimize J_i with respect to $\tilde{\mathbf{w}}_i$, I set

$$\frac{\partial J_i}{\partial \tilde{\mathbf{w}}_i^*} = E[\mathbf{Y}_t^H \mathbf{q}_i \mathbf{q}_i^H \mathbf{Y}_t] \tilde{\mathbf{w}}_i - E[\mathbf{Y}_t^H \mathbf{q}_i X_{t,i}] = 0 \quad (5.10)$$

Only second-order input-output statistics are required to solve this linear estimation problem. In other words, this approach is not based on channel estimation. Also, blind equalization is feasible provided that we have pre-knowledge of input distributions. However, we have the luxury of training sequence offered in many wireline communications standards. A practical solution to train CTEQFB for a wireline multicarrier receiver is formed as follows:

1. Use training sequence to get time average estimations of all expectation items in (5.10).

1. For loaded subchannel i , estimate time average of $\mathbf{A}_i = (X_i^* \mathbf{q}_i^H \mathbf{Y}_t)^T$ and $\mathbf{B}_i = (\mathbf{q}_i^H \mathbf{Y}_t)^T (\mathbf{q}_i^H \mathbf{Y}_t)^*$ over a number of blocks
2. Start with non-zero initial guess \mathbf{w}_i^0
3. Choose step size μ_i satisfies $0 < \mu_i < \frac{1}{2 \times \text{trace}(\mathbf{B}_i)}$
4. Pre-compute $\Lambda_i = (I - \mu_i \mathbf{B}_i)$ and $\Phi_i = \mu_i \mathbf{A}_i$
5. For $k = 1, 2, \dots$, $\mathbf{w}_i^{k+1} = \Lambda_i \mathbf{w}_i^k + \Phi_i$
6. When iteration stops, $\mathbf{w}_i = \mathbf{w}_i^*$

Figure 5.3: Proposed iterative CTEQFB design method.

2. Solve the linear equation in (5.10). The \mathbf{Y}_t terms are observed to be linear independent between symbols. Time average of $\mathbf{Y}_t^H \mathbf{q}_i \mathbf{q}_i^H \mathbf{Y}_t$ is always full rank. Thus, a unique solution

$$\tilde{\mathbf{w}}_i = \hat{E}[\mathbf{Y}_t^H \mathbf{q}_i \mathbf{q}_i^H \mathbf{Y}_t]^{-1} \hat{E}[\mathbf{Y}_t^H \mathbf{q}_i X_{t,i}] \quad (5.11)$$

can be obtained.

An iterative solution is provided in Fig. 5.3 based on a complex-valued steepest decent searching method.

Usually one needs to perform delay optimization to obtain the highest achievable bit rate out of possible transmission delays. In the conventional TEQ-FEQ structure, optimization ends up at one optimum Δ for all frequency components of the signal. To see the true capability of the CTEQFB structure, I can actually introduce distinct optimum transmission delay Δ_i on path i for signals on subchannel i . A better bit rate performance is expected under this frequency selective delay optimization. Simulation results are given in Chapter 6.

5.3 Dual Path Equalizer: A Practical Implementation

In previous section, a CTEQFB structure is constructed with the aim of maximizing the bit rate performance. To do a better comparison with conventional TEQ-FEQ structure, I compare not only the sum of bits allocated to the channel but the distribution of allocated bits as well.

Fig. 5.4 shows sample bit allocation schemes for an ADSL system over ANSI loop 13 with NEXT from 24 DSL disturbers. The loop transfer function and crosstalk transfer function can be obtained by using data provided in [8]. The receiver calculates the bit allocation table when TEQ is trained by MMSE, Min-ISI, MSSNR, and MBR, respectively. It also calculates the bit allocation table when a CTEQFB scheme is applied. Since no single tone delay optimization is performed, CTEQFB and per tone equalizer have equivalent bit rate performance in this case.

Based on simulations, I make the following observations on the performance of CTEQFB equalization vs. that of single TEQ structures:

1. CTEQFB equalization not only achieves higher aggregate bit rates, but also benchmarks Achievable Bit Rate (ABR) for any single tone.
2. The performance gap tends to be larger in favor of CTEQFB equalization as the transmission environment becomes more sophisticated.
3. The performance gap for any single tone is not universally wide. In tones associated with higher SNR, the improvement of CTEQFB tends to be significant. For other tones, the improvement is not significant.

Based on the above observations, especially observation 3, I conclude that it is not necessary to use a separate TEQ for each single tone. Alternately, I propose to use a second TEQ whose goal is to optimize those subchannels with the best chance of improving the bit rate. These subchannels with the potential for the best SNR are generally known before equalizer training. For example, they can be

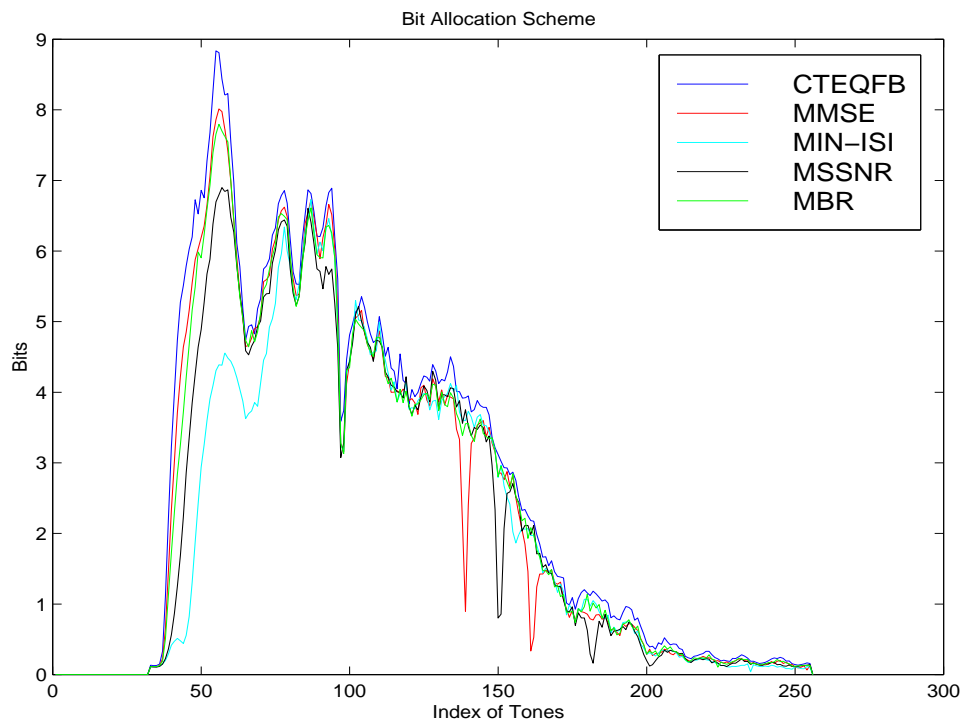


Figure 5.4: Sample bit allocation schemes for ANSI loop 13 with NEXT.

estimated from a periodic sequence, which thus needs no TEQ and occurs earlier in the training stage.

Another motivation to design a second TEQ is reported in [54]. It has been observed that most single TEQ designs produce an equalizer with poor frequency domain behavior for frequency division multiplexing (FDM) transmission, for which a TEQ usually produces deep nulls in the transition band. ISI power is boosted in this region. In this case, a transition band TEQ developed under a spectral flatness constraint is put on the second path.

5.3.1 Model

A dual-path TEQ structure for the DMT receiver passes the received data through two paths instead of one path. One possible approach is to give each path its own TEQ, FFT and one-tap FEQs. The FEQ outputs would be fed into a path selection block, namely, a switch. For each tone, I choose output from one of the two paths according to a preset rule. The rule should be set during initialization stage. A possible criterion could be to choose the path with a higher subchannel SNR after FEQ for each tone. In other words, the FEQ output for each tone i could be

$$\tilde{x}_i = \begin{cases} \tilde{x}_{i1} & \text{if } \text{SNR}_{i1} > \text{SNR}_{i2} \\ \tilde{x}_{i2} & \text{otherwise} \end{cases} \quad (5.12)$$

In Fig. 5.5, I simplify this dual-path TEQ structure to move the path selector before the one-tap FEQ. This modification works well provided that a well-defined metric after the FFT was available. In this case, only one set of FEQs are implemented in the receiver.

One choice is that each TEQ optimizes a different part of the bandwidth and the subchannels of interest span the entire bandwidth. However, such a partition is difficult to optimize. I choose a slightly different approach as follows:

1. Path 1 is a path with normal TEQ, which optimizes the entire bandwidth.

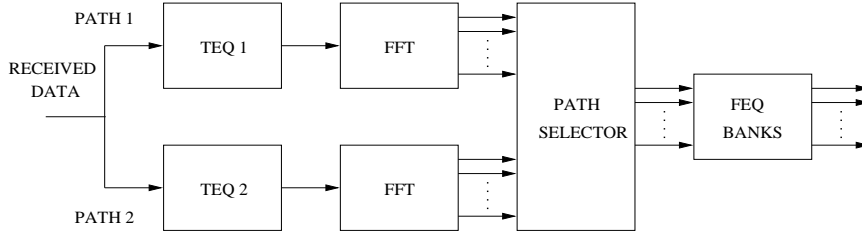


Figure 5.5: Structure of a dual-path TEQ.

2. Path 2 exploits a second TEQ, which optimizes the subchannels within a preset window of frequencies.

The subchannels with higher SNR as seen in Fig. 5.4 generally have more room for bit rate improvement via per tone equalization. Accordingly, these subchannels should be put into the window. A simple subchannel selection method is to slide a window through all subchannels, and the desired start tone index i can be determined by

$$i_{\text{start}} = \arg \max_i \sum_{k=i}^{k=i+WL-1} S_{x,i} |H_i|^2 / S_{n,i} \quad (5.13)$$

where WL is the window length, and $S_{x,i}$, $S_{n,i}$ and H_i are the transmitted signal power, channel noise power, and frequency response for the i th tone, respectively.

5.3.2 Design

Any existing algorithm can be used for training the first TEQ. However, only TEQ design methods that have some control over the TEQ frequency response are good candidates for designing the second TEQ. In fact, all methods fall into the products of quotients cases are potential choices. However, these methods need complicated search routines to reach local optimum, which may not be amenable to a fixed point implementation. Given the consideration of a real-time implementation, I single out Min-ISI as the method for the second path. Min-ISI ends up at a TEQ has minimum

sum of weighted ISI on the set of chosen subchannels on the second path.

Another possibility is to use a suboptimum approach. First, I choose a typical subchannel out of the chosen set for second path and design a TEQ for this subchannel using either pertone or TEQFB approach. Second, I use this TEQ as the TEQ for the second path. It obviously is not an optimal solution for the second path. But if I carefully choose the subset and also the typical subchannel, it may have fairly good performance. To achieve this goal, I might keep the size of the subset small and choose the middle subchannel in the subset for optimization.

5.4 Conclusion

A complex valued TEQ filter bank has been constructed to evaluate the upper bound achievable bit rate of a DMT based transceiver. By carefully inspecting the distribution of bit rate improvement over the subchannels, I propose to use a dual-path TEQ. The dual-path TEQ gives in a higher achievable bit rate than a single-path TEQ, if an appropriate design technique is available, but keeps the training complexity down. The second TEQ used for equalization of selected subchannels can be designed in the time domain with some frequency control, or more naturally, the frequency domain. Min-ISI seems to be a design choice of the second TEQ with a good compromise between performance and complexity.

Chapter 6

Performance Evaluation

6.1 Introduction

Performance measure is necessary to justify the goodness of a new design. This chapter presents details of performance measurement to evaluate various structures, design methods and complexity-reduced implementations that have been proposed in this dissertation. It also compares the performance of proposed ones with other existing designs. To ensure fairness, achievable bit rate (ABR) has been chosen as a common performance metric. Downstream transmission, which means from central office to customer end, of an ADSL G.DMT system has been setup as a common test environment. Section 6.2 describes physical channel characteristics of an ADSL loop. Section 6.3 reviews major impairments encountered in a typical ADSL transmission. Section 6.4 and 6.5 report bit rate performance of simulations over synthesized channels and real channels, respectively.

6.2 Physical Channel Characteristics

For a typical ADSL transmission, three information channels coexist over telephone lines. The high speed unidirectional downstream channel is composed of up to

four subchannels based on 1.536 Mbps or three subchannels of 2.048 Mbps. As a result, downstream information rate ranges from 1.536 Mbps to 6.144 Mbps. The moderate rate bi-directional channel can be viewed as combinations of several duplex subchannels including one mandatory control (C) channel over which the user-to-network control signals are transmitted. The C channel operates at 16 kbps or 64 kbps, and the maximum aggregate rate of the bi-directional channel is 640 kbps.

The separation of downstream and upstream channels is achieved by either frequency division multiplexing (FDM) or echo cancelation. In the FDM approach, the upstream channel occupies the lower frequencies whereas the downstream channel spans a wider high frequency band. The second approach is to allow the downstream channel to overlap with the upstream channel in frequency domain. It provides more bandwidth to downstream. However, local echo cancelation is mandatory to cancel the interference between the two channels. In this dissertation, I only consider the FDM approach, which is dominant in practical mid-range ADSL connections due to the ease of implementation.

The physical media of the ADSL channels is a metallic twisted pair of wires. In practice, it is normal to encounter nonuniform transmission lines. Namely, several segments of wire each of different gauge are connected together to form a subscriber loop. The common gauges are 0.32 mm, 0.4 mm (US gauge 26), 0.5 mm (US gauge 24), and 0.63 mm. Twisted pairs of wires are usually bundled together in large cables. A typical configuration towards a customer is fifty pairs with larger gauge in one cable. In contrast, a configuration for central office often contains a much larger number of pairs with smaller gauge. These gauge channels introduce a slight discontinuity in impedance. A more serious problem in subscriber line is the presence of *bridged taps*, open circuited wire pairs bridged onto the main cable pair. Bridged taps are intended to offer flexibility for future alterations in transmission lines, trading for the significant reflection of signals.

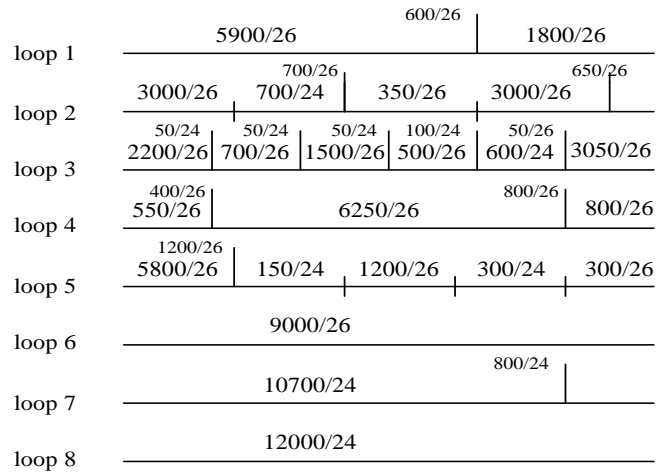


Figure 6.1: Test loops under study within the CSA.

The maximum loop length supported by ADSL is 18,000 feet. However, 85% of the currently installed copper loops are within a so-called carrier serving area (CSA) that extends no longer than 12,000 feet. For instance, Fig. 6.1 shows a set of CSA test loops proposed by Bellcore for HDSL and ADSL system evaluation purposes [15].

I obtain impulse responses of these test loops by using *LINEMOD* program maintained by Prof. J. M. Cioffi's group at Stanford University [87].

Shaped by a fifth order high pass IIR filter with passband frequency at 138 kHz to separate the downstream data from the upstream data, magnitude responses of the eight test loops are plotted in Fig. 6.2 and Fig. 6.3. It is shown that subscriber lines experience severe magnitude distortion over the band of interest, which ranges from 138 kHz to 1.1 MHz. In particular, significant attenuation is observed at higher frequencies. Bridge taps create spectrum nulls that lower the capacity of the channel.

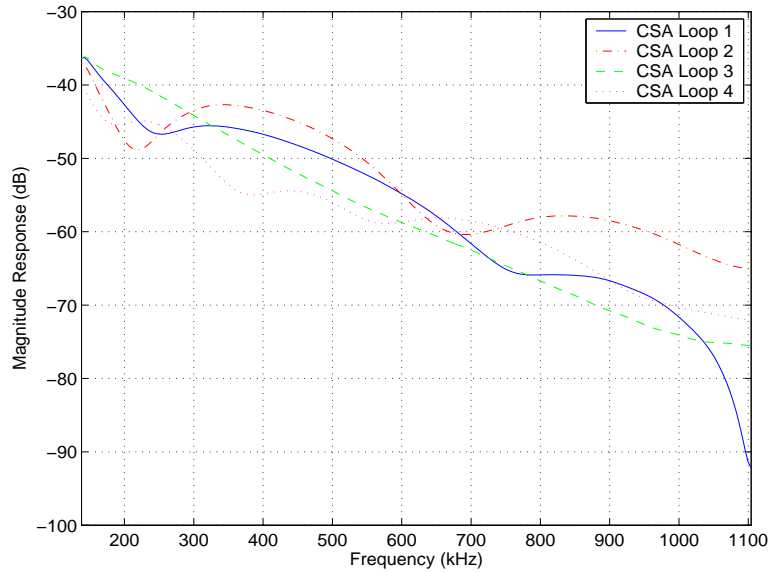


Figure 6.2: Magnitude responses of CSA loops 1,2,3, and 4 over the ADSL transmission bandwidth. A 5th order high pass IIR filter is cascaded to separate the upstream and downstream transmissions in FDM-ADSL

6.3 Noise Environment

In addition to the impairments caused by network itself, such as channel attenuation, micro-interruptions, and corrosion resistances [88], an ADSL system has to deal with a variety of electrical noise. In this section I provide a brief review of ADSL noise sources.

6.3.1 Crosstalk noise

In United States fifty unshielded twisted pairs are typically installed in a single cable. It is thus expected that various copper access transmission systems such as DSL, HDSL, ADSL, and even T1 share a multi-pair cable. One of the major concerns with such systems is crosstalk interference generated by various systems within the

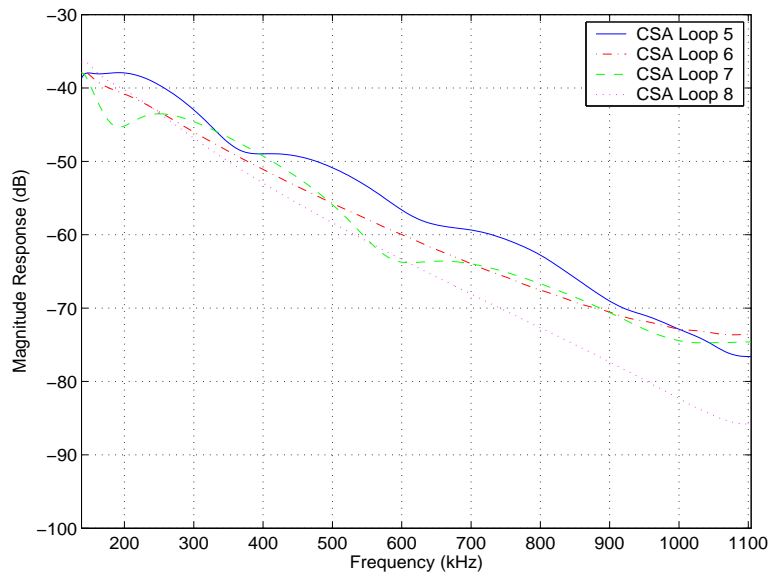


Figure 6.3: Magnitude responses of CSA loops 5,6,7, and 8 over the ADSL transmission bandwidth. A 5th order high pass IIR filter is cascaded to separate the upstream and downstream transmissions in FDM-ADSL

cable.

To model crosstalk noise, we must take issues listed below into account:

- A particular disturbed system
- A particular disturbing signal
- The number of disturbing wire pairs
- A crosstalk transfer function

There are two basic types of crosstalk: near end crosstalk (NEXT) and far end crosstalk (FEXT). Fig. 6.4 illustrates the two mechanisms.

NEXT is defined as a crosstalk interference between a local transmitter and a local receiver, i.e., transmit and receive pairs at one end of a telephone cable.

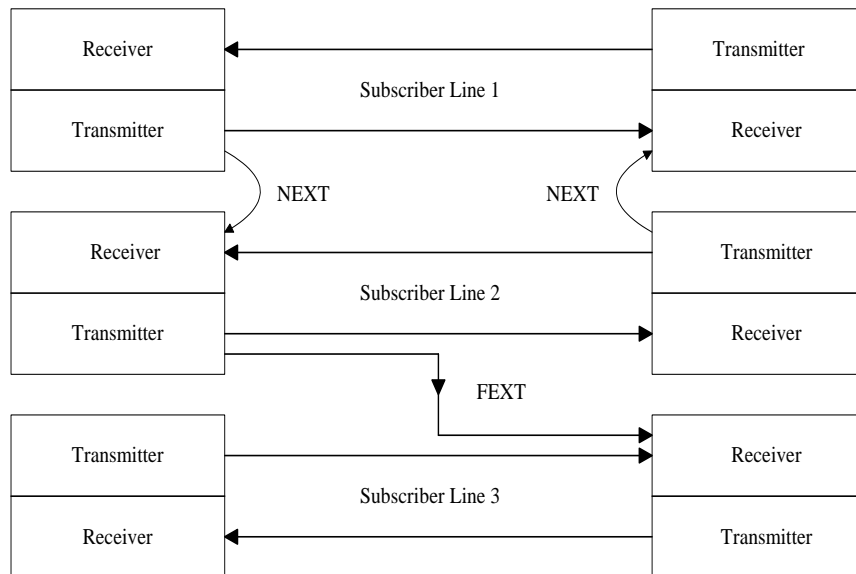


Figure 6.4: Illustration of NEXT and FEXT

NEXT generated by signals from the same service is called self NEXT, which is quite common in bi-directional systems such as T1, ISDN, and HDSL. It introduces serious interference between downstream and upstream data in such duplex systems. In ADSL systems, the upstream ADSL signal normally occupies the band from 25 to 138 kHz. As a result, the effect of ADSL-induced NEXT from other pairs within the same binder group is severe only in the limited range near the DC end. To obtain power spectral density (PSD) of induced self NEXT, one can use PSD of the disturbers as the input to a NEXT filter that has a transfer function suggested in standards. The NEXT from other services including HDSL and ISDN in the same bundle or T1 line in an adjacent binder group can be analyzed in a similar way.

FEXT is defined as a crosstalk from a local transmitter into a remote receiver. Unlike the NEXT, the channel attenuation should be included in the FEXT loss transfer function. Normally NEXT dominates FEXT because FEXT comes from

the other end of the channel and hence has lower power.

6.3.2 Other impairments

Impulsive noise

Impulsive noise is almost unpredictable and much less understood. Some research shows that high-power switching activity, lightning and impulses from other electrical machinery may be several kinds of sources. Concatenated coding and interleaving technique has been adopted by the ADSL standard [8] as a type of precaution to combat the impulsive noise. I do not include impulsive noise in my noise modelling.

Radio Frequency Interference

ADSL spans bandwidth from DC to 1.1 MHz. The radio frequency interference (RFI) within this band is typically narrow band interferences from amplitude modulated (AM) media wave broadcast signals, which in the US occupy 550 kHz - 1700 kHz. Signals from AM broadcasting stations couple into DSL lines through both aerial and buried telephone lines, and the coupling is accentuated by poor balance of the cable and unterminated lines [89].

Background noise

According to a recent Bellcore study, the background noise such as quantization noise from the A/D converter and the thermal noise in the analog portion of receiver in the band of interest can be modeled as additive white Gaussian noise (AWGN) with a conservative estimated level at -140 dBm/Hz.

In total, the ADSL system should combat a variety of crosstalk noise sources including NEXT from ISDN, HDSL, ADSL and T1, RFI, and AWGN background

noise. In the following simulations, I choose different combinations of these noise sources.

6.4 Achievable Bit Rates On Synthesized Loops

First I consider a first generation ADSL downstream transmission over CSA loops. In ITU ADSL standard specifications, the IFFT and FFT lengths are 512 and the cyclic prefix length is 32. I choose the channels to be the eight typical carrier service area (CSA) loops recommended by Bell Labs [82]. Full ADSL data transmission bandwidth is from 25 kHz to 1.104 MHz. A common practice in industry is to use frequency division multiplexing to allocate bi-directional transmission to different frequency bands. I adopt this approach and introduce a 5th order high pass IIR filter with passband frequency at 138 kHz to separate the downstream data from the upstream data. The signal power spectral density at the transmitter output is set equal to -40 dBm/Hz. Channel noise is modeled as an additive white Gaussian noise (AWGN) with -140 dBm/Hz power density, plus NEXT noise from 5 integrated services digital network (ISDN) disturbers.

Number of bits assigned to i th subchannel is then determined by

$$b_i = \log_2 \left(1 + \frac{\text{SNR}_i}{\Gamma} \right) \quad (6.1)$$

where Γ is SNR gap for achieving Shannon channel capacity and is constant over all subchannels given the same target bit error rate for all subchannels. Bit rate of the system is calculated as

$$R = f_b * \sum_{i \in \mathcal{S}} b_i \quad (6.2)$$

where f_b is symbol rate and \mathcal{S} is the set of all used subchannels.

In simulations SNR_i is derived from average QAM error energy over 1000

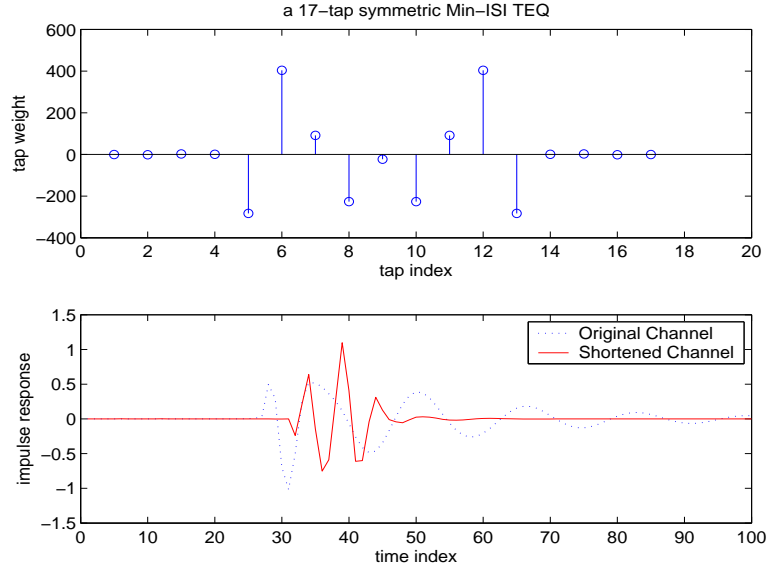


Figure 6.5: Channel shortened by a length-17 symmetric TEQ

symbols at the i th subcarrier

$$\text{SNR}_i = 10 \log_{10} \left(\frac{1000 S_x}{\sum_{t=1}^{1000} |X_{t,i} - \hat{X}_{t,i}|^2} \right) \quad (6.3)$$

The SNR gap to Shannon capacity is chosen as

$$\Gamma_{sim} \quad (\text{in dB}) = \Gamma_{gap} + \text{system margin} - \text{coding gain} \quad (6.4)$$

where $\Gamma_{gap} = 9.8$ dB for an uncoded QAM system with a target 10^{-7} bit error rate, system margin is 6 dB, and coding gain is assumed to be 5 dB.

With all these parameters set, symmetric designs are simulated and compared to performance with unconstrained cases. A sample symmetric TEQ design is presented in Fig. 6.5. The original channel and the channel shortened by this 17 tap symmetric Min-ISI are also plotted in the same figure.

Figures 6.6, 6.7 and 6.8 compare the achievable bit rate versus TEQ length between a optimum TEQ and a corresponding linear phase constrained TEQ under

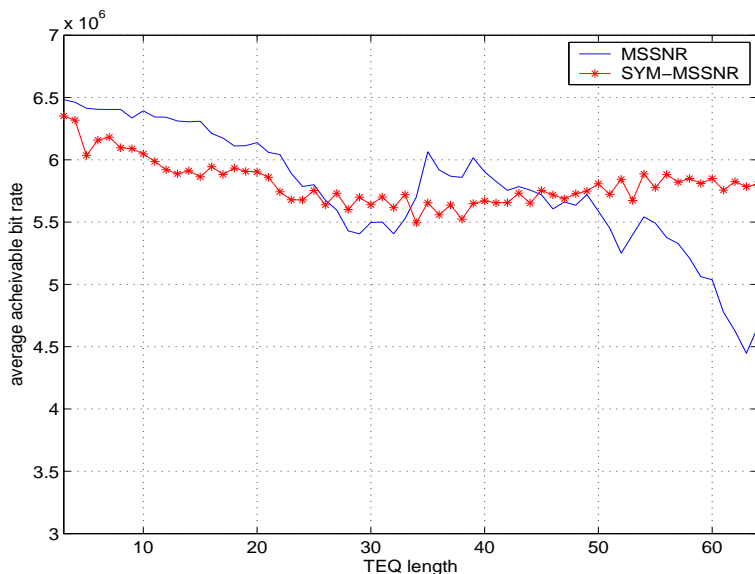


Figure 6.6: Average achievable bit rate vs. TEQ length for 8 CSA loops. Coding gain is 5 dB, margin is 6 dB, input power is -40 dBm/Hz, AWGN power -140 dBm/Hz, NEXT noise is from 5 ISDN disturbers. Equalizer is trained by the MSSNR and SYM-MSSNR.

MSSNR, Min-ISI and MMSE criteria, respectively. TEQ length varies from 3 taps to 64 taps. The channels were the eight standard CSA test loops [26]. The average performance loss for the proposed symmetric algorithm is 1% for Min-ISI, 4% for MMSE, and -1% (1% improvement actually) for MSSNR. I notice the bit rates of original MSSNR and original Min-ISI drastically decrease when TEQ length is longer than 50. This loss is partially due to the magnitude nulls effect caused by longer TEQ, which has been discussed in Chapter 3. But another important factor contributing to this performance degradation is the inaccurate eigen-decomposition for large dimensional matrix even in floating point simulations. Condition number becomes larger as the matrix size increases. Symmetric designs appear to be more robust since they operate on matrices with only half of the dimensions. The MMSE

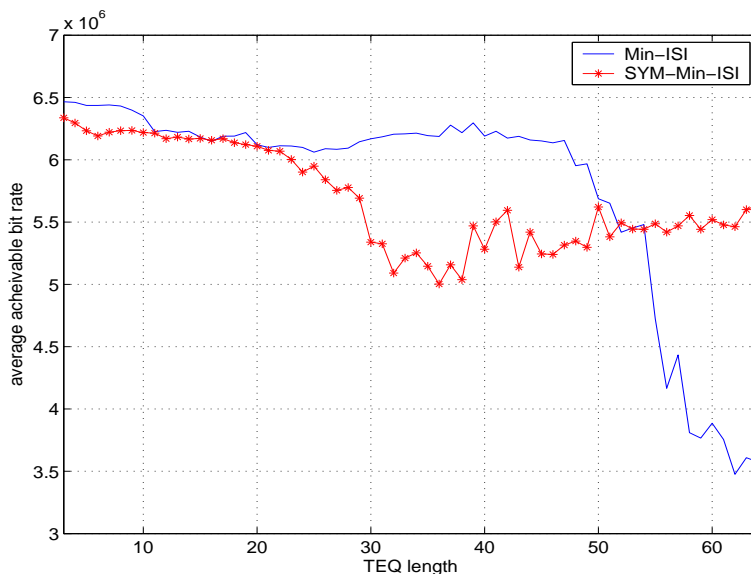


Figure 6.7: Average achievable bit rate vs. TEQ length for 8 CSA loops. Coding gain is 5 dB, margin is 6 dB, input power is -40 dBm/Hz, AWGN power -140 dBm/Hz, NEXT noise is from 5 ISDN disturbers. Equalizer is trained by the Min-ISI and SYM-Min-ISI.

performance is relatively flat because the fixed length TIR is used in the symmetric training instead of a TEQ. Hence, eigen-decomposition is applied to a fixed-size matrix. The bit rates of three optimum methods and their symmetric counterparts for a typical 17-tap TEQ over 8 CSA loops are summarized in Fig. 6.9. In total, symmetric designs achieve very close performance to unconstrained designs. For TEQs with longer length, symmetric designs tend to outperform unconstrained designs of MSSNR and Min-ISI. A similar observation can be made from simulation results in [81] for linear phase equalizers of VDSL channel models.

Fig. 6.10 shows the average bit rate performance of three methods from Min-ISI family for 8 CSA loops vs. TEQ length. Channel noise is modeled as near-end-cross-talk (NEXT) from 24 high speed DSL (HDSL) disturbers plus additive

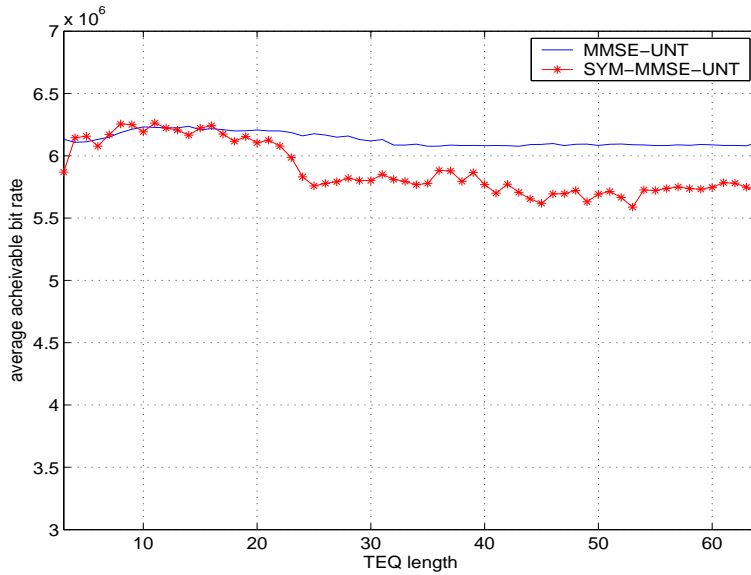


Figure 6.8: Average achievable bit rate vs. TEQ length for 8 CSA loops. Coding gain is 5 dB, margin is 6 dB, input power is -40 dBm/Hz, AWGN power -140 dBm/Hz, NEXT noise is from 5 ISDN disturbers. Equalizer is trained by the MMSE with a unconstraint TIR and MMSE with a symmetric TIR.

white Gaussian noise (AWGN) with -140 dBm/Hz power density. In this case, crosstalk power is far stronger than that of a 5-ISDN disturber case. I compare the non-iterative Min-ISI method and the proposed iterative Min-ISI method with non-quantized SNR weighting as well as on-off weighting. For the iterative methods, the initial guess is $\mathbf{w}_0 = [\mathbf{1} \ \mathbf{0}_{(L_w-1) \times 1}]^T$, the step size is set to 10^{-7} , and the number of iterations is 30. The results suggest that the iterative Min-ISI method with SNR weighting eventually achieves the same bit rates as the eigen-filter Min-ISI method. There is no noticeable difference in the achievable bit rate between iterative implementation with on-off weighting and original weighting. Bit allocation of matched filter bound (MFB) is also provided as an external reference to evaluate

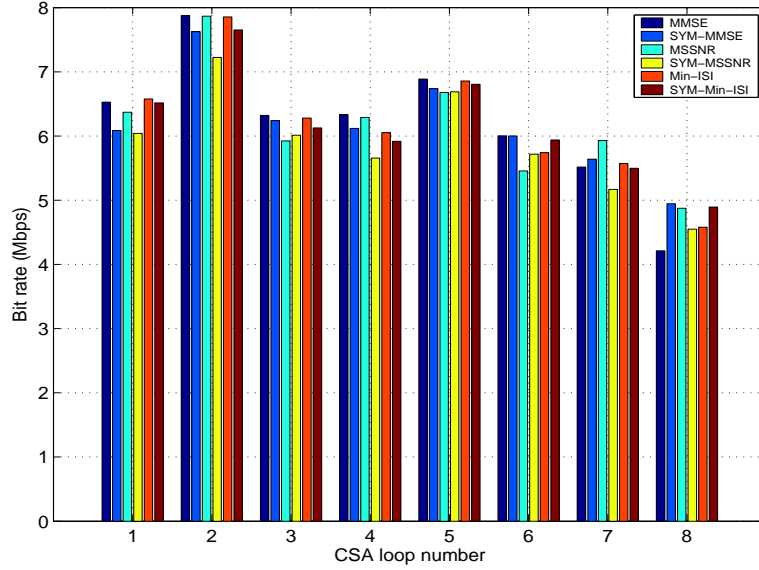


Figure 6.9: Achievable bit rates for 8 CSA loops with length 17 equalizers. Coding gain is 5 dB, margin is 6 dB, input power is -40 dBm/Hz, AWGN power -140 dBm/Hz, NEXT noise is from 5 ISDN disturbers, Equalizer is trained by MMSE, SYM-MMSE, MSSNR, SYM-MSSNR, Min-ISI and SYM-Min-ISI[5].

the performance. In this case, number of bits assigned to subchannel i is

$$b_i = \log_2 \left(1 + \frac{S_{x,i}|H_i|^2}{S_{n,i}\Gamma} \right) \quad (6.5)$$

where $S_{x,i}$ and $n_{,i}$ are the transmitted signal and noise power, respectively H_i is the gain of channel spectrum in the i^{th} subchannel. It appears that average performance loss to MFB bound for Min-ISI, iterative Min-ISI and iterative method with on-off weighting are 5%, 5%, and 7%, respectively.

To show CTEQFB is an achievable performance upper bound, Fig. 6.11 presents a summary of the results that we obtained for various equalizer designs [40]. Min-ISI is chosen to optimize a conventional TEQ-FEQ structure, which is explained in detail in [26]. Least squares design (LS-PTE) is chosen for the per tone structure [34]. Bit rate maximizing TEQFB algorithm presented in [27] is used

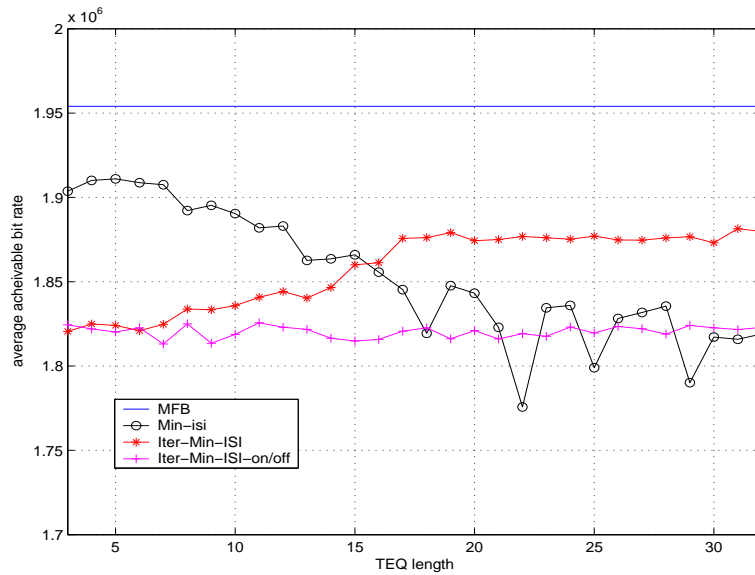


Figure 6.10: Average achievable bit rate vs. TEQ length for 8 CSA loops. Coding gain is 5 dB, margin is 6 dB, input power is -40 dBm/Hz, AWGN power -140 dBm/Hz, NEXT noise is from 24 HDSL disturbers. Equalizer is trained by the Min-ISI and Iterative Min-ISI, with SNR weighting and on-off weighting.

for TEQ filter bank structure. MMSE criteria is used for CTEQFB. The results of CTEQFB with and without delay optimization are both presented. Conventional TEQ-FEQ structure has much lower bit rate in this test setup that contains severe channel distortion and multiple impairments. Especially RFI noise creates deep notches in transmission band. BRM-TEQFB performance is somewhat lower than per-tone and CTEQFB due to its incomplete noise modelling. RFI, which is not included in TEQFB's SNR modelling, killed about 10% bit rate when compared to LS-PTE or CTEQFB. LS-PTE and CTEQFB have equivalent performance. But if delay optimization is performed, CTEQFB has 2% performance improvement, which benchmarks the bit rate performance.

Fig. 6.12 shows the resulting bit allocation for a dual-path TEQ ADSL system

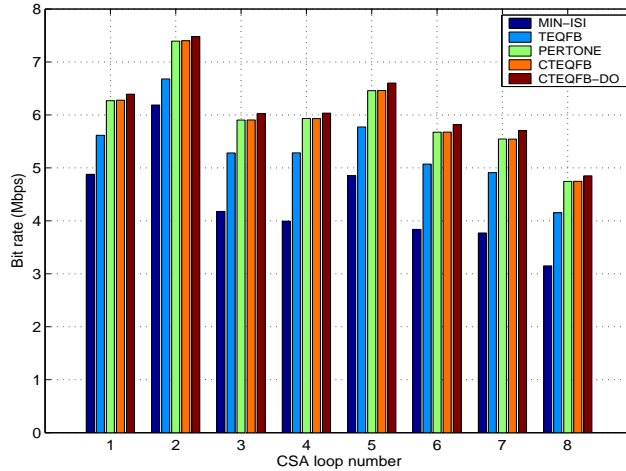


Figure 6.11: Achievable bit rates for 8 CSA loops with length 17 equalizers. Coding gain is 5 dB, margin is 6 dB, input power is -40 dBm/Hz, AWGN power -140 dBm/Hz, NEXT noise is from 5 ISDN disturbers, RFI noise from 7 AM radio frequencies. Equalizer is trained by Min-ISI , bit rate maximizing TEQFB , least squares per-tone and the proposed method.

over ANSI loop 13 with NEXT from 24 DSL disturbers. Both TEQs are trained by the MBR method. It exploits the partially occupied bandwidth optimization capability of the MBR method. The final bit allocation scheme would be the outer envelop of the two overlapped curves. While the first TEQ is an optimum solution for all used tones, the second TEQ optimizes tones 55–85 only. Fig. 6.12 shows that for some tones with higher SNR, especially those with peaks, the second TEQ performs better. For other tones, the second TEQ has a deep notch. The dual-path TEQ increased the ABR by 4% from 2.508 Mbps to 2.602 Mbps.

More simulations for dual-path TEQ are done in CSA loops. Fig. 6.13 compares performance of optimum single equalizers versus performance of a dual TEQ structure. The optimum TEQ designs under consideration are MMSE, MSSNR, Min-ISI and MDS. Min-ISI is chosen for the second path because it is the only one that can be tuned to a subset of used subchannels. The first path is trained by the

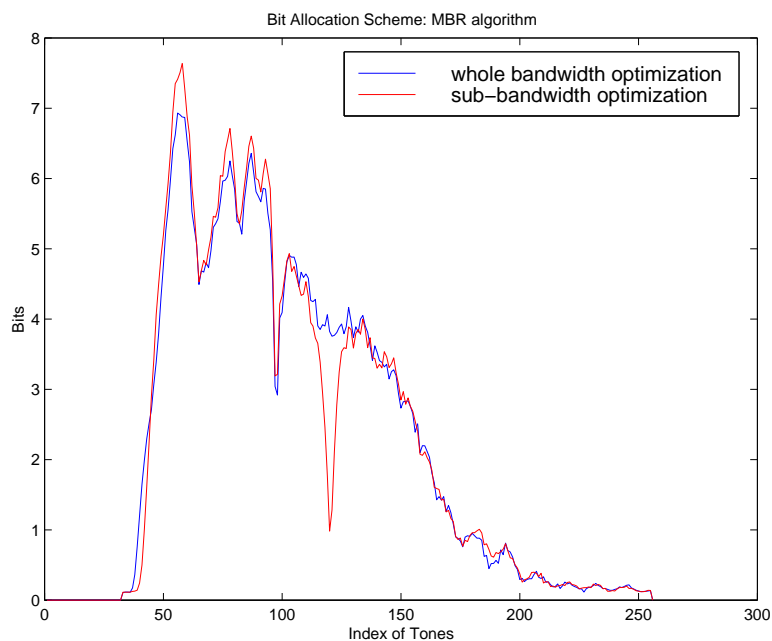


Figure 6.12: Bit allocation scheme for a dual-path TEQ.

method which has the highest ABR for a given loop. Data rate improvements of dual-TEQ vary from 2% to 10%.

6.5 Achievable Bit Rates on Measured Real Channels

Applied Signal Technology has generously provided the author with several measured ADSL data signals. The voltage signal from a telephone line was recorded, sampled at 2.5 MHz, and digitized. The signal was frequency-duplexed so that the upstream and downstream channels lay in two distinct frequency bands [65].

The data has been resampled to exactly 2.208 MHz. The C-REVERB2 training sequence is used to perform a (downstream) channel estimate. The estimated

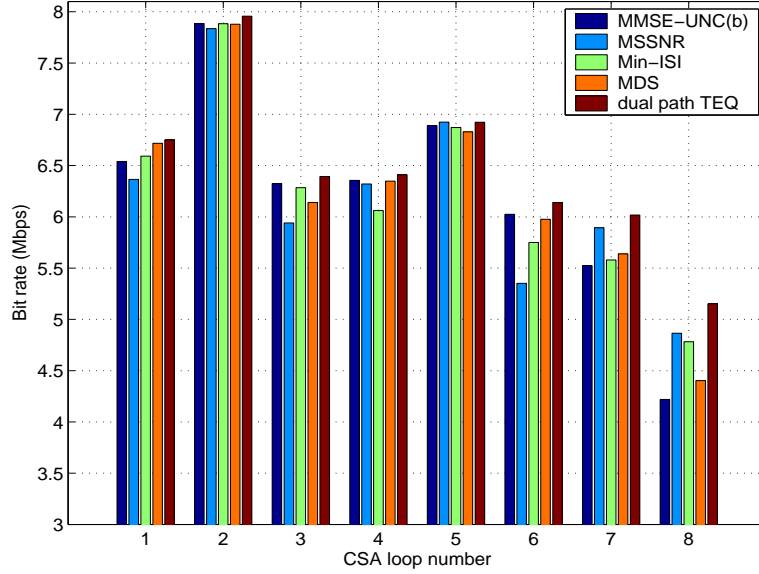


Figure 6.13: Achievable bit rates of a dual-path TEQ for CSA loops.

channel is given by

$$\hat{\mathbf{h}} = \mathcal{F}_N^{-1} \left(\frac{1}{1000} \sum_{k=1}^{1000} \frac{\mathcal{F}_N \mathbf{x}^k}{\mathcal{F}_N \mathbf{y}^k} \right), \quad (6.6)$$

where vector division is performed pointwise. Here, \mathcal{F}_N is the DFT matrix, \mathbf{x}^k is the k^{th} period of the chosen C-REVERB2 signal, and \mathbf{y}^k is the corresponding received signal over the same period. The C-REVERB2 signal is generated according to the definition in [8, Sec. 10.4.5]. Details of the estimation process and the impulse responses of the estimated channels for two sets of recorded data can be found in Appendix A.

Fig. 6.15 shows the achievable bit rate for the 16 TEQ designs available in literature, except now they have been used to equalize the two AST channels with magnitude responses shown in Fig. 6.14.

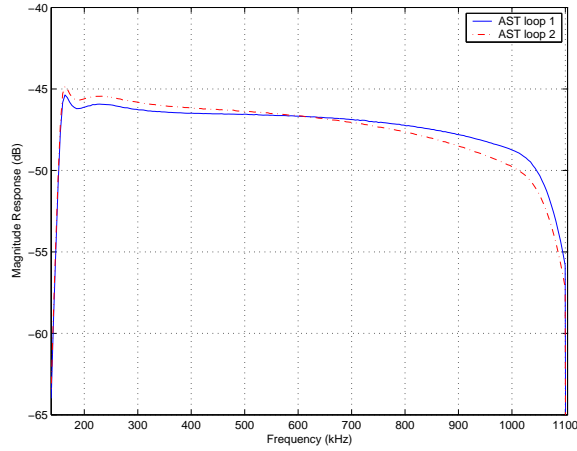


Figure 6.14: Magnitude responses of the two AST channels

6.6 Conclusion

Through extensive computer simulations, bit rate performance of a downstream ADSL receiver with various channel equalizers has been presented in this chapter. The simulation results confirmed that CTEQFB structure provides an upper bound on achievable bit rate among all existing linear equalizer structures.. Iterative Min-ISI method with quantized weighting eventually achieves the bit rate performance of original Min-ISI design with much lower complexity. It is also better suited for a fixed point implementation than the original design since it avoids Cholesky Decomposition completely, hence less sensitive to quantization errors. The bit rate performance of suboptimum linear phase designs under MMSE, MSSNR and Min-ISI criteria has been evaluated to show that bit rate loss between symmetric designs and optimum designs is negligible. Symmetric TEQs have better numerical stability when TEQ length is longer than 50. Simulation results also show that the best tradeoff between performance and complexity comes from a dual-path TEQ design.

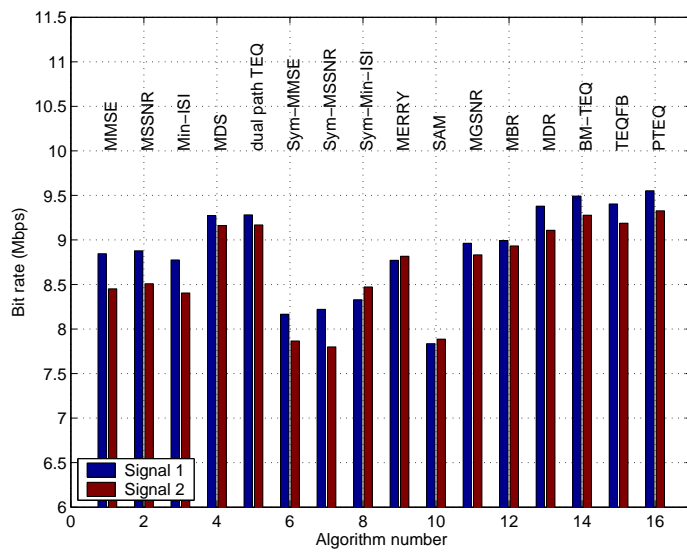


Figure 6.15: Bit rate achieved using the two measured AST channels. The channel magnitude responses are given in Fig. 6.14.

Chapter 7

Conclusions

7.1 Summary

Slowly time-varying DMT channels make it possible to perform dynamic bit loading to maximize bit rate for a target bit error rate. The bit rate optimization of each subsystem in a DMT transceiver should serve as the ultimate design goal. The equalizer should not be an exception. However, it is always necessary to find a compromise between bit rate performance and implementation complexity from a system engineering perspective due to limited memory and computational power in practical implementations. In a conventional DMT receiver with a single TEQ, the bit rate has been directly represented as a log-sum of Rayleigh quotients that are functions of TEQ taps. Bit rate maximization can be achieved by directly optimizing this log-sum function. However, direct optimization turns out to be highly non-linear and memory intensive and has neither closed-form solutions nor guaranteed globally optimal solutions. The TEQ designs resulting in a mathematically tractable problem via generalized eigen-decomposition are of interest in industry. Although these designs do not truly maximize the bit rate, some of them make reasonable approximations of achievable bit rates and achieve high bit rates in the field.

In the first part of my dissertation, I address complexity reduction issues for several suboptimum but practical TEQ design methods. Because the TEQ design methods under consideration do not directly optimize the bit rate, complexity reduction does not necessarily result in bit rate loss. Achieving higher bit rates with lower complexity is possible in the complexity-reduced designs. In the second half of my dissertation, I explore possibilities to surpass the bit rate performance upper bound set by directly optimizing a log-sum bit rate function. An achievable upper bound in a multi-TEQ receiver is found and a practical implementation in the form of a dual-TEQ structure is proposed, which provides a good tradeoff between achievable bit rate and implementation complexity.

In Chapter 3, I describe magnitude and phase responses of infinite length MMSE and MSSNR TEQs. I show that in the limit, the target impulse response of a MMSE TEQ becomes symmetric with all of its zeros on the unit circle. Similarly, an infinite length MSSNR TEQ will have symmetric taps and ν dominant zeros on the unit circle. In the case of finite length TEQs, the average distance of zeros of a TIR for MMSE to unit circle becomes smaller as the length of a TEQ becomes longer. The locations of zeros of a MSSNR TEQ move closer to the unit circle in the same fashion. On the other hand, MMSE TIRs and MSSNR TEQs become more and more symmetric as the number of taps increases. These observations suggest that MMSE/MSSNR TEQs with symmetry in TIR/TEQ can be designed. Exploiting symmetry significantly reduces the computational complexity to find optimum solutions of MMSE/MSSNR TEQs because some operations associated with TEQ training are growing exponentially with the length of the TEQs. Symmetric FIR filters display linear phase property, which also enables parallel design of FEQs for a constant modulus training sequence because the TEQ phase is known. I propose a symmetric Min-ISI design as a general extension from a symmetric MSSNR TEQ as well.

Chapter 4 analyzes the Min-ISI method in great detail. It aims at overcoming several shortcomings that are embedded in the original Min-ISI proposal. When the TEQ length is longer than the cyclic prefix length, the matrix \mathbf{B} in the original formulation becomes rank deficient, and hence computation of eigenvector becomes infeasible. The matrix \mathbf{B} needs to be recalculated at each single delay when performing delay optimization, which introduces many redundant operations. The generalized eigen-decomposition is handled by Cholesky decomposition, which displays undesirable numerical error behavior when TEQ length is longer than a threshold value. This chapter derives a new cost function that is capable of designing Min-ISI TEQs with length up to N (512 for ADSL). The reformulation of cost function makes \mathbf{B} independent of delay, which reduces the number of Cholesky decompositions to one. I introduce quantized ISI frequency weightings to reduce computational complexity with possible bit rate improvement. Based on the new cost function, I derive an iterative Min-ISI method. The iterative Min-ISI method avoids Cholesky decomposition entirely, and achieves the bit rate performance of the original Min-ISI method. The iterative Min-ISI method is amenable to implementation on fixed-point programmable digital signal processors.

Chapter 5 begins with constructing a complex time domain filter bank structure and ends up at a dual-FIR TEQ structure. The methodology here is to find a theoretical maximum first, then try to find an acceptable tradeoff between the bit rate performance and the implementation cost. The constructed complex time domain equalizer filter bank structure passes the received signals through a number of logical paths. Each path takes care of one data carrying subcarrier. More specifically, each path cascades a finite impulse response frequency selective equalizer and a Goertzel filter computing a single discrete Fourier transform coefficient. The equalizers can be trained by MMSE criteria on a per tone basis. Delay optimization on each single path can be performed to maximize the bit rate. CTEQFB

provides designers most freedom to train equalizers hence gives an performance upper bound for all equalization schemes for a DMT receiver. However, the associated high complexity drives me to find a practical solution with much lower complexity than CTEQFB, but higher bit rates than any conventional DMT receiver with a single TEQ. The proposed dual-path TEQ structure seems attain this goal nicely. A dual-TEQ structure utilizes a second TEQ targeted to a subset of the data carrying subchannels to boost performance on the chosen subset. It guarantees higher bit rates than a single TEQ receiver because it realizes the maximum a single TEQ can do on the first path.

Chapter 6 compares bit rate performance of a downstream ADSL receiver by applying various channel equalization schemes developed in this dissertation. The simulation results confirm that the constructed CTEQFB structure gives a bit rate performance upper bound among all existing channel equalization schemes. It shows 2% improvement over a per tone equalizer that is trained without delay optimization per tone. When narrow band interference is presented in the transmission, CTEQFB carries up to 20% more data rates than a practical single TEQ structure. The two iterative Min-ISI methods with quantized weighting eventually achieves the bit rate performance of the original Min-ISI design with much lower complexity. They are also better suited for a fixed point implementation than the original design since they are less sensitive to quantization errors by avoiding Cholesky decomposition completely. The bit rate performance of suboptimum but linear phase designs under MMSE, MSSNR and Min-ISI criteria has been evaluated to show that bit rate loss between symmetric designs and optimum designs is negligible. Symmetric TEQs have better numerical stability when TEQ length is longer than 50. Simulation results also show that the best tradeoff between performance and complexity comes from a dual TEQ design.

7.2 Future Directions

After one decade of active research on the topic of time domain equalizer design, it seems there is not much left for continued research. This dissertation presents an optimal complex time domain equalizer structure that benchmarks the bit rate performance of any existing linear equalization scheme developed for a DFT based implementation of a multicarrier system. I also proposed a dual TEQ structure that outperforms any conventional equalizer while keeping a good balance between implementation complexity and capacity performance. However, it is still worth trying in several directions to make improvements or fill some vacancies in this area.

For a linear equalizer scheme, the design freedom is maximized in a CTEQFB structure. The CTEQFB structure enjoys different delays on subchannels, variable TEQ lengths, even adjustable demodulation frequencies [66] of Goertzel filters. All of the noise sources can easily be taken care of since the detection/demodulation error on each subchannel is ready to be included in the optimal training of the TEQ. However, it is well known that a decision feedback equalizer outperforms a linear equalizer counterpart in a single carrier system. It remains unknown how much improvement it can make if decision feedback equalizers are exploited in a DMT system.

Some attempts can be found in literature for non-DFT based receiver such as [90], which proposed one-tap DFE for a wireless OFDM system. It claims this one-tap DFE based OFDM system performs better in both symbol error rate and the mutual information between the input of decision device and transmitted symbols. The design of a feedforward filter for each subchannel in the proposals involves matrix inversion and singular value decomposition. It is not practical in cost-effective real-time implementations. This proposal did not exploit DFT at the receiver to decouple the different frequency components of the received signal. This makes the design of the feedforward filter extremely difficult. It seems there are several choices

to introduce DFE into a DFT based receiver. In a conventional structure with TEQ prefiltering, a straightforward way is to use a normal FEQ as the feedforward filter, and add one feedback path feeding the decision back to FEQ output. One tap is enough because only one previous symbol has been involved in the residual ISI/ICI after channel shortening performed by the TEQ. Another possibility is to feed the decision back to the time domain. Because intersymbol interference within one block has been taken care of by FEQs that invert the circular convolution in the frequency domain, the feedback filter is supposed to approximate the path introducing inter-block interference. Assuming previous decisions are correct, IBI can be subtracted in the time domain. This method actually divides the whole feedforward filtering into two steps: scaling plus decoupling. The decoupling is efficiently performed by DFT. The scaling filter is easily designed as a normal FEQ. The first approach makes assumption that the inter-block interference on different subchannels are orthogonal to each other. The second approach does not make this assumption but introduces more operations to transfer data back to the time domain. TEQ is not necessary in the second approach since the IBI is calculated at the feedback filter output and subtracted before FFT demodulation. In a CTEQFB structure, DFE could also be introduced in the format of a decision feedback filter bank. Each forward path contains a one tap complex-valued scaler cascaded by a Goertzel filter. Each feedback path will pass a previous decision through a Goertzel filter that calculates one point of an FFT cascaded by a feedback filter, which also should be a complex valued scalar. DFE in a DMT system may achieve better performance than even a CTEQFB structure with a bank of linear equalizers. It also looks a more practical solution than other non-DFT based DFE multicarrier receivers due to the efficient decoupling of subchannels by a DFT.

This dissertation discusses linear phase designs of time domain equalizers, which have advantages of much lower complexity and linear phase response prop-

erty. It is well-known that given the optimum filters that meet the same magnitude specifications, a minimum phase filter will have two key advantages over a linear phase filter [91]: (1) reduced filter length that is one half to three fourths of the linear phase filter length and (2) minimum group delay that concentrates energy in the low delay instead of medium-delay coefficients. This means minimum phase filters can meet delay and magnitude design specifications but require fewer computations and less memory than linear phase filters. It has not been reported in literature how a minimum phase TEQ could be applied in a DMT transceiver. There are many algorithms to design a minimum phase filter by converting from a linear phase filter. Since I have proposed a linear phase design, I may use it as a start point to reach a minimum phase design. It may add some complexity in the training process, but the savings of computations and memory during the data transmission stage are obvious and desirable.

All the channel equalization schemes discussed in this dissertation are applied to a single input single output (SISO) system. Most wireline communication systems such as HDSL and ADSL fall into this category. However, multiple-input multiple-output systems (MIMO) are receiving more attention in current wireless communications in which the signals from multiple paths are equalized simultaneously. Future generation of multicarrier wireline communications such as VDSL also introduce MIMO concept into system design [92]. It is possible to extend methods proposed in this thesis to be applicable to a MIMO channel. Several approaches like MMSE, MERRY, and PTEQ are already adapted to be applied to a MIMO system [93] [94] [95]. Other methods such as MSSNR, MDS and Min-ISI should be easily adapted as well.

In this dissertation I assume that digitized output of an analog matched filter at the sample rate has been fed into the equalizers. However, to lessen the burden of designing an accurate analog matched filter, a fractionally spaced equalizer (FSE)

is often used in practice. A FSE performs matched filtering and equalization at an over-sampling rate (at least greater than $2F_s$) in the digital domain, which is far less sensitive to sampling phase errors and much easier to be implemented adaptively. A FSE needs more memory to store the filter coefficients, but only output signals at sampling rate need to be computed. Some methods such as MMSE and MGSNR have been presented or extended in an FSE structure. MSSNR related methods such as MDS and Min-ISI could be extended to an FSE context in a similar fashion.

Finally, this dissertation focuses on the subsystem design of channel equalizer with the assumption that other parts of the transceiver are working perfectly. However, with imperfections present in other subsystems such as time recovery error, imperfect echo cancelation, carrier frequency offset (in a RF setup) and non-perfect channel knowledge (which has been addressed a bit in appendix B), joint optimization between equalizer and other units is of interest with potential performance gain. It brings more interaction with other units and it benefits the seamless integration of the whole system.

Appendix A

Applied Signal Technology Data Study

A.1 Observations of Provided ADSL Demonstration

The AST CD-ROM contains two directories: *Bin* and *Signals*. The executable files in *Bin* provide a dos-based demonstration of ADSL transmission:

1. **Goto /bin**

Run `adsl_main 1 ../Signals/Train_09_28_01_13.bin`

The program runs both upstream and downstream receivers. It follows the standard procedure to train both of them. When *INITIALIZATION* stage is over, both of the transceivers enter the *SHOWTIME* stage. The demo program performs data transmission between them. When the data in /Singals runs out, the simulation ends.

The output files contains binary data for ATM packets :

Up_Down_Atm_Active_Packets.bin 30 KB binary file

2. **Run `AdslProtocolDecoder`**

it takes Up_Down_Atm_Active_Packets.bin as input, and generates two output files:

Up_Down_Atm_Active_Packets.txt 118 KB

Up_Down_EtherNet_Packets.txt 74 KB

3. Run StrFileWriter

It converts EtherNet packets to Structured File Format .SF output file:

Up_Down_EtherNet.sf 21 KB

4. The Up_Down_EtherNet.sf is supposed to send to PCX Protocol Decoder and get a html file as output, which is the real application data transmitted in the process. The PCX Decoder is not included in the CD-ROM.

If you open the output files in a binary file reader (you can use the Microsoft Visual C++ IDE), you should be able to read the text files that were transferred via FTP. The packets header will look like binary garbage, but the text will stand out. You can also determine which are the ATM, AAL5, ENET, TCP and IP headers, as they repeat for each packet.

A.2 Description of Data Under Study

The three files in the /Signals directory are the recorded ADSL signals in binary format. They tapped the physical telephone line and used an A/D to digitize the signal on the telephone line. The three files are the physical layer signals. they recorded the voltage on the telephone line and digitized it with the sampling rate is 2.5 MHz. There is only one voltage signal, but ADSL is frequency duplexed so when you perform a specgram you will see the separate up and downstream channels in two distinct frequency bands.

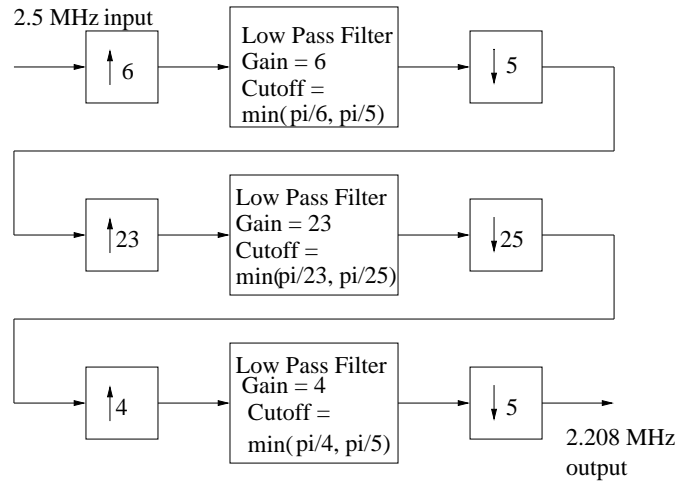


Figure A.1: 3-stage Resampler structure

A.2.1 Accessing the data

The data can be read out using embedded MATLAB functions. For instance,

1. `fid = fopen('Train_09_28_01_13.bin','r');`
2. `A = fread(fid, 100000, 'int16');`

The column vector `A` contains 100000 voltage data samples of data type 'int16'. The sampling frequency is 2.5 MHz.

A.2.2 Resampling the data

ADSL standard sampling frequency is 2.208 MHz. To resample the data from 2.5 MHz to 2.208 MHz, I use the approach described in p.177 of [96]. I design a resampler with three stages, which is shown in the figure (A.1).

I use the Matlab function `fircls1` to design the linear phase FIR interpolation filters. The three filters have frequency responses and phase responses shown in figures (A.2)(A.3)(A.4), respectively.

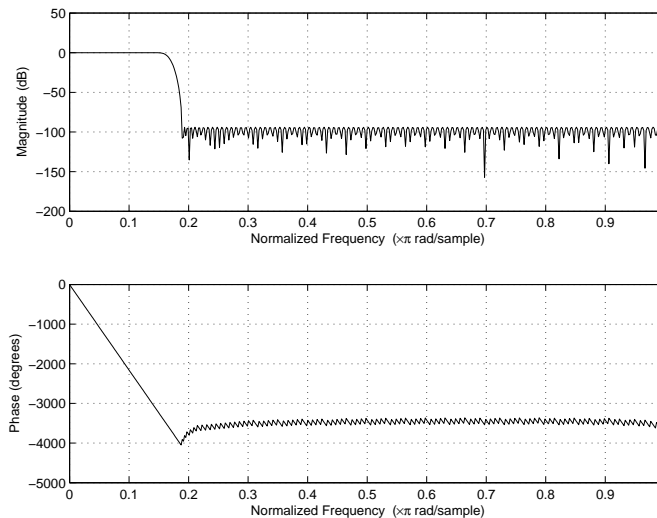


Figure A.2: Frequency and phase response of low pass filter 1

A.2.3 Short review of ADSL initialization sequence

This part is written based on chapter 10 of ITU-T standard G.992.1(ex:G.dmt) titled “Asymmetrical Digital Subscriber Line (ADSL) transceivers” [8].

During the transceiver training, ATU-C (operator end) and ATU-R (customer end) exchange information by sending some special signals. Both of them will go through a set of predefined states associated with corresponding training sequences. If lucky enough, a successful initialization ends up into the *SHOWTIME* stage.

The whole process contains four stages: Handshake Procedures, Transceiver training, Channel Analysis, and Exchange.

Handshaking

In the Handshake stage, the transceivers are powered on and connections (upstream: ATU-R→ATU-C, downstream ATU-C→ATU-R) between them are built.

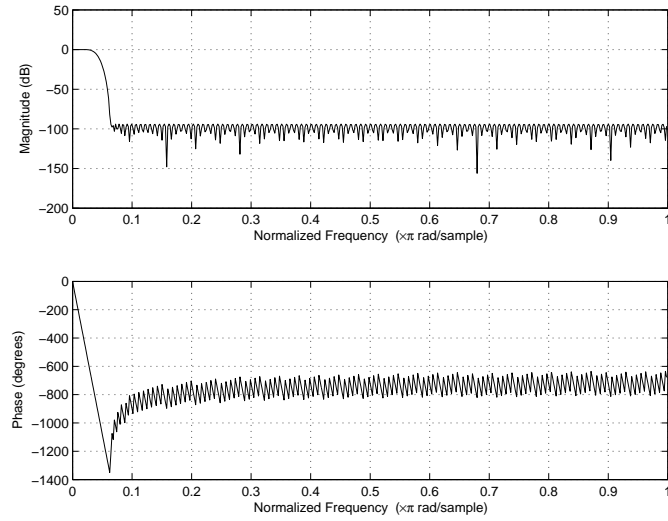


Figure A.3: Frequency and phase response of low pass filter 2

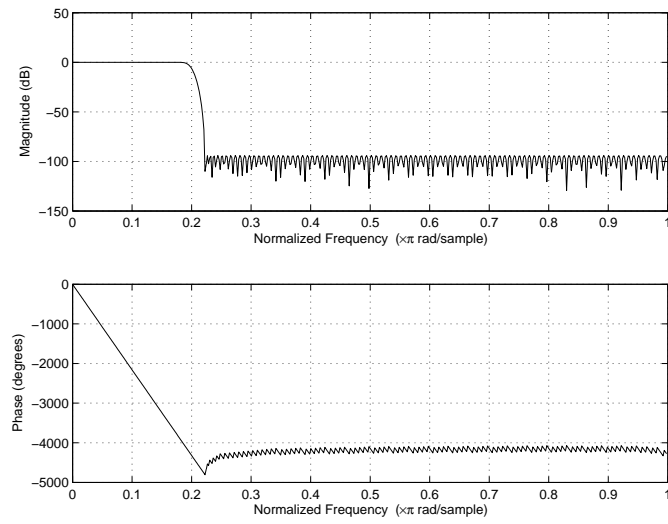


Figure A.4: Frequency and phase response of low pass filter 3

Transceiver training

Synchronization of the mutual training begins with the transmission of R-REVERB1, and is maintained throughout training by both transceivers counting the number of symbols from that point on.

The several important signals in this stage are:

- QUIET: zero output voltage from the DAC
- PILOT: single frequency sinusoid at 276 kHz, tone 64
- REVERB: pseudo-random sequence, 512 bits per symbol, each symbol is identical
- ECT: echo canceller training sequence, vendor-defined

No cyclic prefix is introduced in this stage. Equalizer training should be accomplished by the end of C-REVERB3.

Channel Analysis

Cyclic prefix is used in this stage. Transceiver analyzes the channel and determines transport capacity measured in bearer channels. An ADSL system may transport up to seven user data streams on seven bearer channels (AS0-3: simplex; LS0-2: duplex). The rates for all bearer channels are based on integer multiples of 32 kbps. Important signals are:

- RATES: data rates and formats for bearer channels.
- MSG: vendor information and various options
- MEDLEY: non-periodical, cp-lengthened pseudo-random sequence, estimation of SNR.

Exchange

During this stage each receiver shares with its corresponding transmitter the number of bits and relative power levels to be used on each DMT subcarrier, as well as any messages and final data rates information. Important signals are:

- RATES-RA: refined rates information
- MSG-RA: SNR margin
- MSG2: total bits, loop attenuation, performance margin
- B&G: bit allocation table, scale table.

A.2.4 Channel estimation based on real data

identification of data sequence in initialization

The Matlab script $\mathbf{B} = \text{SPECGRAM}(\mathbf{A}, \text{NFFT}, \text{Fs}, \text{WINDOW}, \text{NOVERLAP})$ calculates the spectrogram for the signal in vector \mathbf{A} . **SPECGRAM** splits the signal into overlapping segments, windows each with the **WINDOW** vector and forms the columns of \mathbf{B} with their zero-padded, length **NFFT** discrete Fourier transforms. Thus each column of \mathbf{B} contains an estimate of a short-term, time-localized frequency content of the signal \mathbf{A} .

I apply this **specgram** analysis to the first 4 seconds of data of the resampled signal “**Train_09_28_01_13.bin**”. The results are shown in the following figures: A.5, A.6, A.7 and A.8.

Form the spcgrams, I can roughly tell that the transceiver runs though **Handshaking** and **Transceiver training**, and enters the stage of **Channel Analysis**. Noted downstream and upstream signals occupy different bandwidth in this Frequency Division Multiplexing ADSL system.

Look at figure A.7, I see the part between two pilot signals (with red power lines centered at 276 kHz) are 512 C-ECT signals followed by 1536 blocks C-REVERB2. C-ECT signals are vender dependent. I guess it is defined as REVERB in this particular system. At the same time, the synchronized ATU-R is transmitted R-QUIET 3 (no transmission actually). Thus, I can use C-REVERB2 to estimate the channel impulse response without separating the upstream signals by a high-pass filter.

More specifically, the estimated channel is given by

$$\hat{h} = \mathcal{F}^{-1} \left(\frac{1}{1000} \sum_{k=1}^{1000} \left\{ \frac{\mathcal{F}\{x_k(n)\}}{\mathcal{F}\{y_k(n)\}} \right\} \right) \quad (\text{A.1})$$

where \mathcal{F} and \mathcal{F}^{-1} represent the forward and inverse 512-point FFT, $x_k(n)$ is the k^{th} period of the chosen C-REVERB2 signal and $y_k(n)$ is the corresponding receiver signal over the same period.

The C-REVERB2 signal is generated according to the definition in 10.4.5 of [8]. The transmit power spectral density is set to -40 dBm/Hz.

Figure A.9 and A.10 show the impulse responses of the estimated channels of recorded data **Train_09_28_01_13.bin** and **Train_09_28_01_14.bin**, respectively.

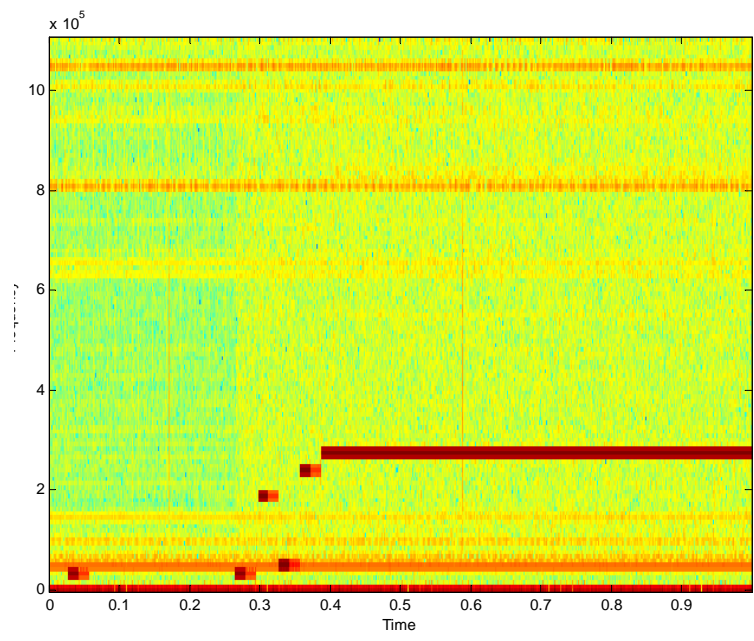


Figure A.5: Spectrogram of signal 1: second 1

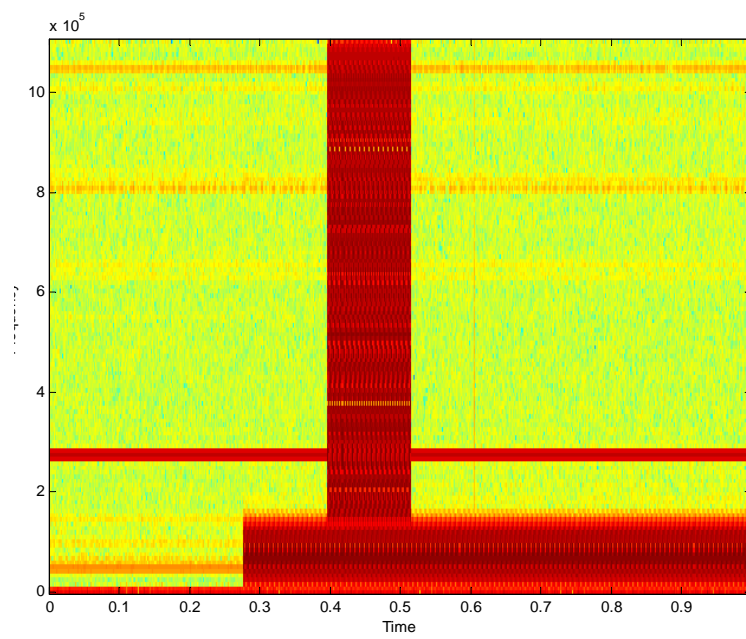


Figure A.6: Spectrogram of signal 1: second 2

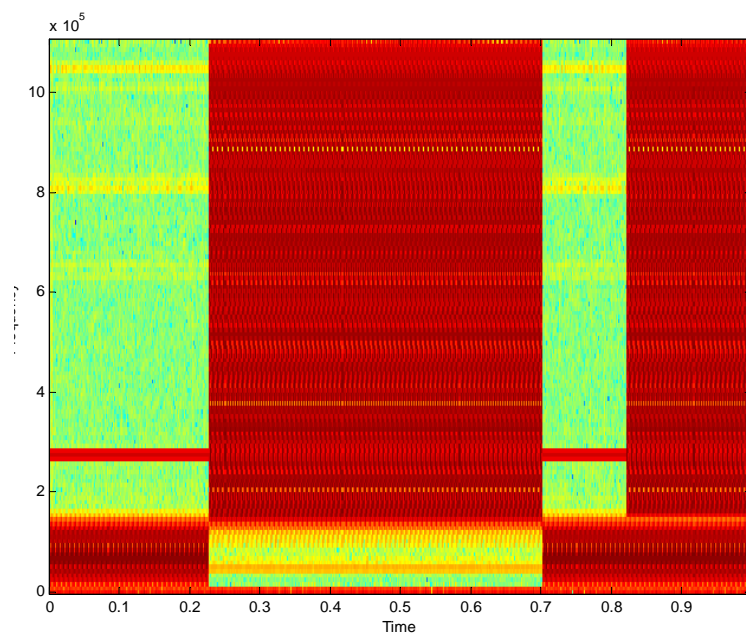


Figure A.7: Spectrogram of signal 1: second 3

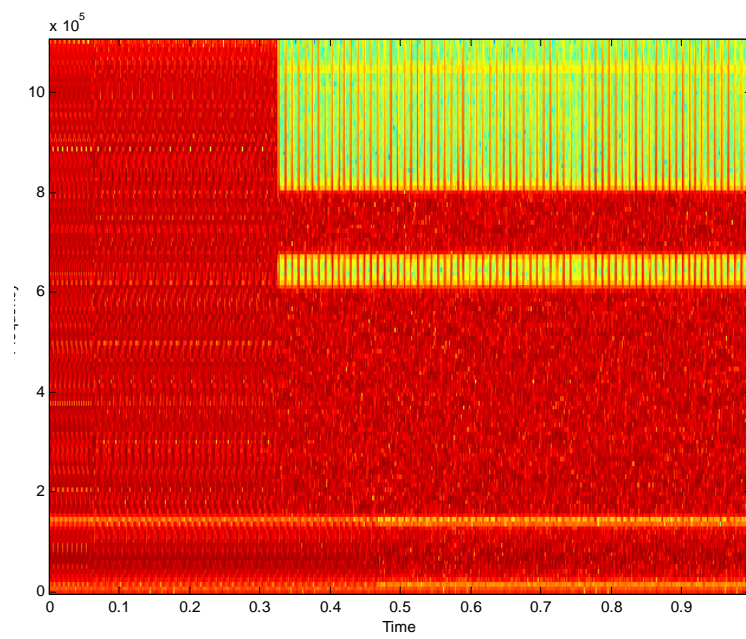


Figure A.8: Spectrogram of signal 1: second 4

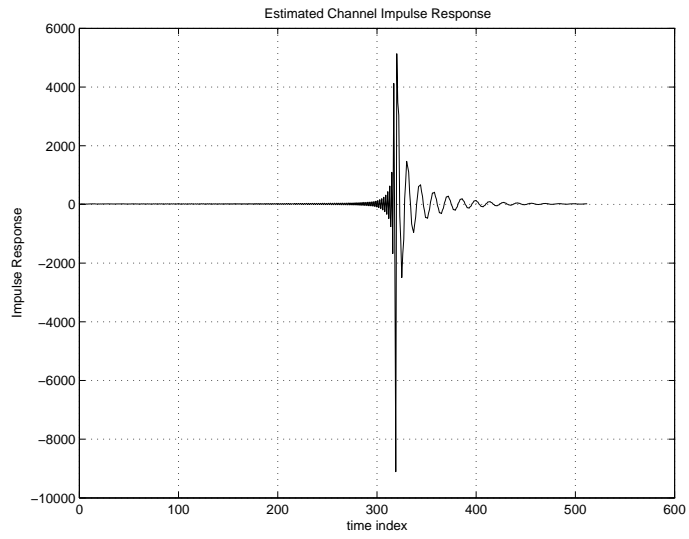


Figure A.9: Estimated Channel Impulse Response for Signal 1

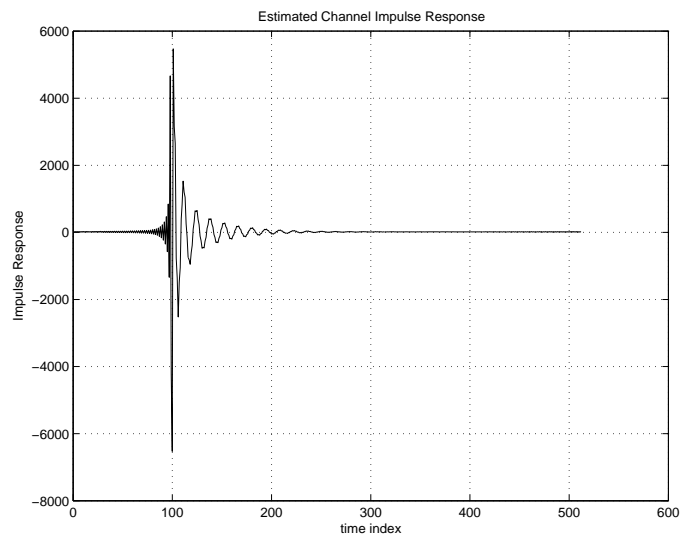


Figure A.10: Estimated Channel Impulse Response for Signal 2

Appendix B

Effect of Channel Estimation Error to Performance

In this appendix, I analyze the impact of imperfect channel estimates on the bit rate performance of four time domain equalization methods. I derive a closed-form expression for the bit rate loss due to channel estimation error. I simulate the sensitivity in bit rate performance with a first-generation downstream ADSL transmission. In simulations, the minimum intersymbol interference and minimum mean square error methods are relatively insensitive to channel estimation errors vs. minimum delay spread and maximum shortening signal-to-noise ratio methods.

In a DMT modulation scheme, a transmitter exploits an N -point Inverse FFT (IFFT) to create $N/2$ orthogonal subchannels. For a large N and an adequately long CP, it is reasonable to assume that channel gain and noise power in each subchannel are flat. SNR on i th subchannel is estimated as

$$\text{SNR}_i = \frac{E[|X_i|^2]}{E[|X_i - \hat{X}_i|^2]} \quad (\text{B.1})$$

where E stands for expectation, X_i and \hat{X}_i s are the transmitted and received symbol on the i th subchannel. Number of bits assigned to i th subchannel is then determined

by

$$b_i = \log_2 \left(1 + \frac{SNR_i}{\Gamma} \right) \quad (\text{B.2})$$

where Γ is SNR gap for achieving Shannon channel capacity and is constant over all subchannels given the same target bit error rate for all subchannels. Bit rate of the system is calculated as

$$R = f_b * \sum_{i \in \mathcal{S}} b_i \quad (\text{B.3})$$

where f_b is symbol rate and \mathcal{S} is the set of all used subchannels.

In [39], it is shown that formulation of equalizer design problem is unified as a maximization of a generalized Rayleigh quotient for most available designs including MMSE, MSSNR, Min-ISI and MDS:

$$\mathbf{w}^{opt} = \arg \max_{\mathbf{w}} \frac{\mathbf{w}^T \mathbf{B} \mathbf{w}}{\mathbf{w}^T \mathbf{A} \mathbf{w}} \quad (\text{B.4})$$

where \mathbf{w} is a $L_w \times 1$ vector contains coefficients of TEQ. \mathbf{A} and \mathbf{B} are generally different matrices when formulated under different criteria. The solution is the generalized eigenvector of the matrix pair (\mathbf{B}, \mathbf{A}) corresponding to the largest generalized eigenvalue.

B.1 Bit Rate Loss Model

B.1.1 General Formulation

The received signal \hat{X}_i for the i th subchannel at the FFT output can be written as

$$\hat{X}_i = \phi_i \mathbf{q}_i^H \mathbf{Y} \mathbf{w} \quad (\text{B.5})$$

where \mathbf{Y} is a $N \times L_w$ Toeplitz matrix which contains the received signal at channel output

$$\mathbf{Y} = \begin{bmatrix} y_t(\nu) & \dots & y_t(\nu - L_w + 1) \\ y_t(\nu + 1) & \dots & y_t(\nu - L_w + 2) \\ \vdots & \ddots & \vdots \\ y_t(N + \nu - 1) & \dots & y_t(N + \nu - L_w) \end{bmatrix}, \quad (\text{B.6})$$

\mathbf{q}_i^H is the i th row of DFT matrix and ϕ_i is the one tap i th FEQ. Follow the approaches provided in [28, 40] by choosing an unbiased zero forcing FEQ, I could have

$$\phi_i = \frac{E[|X_i|^2]}{E[\mathbf{q}_i^H \mathbf{Y} X_i^*] \mathbf{w}} \quad (\text{B.7})$$

Substitute (B.5) and (B.7) into (B.1), and after some manipulations, I have

$$\text{SNR}_i = \frac{|E[\mathbf{q}_i^H \mathbf{Y} X_i^*] \mathbf{w}|^2}{\mathbf{w}^T E[\mathbf{Y}^H \mathbf{q}_i \mathbf{q}_i^H \mathbf{Y}] \mathbf{w} - |E[\mathbf{q}_i^H \mathbf{Y} X_i^*] \mathbf{w}|^2} \quad (\text{B.8})$$

With this SNR model, the bit rate is actually a nonlinear function of the TEQ coefficients:

$$R = f_b * \sum_{i \in \mathcal{S}} \log_2 \left(\frac{\mathbf{w}^T \mathbf{V}_i \mathbf{w}}{\mathbf{w}^T \mathbf{U}_i \mathbf{w}} \right) \quad (\text{B.9})$$

where

$$\begin{aligned} \mathbf{V}_i &= \Gamma E[|X_i|^2] E[\mathbf{Y}^H \mathbf{q}_i \mathbf{q}_i^H \mathbf{Y}] \\ &\quad + (1 - \Gamma) E[\mathbf{Y}^H \mathbf{q}_i X_i] E[X_i^* \mathbf{q}_i^H \mathbf{Y}] \\ \mathbf{U}_i &= \Gamma (E[|X_i|^2] E[\mathbf{Y}^H \mathbf{q}_i \mathbf{q}_i^H \mathbf{Y}] \\ &\quad - E[\mathbf{Y}^H \mathbf{q}_i X_i] E[X_i^* \mathbf{q}_i^H \mathbf{Y}]) \end{aligned} \quad (\text{B.10})$$

For the optimum design with perfect channel knowledge, I calculate bit rate by substituting (B.4) into (B.9). However, the TEQ training usually ends up at a non-optimum $\tilde{\mathbf{w}}$ due to the presence of channel estimation error. I replace \mathbf{A} with $\mathbf{A} + \Delta \mathbf{A}$ and \mathbf{B} with $\mathbf{B} + \Delta \mathbf{B}$ in (B.4). Due to the different formulations of \mathbf{A} and \mathbf{B} in various channel estimation based methods, $\Delta \mathbf{A}$ and $\Delta \mathbf{B}$ are not the same error

matrix in general. The generalized eigen-problem of TEQ design can be reduced to finding an eigenvector of $\mathbf{C} = \mathbf{A}^{-1}\mathbf{B}$. Although in practice one considers other approaches to solve it due to numerical implementation concerns, this approach could serve here as an analytic study of channel estimation error effects.

Suppose an $n \times n$ matrix \mathbf{C} has an eigendecomposition with n eigenvalues $\lambda_1, \lambda_2, \dots, \lambda_n$, n corresponding eigenvectors $\mathbf{w}_1, \mathbf{w}_2, \dots, \mathbf{w}_n$ and n left eigenvectors $\mathbf{p}_1, \mathbf{p}_2, \dots, \mathbf{p}_n$, is perturbed by $\tilde{\mathbf{C}} = \mathbf{C} + \Delta\mathbf{C}$. We have

$$\begin{aligned}
\tilde{\mathbf{C}} &= (\mathbf{A} + \Delta\mathbf{A})^{-1}(\mathbf{B} + \Delta\mathbf{B}) \\
&= (\mathbf{A}^{-1} - \mathbf{A}^{-1}(\Delta\mathbf{A}^{-1} + \mathbf{A}^{-1})^{-1}\mathbf{A}^{-1})(\mathbf{B} + \Delta\mathbf{B}) \\
&= \mathbf{A}^{-1}\mathbf{B} - \mathbf{A}^{-1}(\Delta\mathbf{A}^{-1} + \mathbf{A}^{-1})^{-1}\mathbf{A}^{-1}\mathbf{B} \\
&\quad + \mathbf{A}^{-1}\Delta\mathbf{B} - \mathbf{A}^{-1}(\Delta\mathbf{A}^{-1} + \mathbf{A}^{-1})^{-1}\mathbf{A}^{-1}\Delta\mathbf{B} \\
&= \mathbf{C} + \Delta\mathbf{C}
\end{aligned} \tag{B.11}$$

where $\Delta\mathbf{C}$ is the sum of last three terms in (B.11)

In a practical TEQ design, usually \mathbf{C} has only one largest eigenvalue λ_k , and optimum TEQ $\mathbf{w} = \mathbf{w}_k$ in this case. Under the perturbation of $\Delta\mathbf{C}$, λ_k is replaced by $\lambda_k + \Delta\lambda_k$ and \mathbf{w}_k is changed to $\mathbf{w}_k + \Delta\mathbf{w}_k$. Write

$$\Delta\mathbf{w}_k = \sum_{i=1}^n d_i \mathbf{w}_i \tag{B.12}$$

where d_i are projection coefficients. We have

$$\mathbf{w}_k + \Delta\mathbf{w}_k = (1 + d_k)\mathbf{w}_k + \sum_{i \neq k} d_i \mathbf{w}_i \tag{B.13}$$

Since eigenvectors are determined only up to a scalar multiple, we can always set $d_k = 0$ to make $\Delta\mathbf{w}_k = \sum_{i \neq k} d_i \mathbf{w}_i$. I follow the approach in [97] to expand

$$(\mathbf{C} + \Delta\mathbf{C})(\mathbf{w}_k + \Delta\mathbf{w}_k) = (\lambda_k + \Delta\lambda_k)(\mathbf{w}_k + \Delta\mathbf{w}_k). \tag{B.14}$$

Using the facts

$$\mathbf{C}\mathbf{w}_i = \lambda_i\mathbf{w}_i \quad (\text{B.15})$$

$$\mathbf{p}_j^H\mathbf{w}_k = 0 \text{ if } k \neq j \text{ and } \mathbf{p}_k^H\mathbf{w}_k \neq 0, \quad (\text{B.16})$$

it can be shown that

$$\begin{aligned} \Delta\mathbf{w}_k &= \alpha^{-1} \sum_{k \neq i} \mathbf{w}_i \frac{\mathbf{p}_i^H(\Delta\mathbf{C})\mathbf{w}}{(\lambda_k - \lambda_i)\mathbf{p}_i^H\mathbf{w}_i} \\ \tilde{\mathbf{w}} &= \mathbf{w} + \Delta\mathbf{w}_k = \beta\mathbf{w} \end{aligned} \quad (\text{B.17})$$

where

$$\begin{aligned} \alpha &= \mathbf{I} + \sum_{k \neq i} \mathbf{w}_i \frac{\mathbf{p}_i^H(\Delta\lambda_k)}{(\lambda_k - \lambda_i)\mathbf{p}_i^H\mathbf{w}_i} \\ &\quad - \sum_{k \neq i} \mathbf{w}_i \frac{\mathbf{p}_i^H(\Delta\mathbf{C})}{(\lambda_k - \lambda_i)\mathbf{p}_i^H\mathbf{w}_i}, \end{aligned} \quad (\text{B.18})$$

$$\beta = \mathbf{I} + \alpha^{-1} \sum_{k \neq i} \mathbf{w}_i \frac{\mathbf{p}_i^H(\Delta\mathbf{C})}{(\lambda_k - \lambda_i)\mathbf{p}_i^H\mathbf{w}_i}, \quad (\text{B.19})$$

and \mathbf{I} is an $L_w \times L_w$ identity matrix. Hence, the bit rate

$$\begin{aligned} \tilde{R} &= f_b * \sum_{i \in \mathcal{S}} \log_2 \left(\frac{\tilde{\mathbf{w}}^T \mathbf{V}_i \tilde{\mathbf{w}}}{\tilde{\mathbf{w}}^T \mathbf{U}_i \tilde{\mathbf{w}}} \right) \\ &= f_b \log_2 \prod_{i \in \mathcal{S}} \left(\frac{\tilde{\mathbf{w}}^T \mathbf{V}_i \tilde{\mathbf{w}}}{\tilde{\mathbf{w}}^T \mathbf{U}_i \tilde{\mathbf{w}}} \right) \end{aligned} \quad (\text{B.20})$$

Data rate loss due to imperfect channel estimation can be written as

$$\begin{aligned} \Delta R &= f_b \left(\log_2 \prod_{i \in \mathcal{S}} \left(\frac{\mathbf{w}^T \mathbf{V}_i \mathbf{w}}{\mathbf{w}^T \mathbf{U}_i \mathbf{w}} \right) - \log_2 \prod_{i \in \mathcal{S}} \left(\frac{\tilde{\mathbf{w}}^T \mathbf{V}_i \tilde{\mathbf{w}}}{\tilde{\mathbf{w}}^T \mathbf{U}_i \tilde{\mathbf{w}}} \right) \right) \\ &= f_b \log_2 \prod_{i \in \mathcal{S}} \left(\frac{\mathbf{w}^T \mathbf{V}_i \mathbf{w} (\beta\mathbf{w})^T \mathbf{U}_i (\beta\mathbf{w})}{\mathbf{w}^T \mathbf{U}_i \mathbf{w} (\beta\mathbf{w})^T \mathbf{V}_i (\beta\mathbf{w})} \right) \end{aligned}$$

B.1.2 Case Studies

With the unified approach proposed above, I look into each different TEQ design methods to find out what is $\Delta\mathbf{C}$ in each case.

Maximum Shortening SNR

The MSSNR approach [21] is based solely on shortening the channel impulse response. I define a channel convolution matrix as

$$\mathbf{H} = \begin{bmatrix} h(0) & h(-1) & \dots & h(-(L_w - 1)) \\ h(1) & h(0) & \dots & h(-(L_w - 2)) \\ \vdots & \vdots & \ddots & \vdots \\ h(N - 1) & h(N - 2) & \dots & h(N - L_w) \end{bmatrix} \quad (\text{B.21})$$

and a sliding shortening window function as

$$g(n) = \begin{cases} 1 & \text{if } \Delta \leq n \leq \Delta + \nu \\ 0 & \text{elsewhere} \end{cases} \quad (\text{B.22})$$

where Δ is the transmission delay. Further, we define

$$\mathbf{G} = \text{diag}[g(0) \quad g(1) \quad \dots \quad g(N - 1)]^T \quad (\text{B.23})$$

and $\mathbf{D} = \mathbf{I} - \mathbf{G}$, we have

$$\begin{aligned} \mathbf{A} &= \mathbf{H}^T \mathbf{D}^T \mathbf{D} \mathbf{H} \\ \mathbf{B} &= \mathbf{H}^T \mathbf{G}^T \mathbf{G} \mathbf{H} \end{aligned} \quad (\text{B.24})$$

Channel estimation error is defined as perturbation to matrix \mathbf{H} as $\Delta\mathbf{H}$. Assume $\|\Delta\mathbf{H}\|_2 = \epsilon$ is sufficiently small, we have

$$\begin{aligned} \tilde{\mathbf{A}} &= (\mathbf{H} + \Delta\mathbf{H})^T \mathbf{D}^T \mathbf{D} (\mathbf{H} + \Delta\mathbf{H}) = \mathbf{A} + \Delta\mathbf{A} \\ \tilde{\mathbf{B}} &= (\mathbf{H} + \Delta\mathbf{H})^T \mathbf{G}^T \mathbf{G} (\mathbf{H} + \Delta\mathbf{H}) = \mathbf{B} + \Delta\mathbf{B} \end{aligned} \quad (\text{B.25})$$

where

$$\begin{aligned} \Delta\mathbf{A} &= \mathbf{H}^T \mathbf{D}^T \mathbf{D} \Delta\mathbf{H} + \Delta\mathbf{H}^T \mathbf{D}^T \mathbf{D} \mathbf{H} + \mathcal{O}(\epsilon^2) \\ \Delta\mathbf{B} &= \mathbf{H}^T \mathbf{G}^T \mathbf{G} \Delta\mathbf{H} + \Delta\mathbf{H}^T \mathbf{G}^T \mathbf{G} \mathbf{H} + \mathcal{O}(\epsilon^2) \end{aligned}$$

$\Delta\mathbf{C}$ is then easily computed from \mathbf{A} , \mathbf{B} , $\Delta\mathbf{A}$, and $\Delta\mathbf{B}$ using (B.11). TEQ coefficients and bit rate loss computation can proceed in a straightforward manner.

Min-ISI

The Min-ISI method generalizes the MSSNR method by weighting the ISI in the frequency domain [26, 30], e.g., to place the ISI in unused and low SNR sub-channels. Similarly, for Min-ISI, I have $\mathbf{A} = \mathbf{H}^T \mathbf{D}^T \left(\sum_{i \in \mathcal{S}} \mathbf{q}_i^H \frac{S_{x,i}}{S_{n,i}} \mathbf{q}_i \right) \mathbf{D} \mathbf{H}$ and $\mathbf{B} = \mathbf{H}^T \mathbf{G}^T \mathbf{G} \mathbf{H}$, where $S_{x,i}$ and $S_{n,i}$ are signal power and noise power on i th sub-channel, respectively. We can represent perturbations as

$$\begin{aligned} \Delta \mathbf{A} &= \mathbf{H}^T \mathbf{D}^T \left(\sum_{i \in \mathcal{S}} \mathbf{q}_i^H \frac{S_{x,i}}{S_{n,i}} \mathbf{q}_i \right) \mathbf{D} \Delta \mathbf{H} \\ &\quad + \Delta \mathbf{H}^T \mathbf{D}^T \left(\sum_{i \in \mathcal{S}} \mathbf{q}_i^H \frac{S_{x,i}}{S_{n,i}} \mathbf{q}_i \right) \mathbf{D} \mathbf{H} + \mathcal{O}(\epsilon^2) \\ \Delta \mathbf{B} &= \mathbf{H}^T \mathbf{G}^T \mathbf{G} \Delta \mathbf{H} + \Delta \mathbf{H}^T \mathbf{G}^T \mathbf{G} \mathbf{H} + \mathcal{O}(\epsilon^2) \end{aligned}$$

MDS

MDS method [22] is to minimize so called delay spread of the effective channel impulse response. Delay spread is defined as

$$D = \sqrt{\frac{1}{h_e} \sum_{n=0}^{L_h} (n - \bar{n})^2 |h(n)|^2} \quad (\text{B.26})$$

where h_e is the energy of channel impulse response, and \bar{n} is a user-defined center tap of h . I define $\mathbf{A} = \mathbf{H}^T \mathbf{D}^T \mathbf{Q} \mathbf{D} \mathbf{H}$ and $\mathbf{B} = \mathbf{H}^T \mathbf{H}$ for MDS and obtain

$$\begin{aligned} \Delta \mathbf{A} &= \mathbf{H}^T \mathbf{Q} \Delta \mathbf{H} + \Delta \mathbf{H}^T \mathbf{Q} \mathbf{H} + \mathcal{O}(\epsilon^2) \\ \Delta \mathbf{B} &= \mathbf{H}^T \Delta \mathbf{H} + \Delta \mathbf{H}^T \mathbf{H} + \mathcal{O}(\epsilon^2) \end{aligned}$$

where $\mathbf{Q} = \text{diag}\{[(0 - \bar{n})^2, \dots, (L_w + L_h - \bar{n})^2]\}$ is a diagonal weighting matrix.

MMSE

MMSE TEQ design [17, 18] minimizes the mean square error between the output of the physical path consisting of the channel and FIR filter and the output of a virtual

path consisting of a transmission delay Δ and a target impulse response (TIR). In the case of MMSE TIR with unit norm constraint, the solution to the generalized eigenvalue problem is the optimum target impulse response \mathbf{b} .

$$\begin{aligned}\mathbf{A} &= (\Psi^T \mathbf{R}_x \Psi) - \Psi^T \mathbf{R}_x \mathbf{H} (\mathbf{H}^T \mathbf{R}_x \mathbf{H} + \mathbf{R}_n)^{-1} \mathbf{H}^T \mathbf{R}_x \Psi \\ &= [(\Psi^T \mathbf{R}_x \Psi)^{-1} + \mathbf{H} \mathbf{R}_n^{-1} \mathbf{H}^T]^{-1} \\ \mathbf{B} &= \mathbf{I}_{\nu+1}\end{aligned}\tag{B.27}$$

where Ψ is a $(L_h + L_w - 1) \times (\nu + 1)$ windowing matrix defined as

$$[\Psi]_{m,n} = \delta(m + n - \Delta) \begin{cases} 0 \leq m < L_w + L_h - 1 \\ 0 \leq n < \nu + 1 \end{cases}\tag{B.28}$$

Directly compute $\Delta \mathbf{C}$ is easier in this case,

$$\begin{aligned}\tilde{\mathbf{C}} &= (\Psi^T \mathbf{R}_x \Psi)^{-1} + (\mathbf{H} + \Delta \mathbf{H}) \mathbf{R}_n^{-1} (\mathbf{H} + \Delta \mathbf{H})^T \\ \Delta \mathbf{C} &= \mathbf{H} \mathbf{R}_n^{-1} \Delta \mathbf{H}^T + \Delta \mathbf{H} \mathbf{R}_n^{-1} \mathbf{H}^T + \mathcal{O}(\epsilon^2)\end{aligned}\tag{B.29}$$

Once I obtain $\tilde{\mathbf{b}} = \beta \mathbf{b}$, the TEQ $\tilde{\mathbf{w}}$ can be calculated

$$\tilde{\mathbf{w}} = ((\mathbf{H} + \Delta \mathbf{H})^T \mathbf{R}_x (\mathbf{H} + \Delta \mathbf{H}) + \mathbf{R}_n)^{-1} (\mathbf{H} + \Delta \mathbf{H})^T \mathbf{R}_x \Psi \tilde{\mathbf{b}}\tag{B.30}$$

B.2 Simulations

The simulations compare the sensitivity to bit rate performance of the different equalizer designs for a wireline communication transceiver. More specifically, I consider a downstream first generation ADSL transmission. According to the ITU ADSL standard, the IFFT and FFT lengths are 512 and the cyclic prefix length is 32. I test the designs on eight typical carrier service area (CSA) loops recommended by Bell Labs [82]. Full ADSL bandwidth is up to 1.104 MHz. A common practice in industry is to use frequency division multiplexing to allocate bi-directional transmission to different frequency bands. I adopt this approach and introduce a 5th order

high pass IIR filter with passband frequency at 138 kHz to separate the downstream data from the upstream data. The signal power spectral density at the transmitter output is set equal to -40 dBm/Hz. Channel noise is modeled as an additive white Gaussian noise (AWGN) with -140 dBm/Hz power density, NEXT noise from 5 integrated services digital network (ISDN) disturbers.

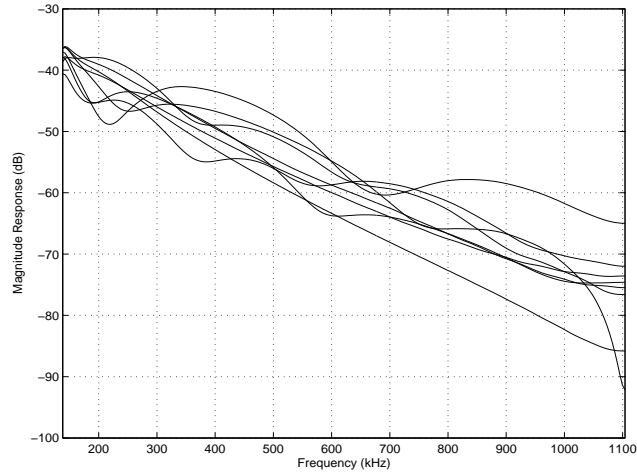


Figure B.1: Magnitude responses in downstream transmission bandwidth for eight CSA loops

Fig. B.1 presents magnitude responses of the eight test loops. The average channel impulse response power is between -43 dBm and -48 dBm. In my system setup, the average received signal power P_r is around -24 dBm and noise power P_n (including crosstalk and AWGN) is about -60 dBm. I model channel estimation error as an AWGN noise with variance σ^2 . According to [13], if I adopt a commonly used frequency domain channel estimates

$$\hat{H}_i = \frac{1}{L} \sum_{k=1}^L \frac{R_{k,i}}{X_i} \quad (\text{B.31})$$

where $R_{k,i}$ is the i th DFT element of received channel output at k th cycle, the channel estimation error is controlled by $\sigma^2 = \frac{1}{L} P_n$. I choose a reasonable σ^2

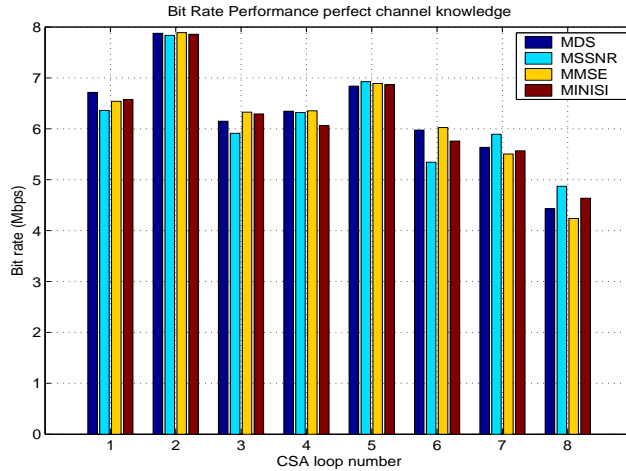


Figure B.2: Achievable bit rate for 8 CSA loops for four TEQ design methods with perfect channel knowledge. Coding gain is 5 dB, margin is 6 dB, input power is -40 dBm/Hz, AWGN power is -140 dBm/Hz, NEXT noise is from 5 ISDN disturbers.

ranging from -90 dBm to -76 dBm, where end points corresponding to averaging on $L = 1000$ cycles and $L = 40$ cycles, respectively. $L = 40$ is also suggested in [13] as a lower bound of estimation cycles. Moreover, my channel estimation error power is corresponding to an AWGN with power spectral density from -153 dBm/Hz to -133 dBm/Hz within my transmission bandwidth, which is significantly below channel gain in this range. It further suggests my choice of estimation error power is fairly conservative.

The SNR gap to Shannon capacity in my simulation is chosen as

$$\Gamma_{sim} \text{ (in dB)} = \Gamma_{gap} + \text{system margin} - \text{coding gain} \quad (\text{B.32})$$

where $\Gamma_{gap} = 9.8$ dB corresponds to 10^{-7} bit error rate, system margin is 6 dB, and coding gain is 5 dB.

Fig. B.2 displays the achievable bit rates for eight CSA loops with perfect channel estimation. Though the four design methods use different metric to opti-

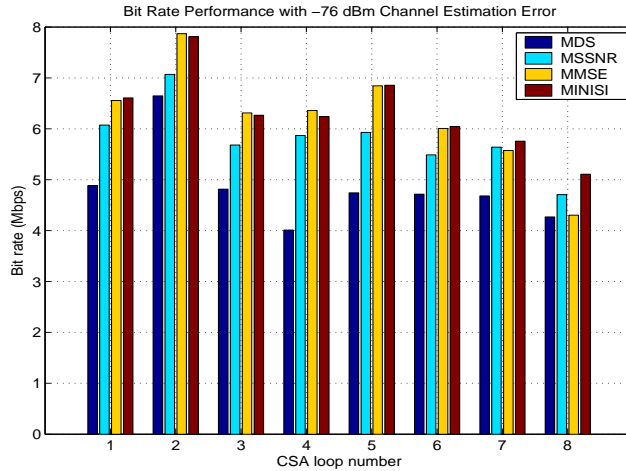


Figure B.3: Achievable bit rate for 8 CSA loops for four TEQ design methods with -76 dBm channel estimation error. Coding gain is 5 dB, margin is 6 dB, input power is -40 dBm/Hz, AWGN power is -140 dBm/Hz, NEXT noise is from 5 ISDN disturbers.

mize TEQ settings, the bit rate performances are quite close with full knowledge of channel impulse response.

Fig. B.3 displays the achievable bit rates for eight CSA loops when -76 dBm power channel estimation error is introduced. It appears that Min-ISI and MMSE outperform MSSNR by roughly 10% and MDS by roughly 20%. The performance gap is universally perceivable among all eight loops. It suggests the Min-ISI and MMSE bit rate performances hold better against channel estimation error than the bit rate performances of MSSNR and MDS.

Fig. B.4 shows bit rate vs. channel estimation error power for loop 5. In Fig. B.4, MSSNR and MDS are significantly affected by channel estimation error. MSSNR and MDS completely depend on the channel impulse response. In addition, MDS uses a \mathbf{Q} weighting matrix to amplify the impulse response as well as the estimation error. On the other hand, Min-ISI and MMSE have already taken noise

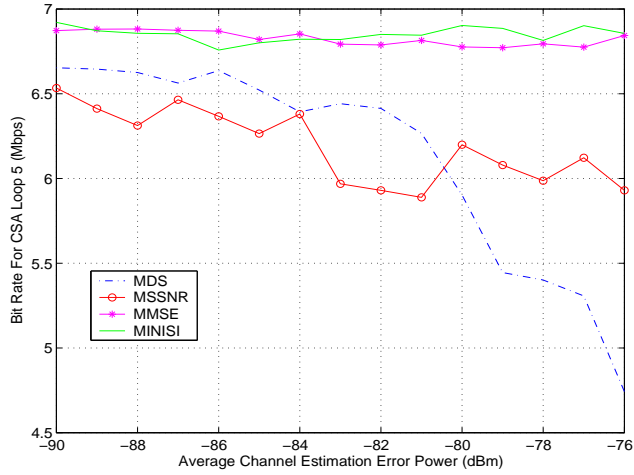


Figure B.4: Achievable bit rate for CSA loop 5 for four TEQ design methods with channel estimation error from -90 dBm to -70 dBm. Coding gain is 5 dB, margin is 6 dB, input power is -40 dBm/Hz, AWGN power is -140 dBm/Hz, and NEXT noise is from 5 ISDN disturbers.

into account, and hence, are relatively insensitive to channel estimation error. With accurate channel gain estimates, estimation error power can be 16 dB lower than additive noise power, which would likely not affect the bit rate performance as much as observed in simulations.

Since none of the four methods directly optimize the bit rate function in (B.2), a TEQ design with small estimation error could achieve a higher bit rate in some cases. This means ΔR of (B.21) might be negative in some cases.

Bibliography

- [1] B. C. Lindberg, “Convergence of Voice, Data, Image and Video, Services and Networks.” available at http://home.earthlink.net/~lindberg_b/converge.htm.
- [2] T. Starr, J. M. Cioffi, and P. J. Silverman, *Understanding Digital Subscriber Line Technology*. Prentice Hall, 1999.
- [3] G. Arslan, *Equalization Techniques for Multicarrier Modulation*. PhD thesis, The Univ. of Texas at Austin, Dec. 2000.
- [4] “Internetworking Technology Handbook.” Cisco Systems, available at http://www.cisco.com/univercd/cc/td/doc/cisintwk/ito_doc/.
- [5] “Learning about DSL.” DSL forum, available at http://www.dslforum.org/about_dsl.htm.
- [6] F. Ouyang, P. Duvaut, O. Moreno, and L. Pierrugues, “The First Step of Long-Reach ADSL: Smart DSL Technology, READSL,” *IEEE Communications Magazine*, pp. 124–131, Sept. 2003.
- [7] J. A. C. Bingham, “Multicarrier Modulation for Data Transmission: An Idea Whose Time Has Come,” *IEEE Communications Magazine*, vol. 28, pp. 5–14, May 1990.

- [8] “Asymmetrical Digital Subscriber Line (ADSL) Transceivers.” ITU G.992.1, 1999.
- [9] J. G. Proakis, *Digital Communications*. McGraw-Hill Inc., 3 ed., 1995.
- [10] S. D. Sandberg and M. A. Tzannes, “Overlapped Discrete Multitone Modulation for High Speed Copper Wire Communications,” *IEEE Journal on Selected Areas in Comm.*, vol. 13, pp. 1571–1581, Dec. 1995.
- [11] S. Kasturia, J. T. Aslanis, and J. M. Cioffi, “Vector Coding for Partial Response Channels,” *IEEE Trans. on Information Theory*, vol. 36, pp. 742–762, July 1990.
- [12] R. Learned, H. Krim, B. Claus, A. Willsky, and C. Karl, “Wavelet-packet Based Multiple Access Communication,” *Proc. SPIE on Math. Imaging*, 1994.
- [13] J. M. Cioffi, *EE379C Course Notes*. Stanford University, 2001.
- [14] J. R. Treichler, I. Fijalkow, and C. Johnson, “Fractionally spaced equalizers,” *IEEE Signal Processing Magazine*, vol. 13, pp. 65–81, May 1996.
- [15] P. Chow, *Bandwidth Optimized Digital Transmission Techniques for Spectrally Shaped Channels with Impulse Noise*. PhD thesis, Stanford University, 1993.
- [16] D. D. Falconer and F. R. Magee, “Adaptive Channel Memory Truncation for Maximum Likelihood Sequence Estimation,” *Bell Sys. Tech. Journal*, pp. 1541–1562, Nov. 1973.
- [17] J. S. Chow, J. M. Cioffi, and J. A. C. Bingham, “Equalizer Training Algorithms for Multicarrier Modulation Systems,” in *Proc. IEEE Int. Conf. on Comm.*, (Geneva, Switzerland), pp. 761–765, May 1993.

- [18] N. Al-Dhahir and J. M. Cioffi, "Efficiently Computed Reduced-Parameter Input-Aided MMSE Equalizers for ML Detection: A Unified Approach," *IEEE Trans. on Info. Theory*, vol. 42, pp. 903–915, May 1996.
- [19] B. Farhang-Boroujeny and M. Ding, "Design Methods for Time-Domain Equalizers in DMT Transceivers," *IEEE Trans. on Comm.*, vol. 49, pp. 554–562, Mar. 2001.
- [20] R. K. Martin, M. Ding, B. L. Evans, and C. R. Johnson, Jr., "Infinite Length Results and Design Implications for Time-Domain Equalizers." *IEEE Trans. on Signal Processing*, vol. 52, no. 1, Jan. 2004.
- [21] P. J. W. Melsa, R. C. Younce, and C. E. Rohrs, "Impulse Response Shortening for Discrete Multitone Transceivers," *IEEE Trans. on Comm.*, vol. 44, pp. 1662–1672, Dec. 1996.
- [22] R. Schur and J. Speidel, "An Efficient Equalization Method to Minimize Delay Spread in OFDM/DMT Systems," in *Proc. IEEE Int. Conf. on Comm.*, vol. 5, (Helsinki, Finland), pp. 1481–1485, June 2001.
- [23] A. Tkacenko and P. P. Vaidyanathan, "Noise Optimized Eigenfilter Design of Time-domain Equalizers for DMT Systems," in *Proc. IEEE Int. Conf. on Comm.*, vol. 1, (New York, NY), Apr.–May 2002.
- [24] R. K. Martin, J. Balakrishnan, W. A. Sethares, and C. R. Johnson, Jr., "A Blind, Adaptive TEQ for Multicarrier Systems," *IEEE Signal Processing Letters*, vol. 9, pp. 341–343, Nov. 2002.
- [25] N. Al-Dhahir and J. M. Cioffi, "Optimum Finite-Length Equalization for Multicarrier Transceivers," *IEEE Trans. on Comm.*, vol. 44, pp. 56–64, Jan. 1996.
- [26] G. Arslan, B. L. Evans, and S. Kiaei, "Equalization for Discrete Multitone

- Receivers To Maximize Bit Rate,” *IEEE Trans. on Signal Processing*, vol. 49, pp. 3123–3135, Dec. 2001.
- [27] M. Milosevic, L. F. C. Pessoa, B. L. Evans, and R. Baldick, “DMT Bit Rate Maximization with Optimal Time Domain Equalizer Filter Bank Architecture,” in *Proc. IEEE Asilomar Conf.*, vol. 1, (Pacific Grove, CA), pp. 377–382, Nov. 2002.
- [28] K. Vanbleu, G. Ysebaert, G. Cuyper, M. Moonen, and K. Van Acker, “Bitrate Maximizing Time-Domain Equalizer Design for DMT-based Systems,” in *Proc. IEEE Int. Conf. on Comm.*, pp. 2360–2364, May 2003.
- [29] D. Love, W. Berglund, and B. L. Evans, “DSP Implementations of Min-ISI Design by UT Austin.” available at <http://www.ece.utexas.edu/~bevans/projects/adsl/index.html> .
- [30] M. Ding, B. L. Evans, R. K. Martin, and C. R. Johnson, Jr., “Minimum Intersymbol Interference Methods for Time Domain Equalizer Design,” in *Proc. IEEE Global Comm. Conf.*, (San Francisco, CA), Dec. 2003.
- [31] S. Celebi, “Interblock Interference (IBI) and Time of Reference (TOR) Computation in OFDM Systems,” *IEEE Trans. on Comm.*, vol. 49, pp. 1895–1900, Nov. 2001.
- [32] S. Celebi, “Interblock Interference (IBI) Minimizing Time-Domain Equalizer (TEQ) for OFDM,” *IEEE Signal Processing Letters*, vol. 10, pp. 232–234, Aug. 2003.
- [33] M. Ding, A. J. Redfern, and B. L. Evans, “A Dual-path TEQ Structure for DMT-ADSL Systems,” in *Proc. IEEE Int. Conf. on Acoustics, Speech, and Signal Proc.*, vol. 3, (San Francisco, CA), pp. 2573–2576, May 2002.

- [34] K. Van Acker, G. Leus, M. Moonen, O. van de Wiel, and T. Pollet, "Per Tone Equalization for DMT-Based Systems," *IEEE Trans. on Comm.*, vol. 49, pp. 109–119, Jan. 2001.
- [35] J.-F. Van Kerckhove and P. Spruyt, "Adapted Optimization Criterion for FDM-based DMT-ADSL Equalization," in *Proc. IEEE Int. Conf. on Comm.*, vol. 3, pp. 1328–1334, June 1996.
- [36] L. Vandendorpe, "Fractionally Spaced Linear and DF MIMO Equalizers for Multitone Systems without Guard Time," *Annals of Telecommunications*, vol. 52, pp. 21–30, Jan.–Feb. 1997.
- [37] L. Vandendorpe, J. Louveaux, B. Maison, and A. Chevreuil, "About the Asymptotic Performance of MMSE MIMO DFE for Filter-Bank Based Multicarrier Transmission," *IEEE Trans. on Comm.*, vol. 47, pp. 1472–1475, Oct. 1999.
- [38] T. Pollet, M. Peeters, M. Moonen, and L. Vandendorpe, "Equalization for DMT-Based Broadband Modems," *IEEE Communications Magazine*, vol. 38, pp. 106–113, May 2000.
- [39] R. K. Martin, K. Vanbleu, M. Ding, G. Ysebaert, M. Milosevic, B. L. Evans, M. Moonen, and C. R. Johnson, Jr., "Unification and Evaluation of Equalization Structures and Design Algorithms for Discrete Multitone Modulation Systems." *IEEE Transactions on Signal Processing*, accepted for publication, 2004.
- [40] R. K. Martin, K. Vanbleu, M. Ding, G. Ysebaert, M. Milosevic, B. L. Evans, M. Moonen, and C. R. Johnson, Jr., "Implementation Complexity and Communication Performance Tradeoffs in Discrete Multitone Modulation Equalizers." *IEEE Transactions on Signal Processing*, in preparation.

- [41] D. S. Watkins, *Fundamentals of Matrix Computations*. John Wiley & Sons, 1991.
- [42] G. H. Golub and C. F. Van Loan, *Matrix Computations*. Baltimore, MD: The Johns Hopkins University Press, 1996.
- [43] C. Yin and G. Yue, "Optimal Impulse Response Shortening for Discrete Multitone Transceivers," *Electronics Letters*, vol. 34, pp. 35–36, Jan. 1998.
- [44] M. Nafie and A. Gatherer, "Time-Domain Equalizer Training for ADSL," in *Proc. IEEE Int. Conf. on Comm.*, vol. 2, (Montreal, Canada), pp. 1085–1089, June 1997.
- [45] I. Djokovic, "MMSE equalizers for DMT systems with and without crosstalk," in *Proc. IEEE Asilomar Conf. on Signals, Systems and Computers*, (Pacific Grove, CA), pp. 545–549, Nov. 1997.
- [46] B. Wang, T. Adali, Q. Liu, and M. Vlatkovic, "Generalized Channel Impulse Response Shortening for Discrete Multitone Transceivers," in *Proc. IEEE Asilomar Conf. on Signals, Systems, and Computers*, vol. 1, pp. 276–280, 1999.
- [47] W. Chiu, W. K. Tsai, T. C. Liau, and M. G. Troulis, "Time-domain Channel Equalizer Design Using the Inverse Power Method," in *Proc. IEEE Int. Conf. on Comm.*, (Vancouver, Canada), pp. 973–977, May 1999.
- [48] B. Lu, L. D. Clark, G. Arslan, and B. L. Evans, "Fast Time-domain Equalization for Discrete Multitone Modulation Systems," in *Proc. IEEE Digital Signal Processing Workshop*, (Hunt, TX), Oct. 2000.
- [49] J. S. Chow, J. C. Tu, and J. M. Cioffi, "A Discrete Multitone Transceiver System for HDSL Applications," *IEEE Journal on Selected Areas in Comm.*, vol. 9, pp. 895–907, Aug. 1991.

- [50] J. S. Chow and J. M. Cioffi, "A Cost-Effective Maximum Likelihood Receiver for Multicarrier Systems," in *Proc. IEEE Int. Conf. on Comm.*, vol. 2, pp. 948–952, June 1992.
- [51] D. Daly, C. Heneghan, and A. D. Fagan, "A Minimum Mean-Squared Error Interpretation of Residual ISI Channel Shortening for Discrete Multitone Transceivers," in *Proc. IEEE Int. Conf. on Acoustics, Speech, and Signal Processing*, vol. 4, pp. 2065–2068, May 2001.
- [52] I. Lee, J. S. Chow, and J. M. Cioffi, "Performance Evaluation of a Fast Computation Algorithm for the DMT in High-speed Subscriber Loop," *IEEE Journal on Selected Areas in Comm.*, vol. 13, pp. 1564–1570, Dec. 1995.
- [53] X. F. Wang, W. S. Lu, and A. Antoniou, "Adaptive equalization for partially bandwidth-occupied ADSL transceivers," in *IEEE Pacific Rim Conf. on Comm. Comp. and Sig. Proc.*, pp. 572–575, Aug. 1999.
- [54] N. Warke, A. Redfern, C. Sestok, and M. Ali, "Performance comparison of teq design techniques for fdm adsl," in *Proc. IEEE Asilomar Conf. on Signals, Systems and Computers*, (Pacific Grove, CA), pp. 367–371, Nov. 2002.
- [55] J. Wu, G. Arslan, and B. L. Evans, "Efficient Matrix Multiplication Methods to Implement a Near-Optimum Channel Shortening Method for Discrete Multitone Transceivers," in *Proc. IEEE Asilomar Conf. on Signals, Systems, and Computers*, vol. 1, (Pacific Grove, CA), pp. 152–157, Nov. 2000.
- [56] R. K. Martin, M. Ding, B. L. Evans, and C. R. Johnson, Jr., "Efficient Channel Shortening Equalizer Design." Dec. 2003.
- [57] W. Henkel, G. Taubock, P. Odling, P. O. Borjesson, and N. Petersson, "The cyclic prefix of OFDM/DMT - an analysis," in *Int. Zurich Seminar Broadband Commun., Access, Transm., Networking*, vol. 2, pp. 1–3, 2002.

- [58] A. Tkacenko and P. P. Vaidyanathan, “Eigenfilter Design of MIMO Equalizers for Channel Shortening,” in *Proc. IEEE Int. Conf. on Acoustics, Speech, and Signal Processing*, vol. 3, (Orlando, FL), pp. 2361–2364, May 2002.
- [59] A. Tkacenko and P. P. Vaidyanathan, “A Low-Complexity Eigenfilter Design Method for Channel Shortening Equalizers for DMT Systems,” *IEEE Trans. on Comm.*, vol. 51, July 2003.
- [60] M. Milosevic, L. F. C. Pessoa, B. L. Evans, and R. Baldick, “DMT bit rate maximization with optimal time domain equalizer filter bank architecture,” in *Proc. IEEE Asilomar Conf. on Signals, Systems and Computers*, (Pacific Grove, CA), pp. 377–382, Nov. 2002.
- [61] K. Vanbleu, G. Ysebaert, G. Cuypers, and M. Moonen, “Bitrate Maximizing Per-Group Equalization for DMT-based Systems.” Submitted to *Elsevier Signal Processing*.
- [62] K. Van Acker, G. Leus, M. Moonen, and T. Pollet, “RLS-Based Initialization for Per-Tone Equalizers in DMT Receivers,” *IEEE Trans. on Comm.*, vol. 51, pp. 885–889, June 2003.
- [63] G. Ysebaert, K. Vanbleu, G. Cuypers, M. Moonen, and T. Pollet, “Combined RLS-LMS Initialization for Per Tone Equalizers in DMT-Receivers,” *IEEE Trans. on Signal Processing*, vol. 51, pp. 1916–1927, July 2003.
- [64] R. K. Martin and C. R. Johnson, Jr., “Blind, Adaptive Per Tone Equalization for Multicarrier Receivers,” in *Proc. Conf. on Information Sciences and Systems*, (Princeton, NJ), Mar. 2002.
- [65] T. Starr, J. Cioffi, and P. Silvermann, *Understanding Digital Subscriber Line Technology*. Upper Saddle River, NJ: Prentice Hall PTR, 1999.

- [66] M. Milosevic, *Maximizing Data Rate of Discrete Multitone Systems using Time Domain Equalization Design*. PhD thesis, The University of Texas at Austin, May 2003.
- [67] N. Al-Dhahir and J. Cioffi, “The Combination of Finite-length Geometric Equalization and Candwidth Optimization for Multicarrier Transceivers,” in *International Conf. on Acoustics, Speech, and Signal Processing*, pp. 1201–1204, May 1995.
- [68] N. Al-Dhahir and J. Cioffi, “A Band-optimized Reduced-complexity Equalized Multicarrier Transceiver,” *IEEE Trans. on Comm.*, vol. 45, pp. 948–956, Aug. 1997.
- [69] N. Al-Dhahir and J. M. Cioffi, “Optimum Finite-Length Equalization for Multicarrier Transceivers,” in *Proc. IEEE Global Comm. Conf.*, (San Francisco, CA), pp. 1884–1888, Nov. 1994.
- [70] N. Lashkarian and S. Kiaei, “Optimum Equalization of Multicarrier Systems: A Unified Geometric Approach,” *IEEE Trans. on Comm.*, vol. 49, pp. 1762–1769, Oct. 2001.
- [71] S. Schaible, “Fractional Programming – a Recent Survey,” *Journal of Statistics and Management Systems*, vol. 29, pp. 845–866, Mar. 2001.
- [72] R. Freund and F. Jarre, “Solving the sum-of-ratios problem by an interior-point method,” Tech. Rep. 3/99, Bell Labs, 1999.
- [73] Y. Almogly and O. Levin, “A Class of Fractional Programming Problems,” *Operations Research*, vol. 19, pp. 57–67, 1971.
- [74] K. Vanbleu, G. Ysebaert, G. Cuyper, M. Moonen, and K. Van Acker, “Bitrate Maximizing Time-Domain Equalizer Design for DMT-based Systems.” June 2004.

- [75] R. K. Martin, C. R. Johnson, Jr., M. Ding, and B. L. Evans, "Exploiting Symmetry in Channel Shortening Equalizers," in *Proc. IEEE Int. Conf. on Acoustics, Speech, and Signal Proc.*, vol. 5, (Hong Kong SAR, China), pp. V-97-V-100, Apr. 2003.
- [76] R. K. Martin, C. R. Johnson, Jr., M. Ding, and B. L. Evans, "Infinite Length Results for Channel Shortening Equalizers," in *Proc. IEEE Sig. Proc. Workshop on Sig. Proc. Advances in Wireless Comm.*, (Rome, Italy), June 2003.
- [77] E. Robinson, *Statistical Communication and Detection*. London: Griffin, 1967.
- [78] J. Makhoul, "On the Eigenvectors of Symmetric Toeplitz Matrices," *IEEE Trans. on Acoustics, Speech, and Signal Processing*, vol. 29, pp. 868-872, Aug. 1981.
- [79] N. Al-Dhahir, *Optimized-Transmitter Reduced-Complexity MMSE-DFE under Finite-Length Constraints*. PhD thesis, Stanford University, 1994.
- [80] A. Cantoni and P. Butler, "Eigenvalues and Eigenvectors of Symmetric Centrosymmetric Matrices," *Linear Algebra and Its Applications*, vol. 13, pp. 275-288, 1976.
- [81] C. Ribeiro, V. Silva, and P. S. R. Diniz, "Linear Phase Impulse Response Shortening for xDSL DMT Modems," in *Int. Telecommunications Sym.*, (Brasil), pp. 368-371, Sept. 2002.
- [82] G. Arslan, M. Ding, B. Lu, M. Milosevic, Z. Shen, and B. L. Evans, "MATLAB DMTTEQ Toolbox 3.1 Release." The University of Texas at Austin, July 27, 2003. [Online.] Available: <http://www.ece.utexas.edu/~bevans/projects/adsl/dmtteq/dmtteq.html>.
- [83] W. W. Hager, *Applied Numerical Linear Algebra*. Prentice Hall, 1988.

- [84] T. K. Moon and W. C. Stirling, *Mathematical Methods and Algorithms for Signal Processing*. Prentice Hall, 2000.
- [85] C. Chatterjee, V. P. Roychowdhury, J. Ramos, and M. D. Zoltowski, "Self-Organizing Algorithms for Generalized Eigen-Decomposition," *IEEE Trans. on Neural Networks*, vol. 8, pp. 1518–1530, Nov. 1997.
- [86] R. C. Younce, P. J. W. Melsa, and S. Kapoor, "Echo Cancellation for Asymmetrical Digital Subscriber Lines," in *IEEE Int. Conf. on Comm.*, pp. 301–306, May 1994.
- [87] D. G. Messerschmitt and A. Salvekar, "Linemod software for transmission line analysis." Dept. of Electrical Engineering and Computer Sciences, University of California, Berkeley. [Online]. Available: <http://www.stanford.edu/~cioffi/linemod/linemod.html>.
- [88] N. G. Cole, "Asymmetric Digital Subscriber Line Technology - a basic overview," *British Telecommunications Tech. J.*, Jan. 1994.
- [89] P. Venugopal, M. J. Carter, and S. A. Valcourt, "Radio Frequency Interference and Capacity Reduction in DSL." *Tech. Report* Dept. of Electrical and Computer Engineering, University of New Hampshire, Available: <http://ftp.iol.unh.edu/CCN/RFLDSL.pdf>.
- [90] Y. Sun and L. Tong, "Channel Equalization Using One-Tap DFE for Wireless OFDM Systems With ICI and ISI," in *Proc. IEEE Sig. Proc. Workshop on Sig. Proc. Advances in Wireless Comm.*, (Annapolis, MD), May 1999.
- [91] N. Damera-Venkata and B. L. Evans, "Optimal Design of Real and Complex Minimum Phase Digital FIR Filters," in *Proc. IEEE International Conf. on Acoustics, Speech, and Signal Processing*, (Phoenix, AZ), pp. 1145–1148, Mar. 1999.

- [92] G. Ginis and J. M. Cioffi, "Vectored transmission for digital subscriber line systems," *IEEE Journal on Select. Area in Comm.*, pp. 1085–1104, June 2002.
- [93] N. Al-Dhahir, "FIR Channel-Shortening Equalizers for MIMO ISI Channels," *IEEE Trans. on Comm.*, vol. 49, pp. 213–218, Feb. 2001.
- [94] G. Leus and M. Moonen, "Per-Tone Equalization for MIMO OFDM Systems," *IEEE Trans. on Signal Processing*, vol. 51, pp. 2965–2975, Nov. 2003. Special Issue on Signal Processing for MIMO Wireless Comm. Systems.
- [95] R. K. Martin, J. M. Walsh, and C. R. Johnson, Jr., "Low Complexity MIMO Blind, Adaptive Channel Shortening." Submitted to *IEEE Trans. on Signal Processing*, Oct. 2003.
- [96] A. V. Oppenheim and R. W. Schaffer, *Discrete-Time Signal Processing, Second Edition*. Prentice Hall, 1999.
- [97] J. Demmel, *Applied Numerical Linear Algebra*. SIAM, 1997.

Vita

Ming Ding was born on July 16th, 1973. He received his Bachelor of Science degree from Department of Electronic Science at Nankai University in 1995 and his Master of Engineering Degree from Department of Electrical and Computer Engineering at National University of Singapore in 1999 respectively. From 1995-1997, he was an R&D engineer with the National Post & Telecom. Industry Co. (PTIC), Shanghai, China. From April 1999 to Aug. 2000, he worked as an R&D Engineer for the Centre for Wireless Communications at the National University of Singapore. Ming is currently a full-time Ph.D. student in Electrical Engineering in The University of Texas at Austin.

In 2000, UT Austin Dept. of Electrical and Computer Engineering employed him as a teaching assistant for the Real-time Digital Signal Processing Laboratory under Prof. Brian L. Evans. From 2001 through 2003, he was a research assistant under Prof. Brian L. Evans, where he developed real-time channel shortening techniques for discrete multitone systems. In the summers of 2001, 2002 and 2003, he was an intern at the DSPS R&D Center, Texas Instruments, Dallas, TX. He has developed and implemented alternative receiver structures for ADSL transmission in TI's commercial modems. He was a non-degree graduate student at Cornell University during Fall 2002. He worked with Prof. Rick Johnson's group there to develop low complexity channel shortening methods.

He has been a student member of the Institute of Electrical and Electronics

Engineers (IEEE) since 2000.

Permanent Address: Xiang Yang Xin Cun 1-1-203,
Changsheng Road, Hangzhou,
Zhejiang, 310006, P. R. China

This dissertation was typeset with L^AT_EX 2_ε¹ by the author.

¹L^AT_EX 2_ε is an extension of L^AT_EX. L^AT_EX is a collection of macros for T_EX. T_EX is a trademark of the American Mathematical Society. The macros used in formatting this dissertation were written by Dinesh Das, Department of Computer Sciences, The University of Texas at Austin, and extended by Bert Kay and James A. Bednar.